Spring 5-15-2022

VCP: A Gatekeeper for Intracellular Proteopathic Seeding

Jiang Zhu
Washington University in St. Louis

WASHINGTON UNIVERSITY IN ST. LOUIS

Division of Biology and Biomedical Sciences
Neurosciences

Dissertation Examination Committee:
Conrad C Weihl, Chair
Yuna M Ayala
Aaron DiAntonio
Timothy M Miller
Erik S Musiek

VCP: A Gatekeeper for Intracellular Proteopathic Seeding

by
Jiang Zhu

A dissertation presented to
The Graduate School
of Washington University in
partial fulfillment of the
requirements for the degree
of Doctor of Philosophy

May 2022
St. Louis, Missouri

Table of contents

List of Figures

List of Tables

Acknowledgments

First, I thank my PI, Chris. He is a great mentor and scientist, and it has been my pleasure to work with him for the past five years. He is sharp and passionate in science, who challenged me when I was over-optimistic with positive data, and guides me to troubleshoot when I was frustrated with a negative result. He trained me to become an independent scientist in every aspect – from paper reading, experimental design, presentation, collaboration, grant writing, publishing, to thinking about science in the big picture. More important, as a mentor, he never stops his people from pursuing what they want and gives any support he can provide. When we started the sequencing project, he questioned that the experiment may not work as I designed. Indeed, it finally failed. However, he still let me do it because he believed it was a good learning process for me. I am in touch at the moment. I can tell so many stories and great personalities I can learn from him. Dr. Weihl definitely deserves the title on his mug – "the best boss of the world." Second, I cannot thank more for my lab mates, especially Sara and Rocio. They are so supportive in the lab and life. They act like my big sisters (something like mom), taught me the ABC of conducting experiments, helped troubleshoot my dirty western blots, and bore me with my mistakes and disorganized benches. They are the spirit of the Weihl lab and maintain a healthy environment for everyone. As the lab grows, I thank my other colleagues, Drew, Jil, Khalid, May, Abu, Eileen Chengcheng, and Michio. They are friendly, supportive, and responsible, and I learned a lot from each one of them. Being a member of the Weihl lab brings so much pleasure to my Ph.D. journey. Third, I would like to thank my committee members, collaborators, and professors, especially Gus and Wille. I cannot finish my research without them. I can come to

Gus whenever I need any help. He will provide the best he knows with great patience. Forth, I must thank my family, especially my mom. My families are at my back, respects my decision, and encourages me to pursue my dream. My mom, a retired born in the 1960s, never stops her curiosity in science and embraces new technology. The last time we chatted, she tried to discuss the Adaboost algorithm and machine learning, which apparently I know nothing about. Her merit and curiosity in science keep inspiring me and encouraging me to go further in research. Her family education and role model are my great fortune in life. Finally, I cannot thank more to my friends at WashU. In the past five and half years, you have been so supportive in both science and life. Whenever Chris and I faced a problem, he always told me, "go ask your friends." At the same time, we shared the Sunday brunches, food, game night, alcohol, and the ups and downs in life.

Although life has been altered since the slash of COVID, I believe the passion for science will never stop.

Jiang Zhu

May 2022

ABSTRACT OF THE DISSERTATION

VCP: A Gatekeeper for Intracellular Proteopathic Seeding

By Jiang Zhu

Doctor of Philosophy in Biology and Biomedical Sciences

Neurosciences

Washington University in St. Louis, 2022

Professor Conrad C Weihl, Chair

Protein inclusions such as β-amyloid, tau, α-synuclein, and TDP-43 are considered the pathologic hallmarks of many neurodegenerative diseases. These proteins are prone to misfold, aggregate, and template new aggregates. Accumulating evidence suggests that those proteins in their high-molecular-weight forms can serve as a "seed", spread through an interconnected brain network, and induce new inclusions. Therefore, it is essential to understand the mechanism of proteopathic seeding.

In this dissertation, we performed a whole genomic CRISPR-Cas9 KO screening to identify gene modifiers of αS seeding. Within the screening, we found several hits of endolysosomal function and trafficking, including VCP. VCP is a versatile protein required for protein homeostasis. Mutations in VCP are associated with type 1 Multisystem proteopathy (MSP1), whose patients can develop multiple neurodegenerative diseases with proteopathic protein inclusions, including Frontotemporal dementia (FTD), amyotrophic

lateral sclerosis (ALS), Parkinson and Alzheimer's. We validated that either VCP dysfunction (inhibition or RNAi knockdown) or VCP disease mutations can exacerbate αS seeding in both αS biosensor cells and hippocampal neurons, in which both VCP knockdown and VCP mutation knock-in neurons show increasing αS aggregation following seeding. Additionally, mice carrying a VCP disease mutation exhibit more αS aggregates than C57 control 90 days after intrastriatal injection of αS pre-formed fibrils *in vivo*. We showed that VCP aggravates endolysosomal membrane damage with the proteopathic seeds. Similarly, seeding activities increased when we co-treated the cells with seeds and LLOMe, a drug specifically permeabilizes the endolysosome. Previously, in our lab, we demonstrated VCP involved in the autophagy-mediated clearance of damaged endolysosome, called lysophagy. Screening different VCP cofactors, we identified that only lysophagy-related cofactor UBXD1 modifies the α-synuclein seeding the same as VCP. We proposed that VCP might regulate αS seeding via UBXD1-dependent lysophagy.

This dissertation also developed two novel TDP-43 seeding assays, which phenocopies hyper-phosphorylated TDP-43 aggregations in patients. We observed the same protective effect of VCP on intracellular TDP-43 seeding and tau. Overall, our results support VCP as a gatekeeper for different intracellular proteopathic seeding in a merging pathway.

Chapter 1: Introduction

1.1 proteopathic seeding and neurodegenerative diseases

Neurodegenerative diseases (NDD) are adult-onset disorders affecting more than 9 million American[1]. It includes Alzheimer's disease (AD), Parkinson's disease, Huntington disease, Frontotemporal dementia (FTD), amyotrophic lateral sclerosis (ALS), multiple system atrophy (MSA), etc. Regardless of diverse phenotypes, NDDs are characterized by progressive neuronal loss, which leads to neurological dysfunctions.

1.1.1 proteopathic seeding hypothesis

Despite their distinct clinic symptoms, most NDDs patients have protein aggregates as a definitive feature. The major components are different from diseases – AD is remarked by Aβ aggregates and tau tangles; Parkinson's and MSA accumulation α-synuclein positive inclusions called Lewy bodies; Huntington is caused by polyQ aggregates; ALS can be divided into different subtypes by the different types of proteins in inclusion (TDP-43 or FUS or SOD1).

The proteopathic seeding hypothesis was proposed in the late 1990s, inspired by infectious prions in prion diseases, since Aβ, tau, and other signatures in NDDs can convert from their native form to amyloid β sheets and turn into insoluble fibrils, same as prions. Numerous studies demonstrated that these amyloid forms could accelerate and template the monomers to form new aggregates. Furthermore, injecting patients' brain lysates into naïve animals can provoke disease-like symptoms and inclusion bodies[2]. Braak's studies identified the different stages of aggregation in AD, Parkinson's, FTD, and ALS, suggesting the

temporal-spatial propagation of those aggregates[3,4]. Fetal neurons transplanted to Substantia Nigra (SN) of the Parkinson patients showed synuclein inclusion in the grafted tissues[5]. It evidences the transformation of those proteins from one region to another in the human brain. Together, scientists declared a proteopathic seeding hypothesis in NDDs and named those infectious proteins as proteopathic proteins (also called prion-like proteins or prionids).

The proteopathic proteins usually have the following features:

1) Those proteins are native unfolded (α-synuclein and tau) or contain an unstructured region (TDP-43)[6], prone to aggregate.
2) The fibrillar or oligomeric(e.g., tau and Aβ) forms of those proteins can specifically template and promote the fibrillization of its monomers[6]. (This process is called seeding. And the high-molecular-weight species are named seed and recognized as seeding compatible.)
3) The aggregate or oligomer form of those proteins is neurotoxic[7–10].
4) The propagation of those protein aggregates (tau, α-synuclein, and TDP-43) can be closely related to disease progression[11].

Some proteopathic inclusions (e.g., synuclein and tau) can precede the first symptoms of NDDs[12] and propagate across brains as disease progress[4]. Previous research showed that blocking the proteopathic intracellular seeding can prevent seed propagation, rescue neuron loss, and benefit motor behaviors in mouse model[13,14]. Therefore, proteopathic seeding could offer new therapeutic targets to a broader range of NDDs patients regardless of their genetic backgrounds.

Of note, other pathological features including inflammation, mitochondria dysfunction, and oxidative stress are shared in many NDDs as well, which are detailed reviewed elsewhere[15,16]. Meanwhile, proteopathic protein might contribute to the diseases in other aspects independent of aggregates and its seeding capacity, like TDP-43, which I will briefly mention below. Furthermore, as the definition suggests, proteopathic proteins are prone to aggregates, but not all aggregated proteins are proteopathic. Moreover, inclusion bodies in NDDs can be highly diverse, deposit up to hundreds of different kinds of proteins[17,18]. Finally, although my research focuses on proteopathic seeding in neurons, some evidence implied the involvement of glia in seeding as well[4,19].

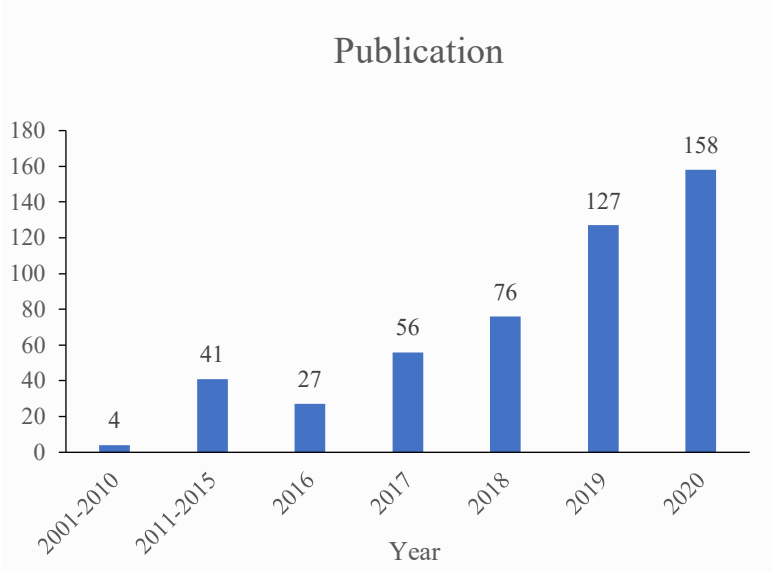

Figure 1. 1: increasing recognition on proteopathic seeding in literature.

1.1.2 αlpha-Synuclein

αS (encoded by SNCA gene) is a 140 amino acid protein highly enriched in the neurons, predominantly in the pre-synaptic terminal. αS locates at the reserved pools of the vesicle and might function in synaptic transmission based on SNAC KO mice[20]. αS is composed of the N- terminal domain, a non-amyloid-β component (NAC) domain, and a disordered C-terminal. It is unfolded monomer or multimers naturally, but upon seeding and pathological conditions, αS is converted to oligomers and amyloid fibrils. αS is identified as the major component of inclusions – Lewy bodies – in the neurons or astrocytes of Parkinson's Disease, Diffuse Lewy body disease (DLB), multiple system atrophy (MSA), and REM sleep behavior disorder (RBD). Meanwhile, SNCA mutations, duplication, or triplication of this locus are associated with PD and MSA[21].

The seeding capacity of αS is well characterized. Because of the disordered secondary structure, αS fibril can seed monomers *in vitro*. Exposure of HEK 293 cells stably overexpressing αS to αS fibrils or brain extract from PD and MSA patients can covert monomeric αS into aggregates within 24 hours[22]. Likewise, adding αS fibril to the primary cells (e.g., neurons[23] and oligodendrocytes[24]) is sufficient to induce novel hyper-phosphorylated detergent-resistant αS aggregates. This seeding event could happen anterogradely and retrogradely in neurons[25]. The novel αS aggregate is seeding compatible as well (called passage), which amplifies αS pathology[22].

Either inoculation of αS purified fibril or extraction from α-Synucleinopathy patients into the brain can generate αS pathology in wild-type mice or monkeys. Regardless of different injection sites (SN, olfactory bulb, or striatum), hyperphosphorylated αS inclusions were observed from the proximal injection area to the more distal area in a time-dependent manner[26–29]. The injected animal also exhibited a neuronal loss in SN and motor deficits.

Several pathways are known to affect the αS seeding process. Although αS monomer can freely diffuse into the cell, αS fibril mainly takes up via endocytosis[30]. HSPG mediates αS fibril via micropinocytosis and, in turn, affects seeding[31]. Alternatively, LAG3 and two other transmembrane receptors were identified to selectively bind to αS fibril and take up αS fibril via endocytosis. LAG3 deletion can alleviate αS neuron-to-neuron transmission and reduce αS pathology and motor deficits in injection model[32].

Once uptake, αS fibril predominantly localizes in the endo-lysosome. The role of lysosomes in αS seeding is mysterious. Lysosome inhibition showed persistent αS fibril in cells, implicate reduced degradation[33]. And knockdown of the lysosomal K^+ channel TMEM175 or drug inhibition of lysosome (CHQ) enhanced the seeding efficiency in primary neurons[34,35]. Permeabilizing endolysosome by LLOMe raises αS seeding efficiency in Jiang et al.'s study[36]. It is consistent with my results in cells and primary neurons. In contrast, lysosome inhibition and knockdown of core lysosomal protein showed a decrease in αS seeding[37]. Those contradictive studies might suggest dual roles of the lysosome in αS seeding (discuss later).

Several polyphenols (EGCG, brazilin, resveratrol, etc.) can antagonize the fibrillation of αS[38]. Brazilin can biochemically ameliorate αS fibrilization and protect neurons from cell death[39], consistent with our result of EGCG on the αS biosensor line (data not shown). Meanwhile, chaperone/co-chaperone, like DNAJB6[40] and Hsp110[13], prevents αS seeding probably by fibril disassembly[41].

αS aggregates might be released extracellularly from dead neurons. However, it cannot explain the fast propagation and wide spreading of αS in patients and mouse injection models. Moreover, Ulusoy et al. showed αS propagation independent of neurodegeneration in rat[42]. Although αS contains no secret signal, αS is found in the CSF of healthy control and synucleinopathy patients[43]. αS aggregates can be secreted extracellularly by exosome[44]. In parallel, exosomes isolated from brain extract or the CSF of DLB patients enrich αS are seeding capable[45]. Besides, αS fibril and TDP-43 can transfer in tunneling nanotubes between cells[46,47].

Apart from the known pathways in seeding, other orphan genes were found, whose role in seeding is still enigmatic or controversial. Three parkinsonism risk genes – LRRK2[48,49], GBA[49] and APOE4[50] – modulate αS seeding efficiency in both cell and mouse models. Both LRRK2 and GBA modulate total αS expression[49], and LRRK2 contributes to many aspects of the lysosome-autophagy pathway[51], which is essential for protein homeostasis and aggregates clearance. APOE4 links with earlier onset[52] and faster cognitive decline of PD [50]. However, the molecular mechanism of these effects needs further investigation.

1.1.3 TDP-43

TAR DNA binding protein 43 (TDP-43) is a highly conserved DNA/RNA binding protein. TDP-43 is ubiquitously expressed in many tissues. It contains an N-term region (aa 1–102) with nuclear localization signal (NLS, aa 82–98), two RNA recognition Motifs RRMs (aa 104–176 and aa 192–262), a nuclear export signal (NES, aa 239–250), followed by an unstructured C-terminal region (aa 274–414) with prion-like glutamine/asparagine-rich (Q/N) domain (aa 345–366) and a glycine-rich domain (aa 367–414). By binding to specific RNA via RRM, TDP-43 can involve in many RNA metabolisms, including transcription, pre-mRNA splicing, mRNA transport, translation, microRNA and long non-coding RNA processing, stress granules, etc[53]. TDP-43 normally acts in the nucleus as a dimer but can translocate to cytoplasm or mitochondria. For instance, TDP-43 can be recruited to stress granules under stress exposure, binds to RNA, and regulates transcription. This regulation can be crucial for some cellular events, like muscle regeneration[54]. Loss of TDP-43 in neuronal-like cells (Neuro-2A) blocks neurite outgrowth and induces apoptosis[55], and homozygous depletion of TDP-43 in mice cause early embryonic lethality[56].

In 2006, TDP-43 was identified as the main component of tau negative inclusion bodies in the spinal cord of both sporadic and familial ALS and the cortex of FTD. The insoluble TDP-43 is ubiquitinated, hyperphosphorylated, cleaved into a C-terminal fragment, and abnormally present in the cytosol. Moreover, studies have found TDP-43 positive inclusions in many other NDDs, including 50% Alzheimer's, 50-60% DLB, and almost 100%

Huntington's. Besides, TDP-43 is a less common gene cause of ALS, accounting for 2% fALS.

Similar to Aβ, tau, and αS, TDP-43 behaves as a proteopathic protein. First, it is the major component of inclusion bodies found in 97% of ALS and 45% of FTD. Second, similar to other proteopathic proteins, its unstructured Q/N rich region is prone to aggregate[53,57]. In addition, most of the TDP-43 mutations identified in familiar ALS-FTD patients are located at C-terminal, and many mutations display increased insolubility, together with higher cytotoxicity compared with WT TDP-43[58–60]. The full-length TDP-43[61] or its fragment[60,62] can self-template and specifically promote the fibrillization of TDP-43 monomers *in vitro*. Third, although TDP-43 seeding is less easy than αS, Multiple studies demonstrated TDP-43 seeding both *in vitro* and *in vivo*. Applying either purified TDP-43 fibril[63] or patients' extract with insoluble TDP-43[64] is sufficient to generate insoluble phosphorylated and ubiquitinated TDP-43 aggregates, which mimics TDP-43 inclusions in patients. The TDP-43 aggregates localize with Multivesicular bodies and can freely transmit between cells[64,65]. Injecting FTD patient extracts with insoluble TDP-43 enables to induce new aggregates and spread across the brain neural network with time on mice[66]. Wang's group[67] recently found TDP-43 seeding events after motor cortex injection with purified recombinant TDP-43 fibril in a time-dependent manner. Those injections also accelerated ALS-like symptoms (motor defect and electrophysiological abnormalities) compared with vehicle controls. However, the pitfalls of both studies are using TDP-43 transgenic mice as mouse model, whereas WT TDP-43 overexpression used in studies above is sufficient to accumulate TDP-43 cytoplasmic

inclusion and generate the neuronal loss, memory loss, and motor dysfunctions at a later stage[68,69]. And the severity of ALS-like symptoms is correlated with the dose of TDP-43 expression[68]. Forth, although under dispute, several studies suggest that oligomer and aggregate form of TDP-43 is cytotoxic[61,62,70]. Intrahippocampal injection of TDP-43 oligomers drove local neuronal loss at CA1 region[61]. Finally, TDP-43 pathology spreads sequentially in stages in ALS and FTD. The sequences of TDP-43 deposits are associated with functional loss and disease progression[71]. In AD, TDP-43 burden is paralleled with cognition impairment and memory loss, and regional atrophy after control for age, APOE, Braak's stage, and other AD pathology[72]. Therefore, decoding the mechanism of TDP-43 seeding and spreading is an essential aspect of TDP-43 pathology.

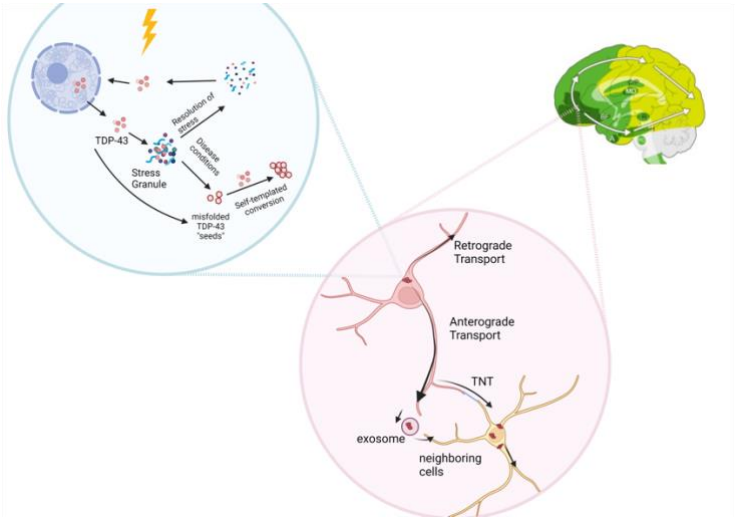

Figure 1. 2: scheme of TDP-43 intracellular seeding and propagation.
It is partially adapted from ref **73** the brain anatomy comes from ref **3**, the figure is made via Biorender.

1.1.4 other proteopathic proteins

Besides α-Synuclein and TDP-43, Aβ, tau, etc., are also considered as proteopathic proteins. While polyQ, SOD1, TIA-1, FUS, and desmin show some seeding capability. The evidence of their seeding property is summarized in Table 2. Of note, proteopathic proteins are not only limited in the brain but other tissues, like the muscle. For example, TDP-43 inclusions have been found in the muscle of MSP and several different myopathies[58,74]. Like TDP-43, Desmin, an intermediate filament protein with two amyloidogenic regions, is the principal inclusion component in myofibrillar myopathies. Its mutations can lead to Eichsfeld type congenital muscular dystrophy[75]. Our group found that WT Desmin monomer can self-assemble into seeding compatible fibril *in vitro*, accelerating further fibrillation. This desmin fibril showed increased myotoxicity *in vitro*[76].

Table 1. 1: summary of properties of proteopathic proteins. It is partially adapted from ref [2]

Misfolded protein	Human diseases associated	Prion-like properties in vitro		Prion-like properties in vivo		Strains	Induced neurotoxicity
		Seeding	Propagation	Seeding	Propagation		
β-amyloid	AD	Yes[77]	Yes[78,79]	Yes[80–82]	Yes[83,84]	Yes[82,85,86]	Not yet
Tau	FTD-Tau, AD, PSP, AGD, PiD, CBD	Yes[87,88]	Yes[87,89,90]	Yes[91–94]	Yes[90,93–97]	Yes[98]	Not yet
α-Synuclein	PD, LBD, MSA	Yes[22]	Yes[44]	Yes[26–28]	Yes[26–28]	Yes[99–102]	Yes (in vitro and in vivo)[25,27,103,104]
PolyQ	HD/SCA	Yes[105]	Yes[106]	Not done	Not done	Not done	Not done
TDP-43	ALS, FTD	Yes[66,107]	Yes	Yes[66,67]	Yes[66,67]	Yes[54]	Yes (in vitro[64])
SOD1	ALS	Yes[108–111]	Yes[108,110,112]	Yes[113]	Yes[113]	Not done	Yes (In vivo)
FUS	ALS	Yes[114]	Not done	Not done	Not done	Not done	Not done
C9ORF72 associated dipeptide	ALS, FTD	Yes[115]	Yes[115,116]	Not done	Not done	Not done	Yes (in vitro[117,118])

1.2 Multisystem proteinopathy & VCP

1.2.1 VCP

Valosin-containing protein (VCP/p97, also called cdc48 in yeast), is an abundant AAA+ ATPase, conserved across species. VCP is widely expressed in many organs and tissues (e.g., muscle, brain, bone, liver, etc.) for various cellular activities, including cell cycle, DNA repair, ER-associated degradation (ERAD), stress granule dynamics, autophagy, etc[119]. VCP is composed of an N terminus (aa 1-187) followed by two ATPase domains, D1 (aa 209–460) and D2 (aa 481–763) and C terminus (aa 764–806). VCP usually forms a homozygous hexamer like a ring and unfolds or segregates its substrates fueled by ATP hydrolysis[120].

VCP diverse cellular functions are mainly achieved by binding to different cofactors at N- or C-terminal and recruiting different substrates. To date, more than 30 proteins have been identified as VCP cofactors, and the number keeps increasing (the cofactors were reviewed in ref [119]). UFD1-NPL4 is the best studied VCP cofactors so far. UFD1-NPL4 facilitates the disassembly or degradation of lysine 48-linked ubiquitin chains (K48) tagged proteins on the membrane or within a large subunit. This UFD1-NPL4-VCP complex is required for many VCP-mediated cellular functions. For example, in ERAD, Ufd1-Npl4 recognizes misfolded proteins in the lumen and assists them to translocate through the central pole of VCP to proteasome degradation in the cytosol; upon DNA double-strand break, UFD1-NPL4-VCP complex recognizes and extracts K48 labeled Ku80, which releases chromatin and propels DNA break joins[121]. Similarly, this complex can target other substrates such as IkBa, Aurora

B, and Nrf1 to regulate NF-kB activation[122], mitosis[123], and homeostatic response[124], respectively.

VCP can impact endo-lysosome trafficking and autophagy-independent of Ufd1 and Npl4. VCP localizes at endosome. Either VCP knockdown or VCP ATPase inhibitors showed enlarged endosome and defect on end-lysosome fusion[125,126]. It is consistent with rimmed vacuoles found in MSP1 patients' muscles. Research suggested that this VCP function is mediated by cofactor UBXD1 binding to ubiquitinated CAV1[126,127]. In autophagy, double-membrane vesicle engulfs selective cargos or cytoplasmic components and degrade them by marge with the lysosome. VCP siRNA knockdown exhibits increased autophagy influx and immature autophagosome[128,129]. The molecular mechanism of VCP in autophagy remains unclear. VCP-Ataxin-3 can stabilize Beclin-1 and promote autophagy initiation[130]. However, the immature autophagosome by VCP knockdown suggests VCP involvement in the downstream autophagy process as well. One candidate cofactor for this process could be UBXD1, a cofactor that binds to VCP exclusively to Ufd1 and Npl4[120], proving to regulate vesicle trafficking and sorting[131]. Furthermore, the VCP-UBXD1 complex has been found essential for selective autophagy of large organelles such as damaged lysosome and mitochondria, called lysophagy and mitophagy, respectively[132,133].

1.2.2 Multisystem proteinopathy

In 2001, Kovach et al. first identified VCP mutations with a unique dominant syndrome—inclusion body myopathy associated with Paget disease of bone and frontotemporal dementia (IBMPFD), which affects muscle, bone, or brain[134]. Among all

patients, ~90% have myopathy, half receive Paget disease of bone (PDB), 30% develop frontotemporal dementia (FTD), whereas ~10% get fALS[135] and a few other sporadic phenotypes. Despite different types of tissues affected, one common feature is ubiquitin and TDP-43 positive inclusions and rimmed vacuoles[136]. With the growth of exon sequencing in clinics, VCP mutations have been identified in other discrete diseases in the last decade. For example, several known VCP mutations were reported in Parkinsonism patients with α-synuclein-positive Lewy bodies in S. Nigra. Parkinsonism symptom can exist alone or proceed IBMPFD[137–139]. Furthermore, in 2020, Lee's group identified two independent families with new heterozygous mutation (D395G) that caused AD with tau tangles and empty vacuoles in the absence of other proteopathic proteins, including TDP-43 and α-synuclein. This new mutation enhances the tau seeding efficiency in the tau overexpressed HEK 293 cell line and mice with tau fibril injection[140]. According to the diversity of affected tissues and diseases, those VCP caused conditions should be better referred to as type1 Multisystem proteinopathy (or MSP1, OMIM #167320). MSP1 is an adult-onset disease, with the onsets at 42 for muscle and bone or 56 for FTD on average[135]. Other genes cause MSP, including HNRNPA2B1, HNRNPA1, SQSTM1, MART3, OPTN, etc[141]. Distinct from other diseases, MSP shows high variability, even carriers within the same family can exhibit mosaic symptoms.

Due to the complexity of VCP protein function, the mechanism of VCP medicated MSP is still controversial. Most VCP mutations exhibit comparable VCP protein expression level, hexametric conformation, and normal or even higher ATPase activities[142,143] (except D395G[140]). However, no clear correlation between ATPase activity and pathological severity

from different mutations has been found. Meanwhiles, our heterozygous knockout mice, showed no distinct phenotypes in both the muscle[144] and the brain[145] by 12 months of age. Hence, MSP1 is not due to the haploinsufficiency of VCP protein. Meanwhile, VCP homozygous knockout mice are embryonic lethal[146]. Given the late onset of the MSP1, the dysfunction of VCP mutations is not due to early embryonic development. Intriguingly, VCP inhibition in Drosophila can alleviate some pathologies of VCP mutations, which supports a gain of toxic function[147]. Other research using VCP knockdown and VCP inhibitors phenocopied VCP disease mutations and MSP1 patients.

Given the proteopathic protein aggregation (TDP-43, tau, or αS) in MSP1, researches focus on protein homeostasis on VCP mutations. ERAD helps the clearance of misfolded proteins and plays an essential role in protein quality control. Some early studies discovered the persistence of ERAD substrate ΔF508-CFTR in cells with VCP disease mutations[142]. While Tresse et al.'s study showed VCP disease mutations have no changes in proteasome degradation and ERAD activities using UbG76V and CD3δ as substrate, respectively[126,129]. In contrast, autophagy is an alternative protein clearance machinery, especially for large aggregates. Rimmed vacuoles in MSP1 patients' muscles are enveloped with double-membrane vesicles and stained positive with autophagy markers LC3 and p62[128]. Overexpressing VCP mutations showed increased autophagy flux (denoted by LC3 II/I), the immature autophagosome, and delayed autophagy clearance[128,129]. This is in accordance with some other MSP genes, such as SQSTM1 and OPTN, which are known as autophagy adaptors[141]. Besides, overexpressing VCP disease mutations leads to the accumulation of large polyQ80 inclusions, which fail to merge to autolysosome markers and delay in

clearance *in vitro*[148]. Proteomic studies on VCP binding protein found VCP disease mutations specifically decrease binding with cofactors UBXD1 and PLAA, but increase with Ufd1, Npl4, and p47[126,149,150], which indicates selective defect on the autophagy-related pathway. VCP disease mutations mimic the effects of VCP siRNA and UBXD1 siRNA on lysophagy and mitophagy[128,129]. UBXD1 N-terminal can stabilize VCP, and its binding reduces VCP ATPase activity by 41% *in vitro* assay[151]. This imbalance towards Ufd1-Npl4 might explain increased ATPase activity seen with some VCP mutations.

Besides, researchers also studied mitochondria since VCP mutations selectively affect high energy expenditure tissues – muscle and brains. VCP mutations impede mitochondria morphology clearance[152], decrease mitochondrial membrane potential and ATP production[153]. VCP might be involved in multiple aspects of mitochondria. VCP can surveille the outer mitochondrial membrane (OMM) protein quality and translocates those proteins via the UFD1-NPL4 proteasome pathway, called MAD[154]. Degradation of OMM proteins like Mfn1 and 2 upon depolarization damage leads to fission and mitochondria fragmentation[155]. At the same time, VCP-UBXD1 can be recruited to damaged mitochondria marked by Parkin for mitophagy (selective autophagy of mitochondria)[156]. The MAD and mitophagy might interconnect, as Mfn2 degraded via MAD upon damages are ubiquitinated by PARKIN/PINK and antagonizes mitophagy[157].

VCP mutations can also impact stress granules dynamics. VCP mutations resulted in constitutive stress granules[158] and delayed disassembly after arsenite washout[159]. TDP-43, the component of inclusion in MSP1, is also recruited to stress granules under stress conditions.

In concert, MSP can be caused by mutations on many RNA-binding proteins, such as HNRNPA2B1, HNRNPA1, and TIA-1, which are components of stress granules[141]. However, the exact role of VCP in stress granules is still indefinite.

1.3 screening method and CRISPR

1.3. 1 screening methods

Genetic screens aim to link genotypes to phenotypes in high throughput assays. Mutagenesis screen on the model organism is the first approach for screening done by Nobel laureates Christiane Nüsslein-Volhard and Eric Wieschaus. DNA mutations are generated by exposure to mutagens, the strains are selected with desired phenotypes, and finally, uncover the mutations in those chosen strains. However, the effect of those random mutations is not predictive. In parallel, the point mutations and affected genes are always not mutually exclusive. This leads to incomplete coverage of the genome, high off-target effect, and moderate repeatability. Additionally, sequentially phenotype selection is usually labor-intensive and inefficient. Therefore, this forward screening method, including the mutagenesis screen, is now largely replaced.

Scientists recently performed screening using full sequenced libraries with known genetic targets. There are three elements of a functional screen: perturbation, model, and an assay/readout. By type of perturbation, screens can be classified as the Open Reading Frame (ORF) screen, the RNA interference screen, or the CRISPR-Cas9 screen. ORF screen is a gain of function screen achieved by overexpressing ORFs from a cDNA library, usually in an

arrayed format. The ORF of each gene is relatively long and less faithful[160,161]. Now ORF screen is largely taken over by the CRISPRa screen (mentioned later). RNAi (using either siRNA or shRNA) targets at transcription level since it might cause incomplete protein depletion and have high off-target effects. CRISPR-Cas9 system-induced double-strand DNA breaks (DSB) at the targeted sequence and induces frame-shift or deletion via NHEJ (discuss more in the next section)[162].

In parallel, the library can be either arrayed or pooled. In an arrayed screen, assays are done in multiple-well plates, and each well has a different perturbation. The arrayed screen provided direct genotype-phenotype correlation. However, it needs an automated platform for large-scale cell culture and assay readout. In comparison, the pooled screen combines all the perturbations together in a single batch, selects desired cells from the mosaic population by their phenotypes, and then recovers the perturbation by NGS. Although the paracrine signaling effect might influence the result of cells as a pool, The pooled screens still take advantage over the arrayed based on the low cost and labor[163].

1.3.2 unbiased screening on α-synuclein

The first αS screen was done in the yeast model since overexpressing human WT or mutated αS in yeast inhibits the growth in a dose-dependent manner[164]. It offers a distinct readout for screening. All genetic screens on αS are summarized in Table 1.2.

Although those screens broaden our knowledge of the nature of α-synuclein, some pitfalls of the current screening are worth highlighting. First, early screens mainly were done

in yeast or *C elegans*, which have only ~30%[165] and ~40%[166] homolog to the human genome. This hinders the conclusion transfer to the disease mechanism in humans. Second, limited by the volume of the library, some early screens are not really "unbiased". For instance, a selection of PD-related genes or vesicle-related genes[167,168] was picked as the total pool, which has been documented associated with αS. This might contribute to a high possibility of hits but low success in secondary validation. Meanwhiles can give rise to the missing genes with a moderate effect on the readout. Hence, we need to alert the conclusion, especially the pathway enrichment. Some pathways (e.g., vehicle trafficking) might be overscored because of library selection. Third, in most of the current αS screens (except [168], [169], and [170]), the readout is based on observation and selected by researchers (e.g., more aggregate in worm muscle wall or more colonies in yeast). It is labor-intensive and relatively subjective.

In addition, we need to think prudently over the readout for each screen. For example, the cell survival in yeast (Ref [171], [172], [173], [174], [175], [176], and [129]) is an indirect measurement of αS expression. Alongside, other "essential" genes involved in cell survival might be picked by the screens independent of αS level. Similarly, in the screen for αS oligomerization (ref [168]), some hits alter the readout signal merely by changing αS expression instead.

1.3.3 CRISPR-cas9 and pooled screening

Cas proteins are DNA endonucleases that can induce DSB guided by a short RNA complement. It is a bacterial defense mechanism against phage infection found in bacteria. Given the repeating sequences in bacteria, the system is named CRISPR (clustered regularly interspaced palindromic repeat)-Cas. The CRISPR loci are intercalated with DNA fragments

from invaders, which can transcribe into RNA to guide the DSB as adaptive immunity.[178] The DSB will be repaired by Non-Homologous End Joining (NHEJ) or Homology-Directed Repair (HDR) with the template. NHEJ is error-prone (insertion or deletion) and results in gene deficit (KO) due to nonsense-mediated mRNA decay[163]. The short RNA, termed CRISPR RNAs (crRNAs) or guide RNA, is effective as short as 20 nt[179]. Scientists first successfully harnessed this CRISPR- Cas system to target gene editing with artificial designed guide RNA in mammalian cells in 2013[180,181]. Cas9 from *Streptococcus pyogenes* (SpCas9) is picked for gene editing since Cas9 can perform endonuclease activities at guide RNA complemental site adjacent to a unique PAM sequence (NGG) downstream solely without other endonucleases. The simplicity and flexibility of this two-component gene-editing system enable scientists to study gene function on a large scale. The very first CRISPR screens were done by Feng Zhang's and Eric Lander's groups in 2014[182,183]. To date, more than 1500 screens[184] have been done so far in yeast, immortalized cell lines, primary cell culture, and even in animals [185–188]. The pooled library usually contains 4-10 different guide RNAs for each gene and abundant non-targeting guide RNAs as scramble controls. And generally more than 500 copies of the cell for each gRNA to minimize systematic false positive or negative[163].

Typically, the CRISPR pooled screening includes the following steps[163]:

Step 1: cell preparation. Deliver cells with both Cas9 and gRNA library and maintain under antibiotic selection for gRNA. Low MOI (usually <0.3) for gRNA is used to ensure most cells get no more than one gRNA.

Step 2: collect cells under selection. The simplest readout is the cell survival/ proliferation. Cells with gRNA KO of essential for survival or cell cycle are deprived with time. Those gRNAs will be identified when comparing the group of cells at early time points to that at late time points. Similarly, based on the cell survival under a particular treatment, researchers can identify genes for drugs resistance in cancer research, cytokines response in inflammation, cell differentiation, or pathogen resistance for infectious diseases[185,189]. Beyond that, some biological phenotypes can be captured with fluorescent reporter and FACS. For example, to study the gene modifiers for a protein, researchers can make a reporter line with the fluorescence tagged protein of interest and sort cells with low and high fluorescence signals by FACS (e.g., ref [170] and [190]).

Step 3: sequencing. In each group, gRNA is PCR amplified from DNA extraction and is subject to Next Generation Sequencing separately.

Step 4: data analysis. The raw sequencing data represent gRNA abundancy in each group. Nowadays, algorithms were built to identify genes responsible for the selection in Step 3. Those tools always combine the effects of each gRNA that targets the same gene upon the treatment and are normalized to non-targeting gRNA controls.

Step 5: Validation. It is performed in multiple ways using sub-library, other models, different perturbation and assays, etc. The goal is to show the effectiveness of the screens and narrow down hits to genes of interest.

Besides traditional KO screening, the CRISPRa/i system is invented with endonuclease-deficient Cas9 fused to transcriptional enhancer or repressor. It empowers transcriptional regulation of targeted genes without DSB. CRISPRa now substitutes ORF screens for gain-of-function screens. Additionally, researchers introduced point mutations via HDR to conduct CRISPR cas9[188,191] mutagenesis screening, which can solve the variants of uncertain significance within genes or genome.

CRISPR pooled screens override other screening methods due to this high throughput, the versatility of library design, relatively low off-target effect, and low cost and labor. Despite the advantage, there are systematic drawbacks of the CRISPR pooled screening. First, Like other gene-editing using complemental pairing, CRISPR has an off-target effect. However, it is minimized with increasing knowledge on the mechanism of the CRISPR-Cas9 system. Better in silico prediction generates more precise guide RNA design[192,193]. Meanwhile, engineered Cas9 and other Cas proteins were innovated with higher fidelity like Cas12a [163]. Second, researchers might lose essential genes in their pool for a long-term screen, as those genes are unfavored in proliferation[163]. Third, restricted by the large coverages needed for the CRISPR screen (usually more than 500 copies per perturbation), the cells can only be sorted and selected to a limited number of groups. The list of hits is not weighted according to the readout. Genes moderately and highly regulate the readout might be enriched in the same group. Therefore, the top hits from screening might not induce the biggest effects in many cases. Some attempts are made to solve this problem. One is to incorporate *in situ* sequencing, optic phenotypes, and automatic microscopy with CRISPR screening, which enables phenotype-genotypes correlation in each gene with their readout

one by one (e.g., ref [194]). Forth, the false positive may occur when CRISPR-cas9 targets high copy number genes, like oncogenes or repeated regions in high ploidy cancer cell lines[163]. Finally, like other pooled screens, the application of CRISPR screens is restricted by limited phenotype to readout other than cell survival and resistance to a certain treatment. The fluorescent reporter is one direction and brings in some success. However, it is incapable of sophisticated phenotypes, like mislocalization or morphology changes. A recent attempt is applying an automatic microscope, AI algorithm, and photoactivatable fluorescent protein into the screening. In brief, the pooled cells are automatically imaged, and cells with want phenotypes are picked photo-activated and then selected by flow sorting. Those more complicated screens require more effort to build and test and might introduce false alarms at the same time (e.g., ref [195] and [196]).

CRISPR functional screening used in NDDs is nascent. Besides the synuclein expression screens I mentioned before, two group screens for the modifier of the expression level of SQSTM1 and PARKIN, the gene associated with ALS and Parkinson's, respectively. Aaron Gilter's group identified the essential role of ER stress components in neuronal survival under dipeptide-repeat (DPR) proteins treatment by screens for DPR resistance[197]. As mature of CRISPR techniques and the build-up of reporters, these screening methods can accelerate the research in NDDs in the future.

Table 1. 2: unbiased genetic screens on α-synuclein

model	library	readout	primary screening result	follow-up	results	Ref.
Yeast overexpressing human WT αSyn	4850 deletion haploid mutation strands	Cell growth affected by αSyn expression			86 genes aggravate αS induced toxicity in yeast.	171
Yeast expressing WT αSyn-YFP under a galactose promoter	Overexpression of 3000 randomly selected ORFs from a genome-wide collection	Cell growth affected by αSyn expression	34 and 20 genes reduced and enhanced αSyn toxicity. Vesicle-mediated membrane trafficking genes were enriched.	Validation in Drosophila, *C. elegans*, and rat midbrain primary cultures	the ER-Golgi transport gene, YPT1 (ortholog of Rab1) expression mitigates αSyn-induced cell death.	172
Yeast expressing αSyn-YFP under a galactose promoter	Overexpression of 5500 randomly selected ORFs in yeast strains (85% of the genome)	Cell growth affected by αSyn expression	55 suppressors and 22 enhancers of a-syn toxicity	A computational approach to identify connectors between yeast genetic screening and transcription data	Identification of 106 proteins that were linked between genetic hits and differentially expressed genes, not identified by either of the individual approaches. Ubiquitin-dependent protein degradation, cell cycle regulation, and vesicle-trafficking pathways are overrepresented.	173
Primary screening in Ref [173]				Validation in *C. elegans* and rat midbrain primary cultures.	PARK9, PLK2, and PDE9A (homolog of YPK9, PLK2, and Pde2 in humans) protect DA neurons from αSyn-induced cell death in both models. PARK9 is a PD gene that protects cells from Mn2+ exposure.	174

Yeast expressing αSyn-YFP under a galactose promoter	CRISPR-aCas9 with randomized gRNA library	Cell growth affected by αSyn expression	two gRNAs suppressed αS toxicity	Transcription analysis to identify gene targets of the gRNAs. Promising gene targets were further validated in yeast and differentiated SH-SY5Y cells expressing human WT αSyn	DJ-1, ALS2, GGA1, and DNAJB1 protected cells from αS toxicity in both yeast and SH-SY5Y models.	175
Yeast expressing A30P mutated αSyn, challenged with H_2O_2 in yeast	High copy yeast genomic library (overexpressing yeast chromosome fragment)	Cell growth after additional challenges with H_2O_2	YPP1 suppressed lethality of A30P but not WT and A53T under ROS.	Screen YPP1 interactors	Class E VPS genes overrepresent for A30P αSyn induce ROS increase.	176
Yeast expressing WT- αSyn, challenged with H_2O_2	High copy yeast genomic library (overexpressing yeast chromosome fragment)	Cell growth after additional challenges with H_2O_2	~100 protected plasmids recovered	testing ROS signal overexpression and deletion strains	5 selective hits, ARG2, ENT3, IDP3, JEM1, and HSP82, suppressed ROS signal with overexpression and increased with deletion.	129
C. elegans expressing human αSyn-GFP in body wall cells	RNAi of a selection of 868 genes associated with PD, involved in protein degradation and interactors of these	Aggregation of αSyn-GFP in body wall cells	20 genes enhance αSyn aggregates at late larva stages.	Overexpression of seven hits, survival of DA neurons in *C. elegans*	5 genes protected DA neurons from αSyn toxicity in *C. elegans,* including worm homolog of ATG7, VPS41, and SEC22. Both VPS41 and SEC22 encode the protein for vesicle trafficking.	167

C. elegans expressing human αSyn-YFP in body wall muscle cells	whole genomic RNAi library (Ahringer) covered 87% of *C. elegans* genes	amount of αS inclusions at adult stage	80 strains enhanced αS aggregation. Quality control and vesicle-trafficking genes expressed in the ER/Golgi complex and vesicular compartments were overrepresented			198
Human H4 neuroglioma cells Bimolecular expressing N-terminal GFP and C-terminal GFP halves linked to αSyn	Lentiviral mediated RNAi library of 1387 genes involved in membrane trafficking and signal transduction related pathways	αSyn oligomerization measured by fluorescence complementation	4 genes encoding Rab proteins (RAB8B, RAB11A, RAB13, and RAB39B) and 5 genes encoding kinases or signal transduction proteins (CAMK1, DYRK2, CC2D1A, CLK4, and SYTL5) were identified	total αS expression, Cell-to-cell trafficking, and αS aggregations and cytotoxicity with silencing of selected hits.	All hits except RAB39B αS aggregation. Silencing of RAB8B, RAB13, or SYTL5 increases aSyn cell-to-cell trafficking. RAB8B silencing increases total αS level, aggregations, and cytotoxicity.	168
human HTB-186 cell with DsRed-IRES-SNCA- EGFP	shRNA library targeting 7787 druggable genes	αSyn level	60 genes modified αS level.	Validated αS expression of 33 αS suppressors by Western blot. Valid candidates were tested in Drosophila, hESC-derived neurons, and mouse brain	10 genes regulated αS induced viability in the Drosophila model. 6 out of 10 selective hits were validated whose knockdown ameliorated αS expression in both hESC-derived neurons and mouse brain.	169

HEK293T cells with tetracycline-inducible α-syn-EGFP	CRISPR-Cas9 genomic-wide library (GeCKO)	αSyn degradation under Canthin-6-one measured by GFP level	Identifies proteasome components -- PSMA1, PSMA6, PSMA7, and PSMD1 regulates Canthin-6-one induced αSyn degradation			170

Table partially Adapted from ref 199.

Chapter 2 VCP protect against proteopathic seeding

This chapter is adapted from VCP protects neurons from proteopathic seeding

Jiang Zhu, Sara Pittman, Dhruva Dhavale, Rachel French, Jessica N. Patterson, Mohamed Salman Kaleelurrrahuman, Yuanzi Sun, Jaime Vaquer-Alicea, Gianna Maggiore, Christoph S. Clemen, William J. Buscher, Jan Bieschke, Paul Kotzbauer, Yuna Ayala, Marc I. Diamond, Albert A. Davis, Conrad Weihl

2.1 Abstract

Background: Neuronal uptake and subsequent spread of proteopathic seeds, such as αS (alpha-synuclein), Tau, and TDP-43, contribute to neurodegeneration. The cellular machinery participating in this process is poorly understood. One proteinopathy associated with dominant mutations in Valosin Containing Protein or multisystem proteinopathy (MSP) has muscle and neuronal degeneration characterized by aggregate pathology that can include αS, Tau and TDP-43.

Methods: We performed a fluorescent cell sorting based genome-wide CRISPR-Cas9 screen in αS biosensors. αS and TDP-43 seeding activity under varied conditions was assessed using FRET/Flow biosensor cells or immunofluorescence for phosphorylated αS or TDP-43 in primary cultured neurons. We analyzed *in vivo* seeding activity by immunostaining for phosphorylated αS following intrastriatal injection of αS seeds in control or disease mutation carrying mice.

Results: 154 genes were identified as suppressors of αS seeding. One suppressor, VCP when chemically or genetically inhibited increased αS seeding in cells and neurons. This was not due to an increase in αS uptake or αS protein levels. MSP-VCP mutation expression increased αS seeding in cells and neurons. Intrastriatal injection of αS preformed fibrils (PFF) into VCP-MSP mutation carrying mice increased 33hosphor αS expression as compared to control mice. Cells stably expressing fluorescently tagged TDP-43 C-terminal fragment (CTF) FRET pairs generate FRET when seeded with TDP-43 PFF but not monomeric TDP-43 (TDP-43 biosensors). VCP

inhibition or MSP-VCP mutant expression increases TDP-43 seeding in TDP-43 biosensors. Similarly, treatment of neurons with TDP-43 PFFs generates high molecular weight insoluble phosphorylated TDP-43 after 5 days. This TDP-43 seed dependent increase in 34hosphor TDP-43 is further augmented in MSP-VCP mutant expressing neurons.

Conclusion: Using an unbiased screen, we identified the multifunctional AAA ATPase VCP as a suppressor of αS and TDP-43 aggregate seeding in cells and neurons. VCP facilitates the clearance of damaged lysosomes via lysophagy. We propose that VCP's surveillance of permeabilized endosomes protects against the proteopathic spread of pathogenic protein aggregates. The spread of distinct aggregate species may dictate the pleiotropic phenotypes and pathologies in VCP associated MSP.

KEYWORDS

CRISPR screen, seeding, alpha-synuclein, TDP-43, Frontotemporal dementia

2.2 Background

α-synuclein (αS) is the principal component of protein inclusions found in a family of neurodegenerative disorders known as synucleinopathies . Synucleinopathies include Parkinson's Disease, Diffuse Lewy body disease (DLB), multiple system atrophy, and REM sleep behavior disorder (RBD)[200]. αS contains an amyloid-like region making it prone to aggregate. Several lines of evidence suggest that aggregated αS can seed the fibrillization of soluble, monomeric αS[201]. This process may relate to disease pathogenesis and progression[4]. αS fibrils enter neurons via endocytosis and template new αS aggregates within the cytoplasm[22]. This leads to synapse loss, neurodegeneration, and ultimately the release of αS fibrils to adjacent cells resulting in aggregate propagation along interconnected neurons[4]. The cellular process of proteopathic seeding consists of several regulated steps. These include seed uptake, vesicular trafficking, endolysosomal escape, and templated conversion of cytosolic αS.

One route of seed uptake is endocytosis. αS seeds can enter cells and neurons via the endocytic system. These seeds then penetrate the endolysosomal membrane facilitating their escape into the cytoplasm[1,2204]. Pharmacologically blocking cellular uptake or increasing endolysosomal membrane damage can decrease and increase seeding efficiency, respectively[204]. Previous studies have identified genetic modifiers of αS toxicity associated with its intracellular expression in yeast or *C. elegans*[1,2205]. However, genetic modifiers of proteopathic seeding have not been explored.

VCP (also called p97, or cdc48 in yeast) is a ubiquitin-directed AAA-ATPase implicated in multiple forms of neurodegeneration[206]. Dominantly inherited mutations in VCP cause multisystem proteinopathy (MSP), associated with multiple variably penetrant phenotypes that include inclusion body myopathy, frontotemporal dementia, ALS, and Parkinsonism . Just as the phenotypes are variable, VCP patients develop varied aggregate pathologies that include αS, TDP-43, Ta u, SQSTM1, and ubiquitin inclusions[140,207–209]. How VCP disease mutations lead to cellular degeneration and protein inclusions is unclear. VCP affects the trafficking and clearance of polyglutamine aggregates *in vitro*[210]. VCP is also necessary for both autophagic and proteasomal degradation of ubiquitylated proteins, including TDP-43 and ER-associated proteins via ERAD[206]. VCP has more recently been proposed to behave as a protein disaggregase specifically acting upon pathologic tau aggregates[140]. By binding to distinct adaptors, VCP alters its functionality, allowing it to participate in its many other functions such as ERAD, vesicular trafficking, DNA repair, and cell cycle regulation[206].

VCP disease mutations alter its association with distinct adaptors[126,211]. Specifically, VCP disease mutations have reduced binding to UBXD1 and increased interactions with Ufd1/Npl4 creating both a loss and gain of function with regard to UBXD1 and Ufd1 dependent processes[126,133,147,211]. Notably, a VCP-UBXD1 dependent complex is recruited to damaged endolysosomes[133]. This complex recruits the deubiquitinase YOD1, which cleaves K48 linked ubiquitin chains from the lysosomal membrane facilitating lysophagic degradation[133]. VCP inhibition, loss of UBXD1, or VCP disease mutant expression lead to a delay in the clearance of

damaged late endosomes resulting in the accumulation of galectin-3 positive puncta in both VCP mouse models and patient tissue-[133,212].

MSP patients are pathologically characterized as a TDP-43 proteinopathy[213]. MSP patient tissue accumulates aggregated and insoluble TDP-43 in affected muscle and CNS tissue[213]. 90% of MSP patients have myopathy that precedes dementia by ~10 years[214]. Whether TDP-43 aggregate pathology spreads from muscle to motor neuron and ultimately the cortex is unknown. TDP-43 contains an intrinsically disordered or prion-like domain that facilitates its templated aggregate conversion[215]. Like αS, TDP-43 aggregates can serve as proteopathic seeds that propagate in cell and mouse models[216,66]

Functional genomic screens are a powerful tool to identify proteins participating in distinct cellular pathways. In this study, we utilized an αS seeding FRET biosensor to screen a CRISPR knockout library. This approach identified multiple suppressors of αS seeding, of which the AAA ATPase, VCP, was further explored both *in vitro* and *in vivo*.

2.3 Methods and materials

αS FRET seeding assay

Generally, HEK 293T αS-CFP/YFP is plated in a black-bottomed 96-well plate with the density of 80k/well in DMEM media with 10% FBS and Penicillin-Streptomycin. Three control cell lines – no-transfected HEK293T cells, αS-CFP, and αS-YFP transduced cells are cultured in the same condition. αS PFF is sonicated and prepared with OPTIMEN and 1 μL Lipofectamine 2000 (Invitrogen) for each well and added dropwise to the cell after 48 hours. The cells are harvested after 24 hours for flow cytometry, the same as reported. Briefly, the cells are detached by 0.05% trypsin-EDTA (Gibco), centrifuged, then fixed with 2% PFA for 15 minutes, and finally resuspended in MACSima Running Buffer. The samples are analyzed by MACSQuant® VYB. FRET signal is excited by 405nm lasers and detected by 525/50 band pass filter. At the same time, the CFP and YFP are excited by 405nm and 488nm lasers and filtered by 450/50nm and 525/50nm, respectively. The data is analyzed with FlowJ v10 software. Each FRET signal is calculated as the percentage of FRET-positive cell timing Median FRET fluorescence intensity and then normalized to its vehicle control.

VCP mcherry vectors are a gift from Hemmo Meyer's lab. The mutations were confirmed by Sanger sequencing (GENEWIZ) with VCP plasmid primers described before. 250ng of the plasmid is transfected with OPTIMEN and 0.5μL Fugene 6 (Promega) in each well 24 hours after plating. The cells were then treated the same way as described above. The mcherry signal is

excited by 561nm laser and filtered via 615/20nm, and the FRET signal is analyzed separately for mcherry positive and negative cells.

Knockdown is achieved by reverse transfection of Human SMARTPOOL siRNA from Dharmacon or Thermo Silencer Select siRNA. 6pmol siRNA is prepared in OPTIMEN and 0.3µL Lipofectamine™ RNAiMAX (Invitrogen) according to its protocol and added to each well in a 96-well plate. Then 80k suspended αS-CFP/YFP cell is plated in each well already with siRNA droplet. The αS PFF is treated 48 hours after plating as described above. The concentration and duration of the drug treatments were summarized in supplemental Table 1.

TDP-43 FRET seeding assay

TDP-43 biosensor plasmids were designed to express the glycine-rich aggregation-prone region of TDP-43 from amino acids 262 to 414. Gene expression was driven by a CMV promoter in a lentiviral FM5 plasmid. At the N-terminus, an alanine codon (GCG) was added to enhance expression, and the C-terminus was fused to a flexible 12-amino acid linker (GGTTCTGCTGGCTCCGCTGCTGGATCCGGCGAATTC) with mClover3 or mRuby3. Lentivirus was generated as previously described and transduced to HEK293T cells to stably express both TDP-43 aa262-414-mClover3 and TDP-43 aa262-414 mRuby3. High-expressing monoclonal cell lines were sorted and tested for responsiveness to TDP-43 aggregates from TDP-43 peptides and brain homogenates from human cases with TDP-43 pathology.

TDP-43 sequence:

ATGGCGAAGCACAATAGCAATAGACAGTTAGAAAGAAGTGGAAGATTTGGTGGTAA
TCCAGGTGGCTTTGGGAATCAGGGTGGATTTGGTAATAGCAGAGGGGGTGGAGCTG
GTTTGGGAAACAATCAAGGTAGTAATATGGGTGGTGGGATGAACTTTGGTGCGTTCA
GCATTAATCCAGCCATGATGGCTGCCGCCCAGGCAGCACTACAGAGCAGTTGGGGT
ATGATGGGCATGTTAGCCAGCCAGCAGAACCAGTCAGGCCCATCGGGTAATAACCA
AAACCAAGGCAACATGCAGAGGGAGCCAAACCAGGCCTTCGGTTCTGGAAATAACT
CTTATAGTGGCTCTAATTCTGGTGCAGCAATTGGTTGGGGATCAGCATCCAATGCAG
GGTCGGGCAGTGGTTTTAATGGAGGCTTTGGCTCAAGCATGGATTCTAAGTCTTCTG
GCTGGGGAATG.

Generally, HEK 293T TDP-43-Ruby/Clover is plated in a black-bottomed 96-well plate with the density of 80k/well in DMEM media with 10% FBS and Penicillin-Streptomycin. Three control cell lines – no-transfected HEK293T cells, TDP-43 Ruby, and TDP-43 Clover transduced cells are cultured in the same condition. TDP-43 PFF is sonicated and prepared with OPTIMEN and 1μL Lipofectamine 20000 (Invitrogen) for each well and added dropwise to the cell after 24 hours. The cells are harvested after 48 hours for flow cytometry, the same as reported. Briefly, the cells are detached by 0.05% trypsin-EDTA (Gibco), centrifuged, then fixed with 2% PFA for 15 minutes at dark, and finally resuspended in MACSima Running Buffer. The samples are analyzed by MACSQuant® VYB. FRET signal is excited by 488nm lasers and detected by 614/50 band pass filter. At the same time, the Clover and Ruby are excited by 488nm and 561nm lasers and filtered by 525/50nm and 615/20nm, respectively. The data is analyzed with FlowJ

v10 software. Each FRET signal is calculated as a percentage of FRET-positive cell timing Median FRET fluorescence intensity and then normalized to its vehicle control.

drug treatment	Drug conc. & duration	PFF/monomer conc. & duration
EGCG	50μM; 0-24hr	10nM; 0-24hr
Bortezomib	10nM; 0-24hr	10nM; 0-24hr
3-MA	1μM; 0-24hr	10nM; 0-24hr
Rapamycin	100nM; 0-24hr	10nM; 0-24hr
LLOME	1μM; 0-4hr	30nM; 0-4hr
NMS-873	5μM; 0-4hr	30nM; 0-4hr
CB-5083	1μM; 0-24hr	10nM; 0-24hr
Eeyarestatin I, EerI	2μM; 0-24hr	10nM; 0-24hr
Dynogo 4a	10μM; -1-24hr	10nM; 0-24hr
thapsigargin	0.3μM; 0-24hr	10nM; 0-24hr
DTT	1mM; 0-24hr	10nM; 0-24hr
Tunicamycin	2.5μg/mL; 0-24hr	10nM; 0-24hr

Table 2. 1: Drug treatments for FRET syn/TDP-43 biosensor assay

Genome-wide CRISPR-Cas9 screens on αS biosensor line

αS-CFP/YFP HEK293T cells were first transduced with WT cas9-blast. Single clones were sorted and cultured. The new cas9 αS CFP/YFP line maintained both αS-CFP and αS-YFP and was capable of seeding. Cas9 functions were validated by a synthetic gRNA and obtained with 99% NHEJ activity. About 50 million HEK293T syn CFP/YFP Cas9-blast cells were plated and then infected with pooled lentivirus with Brunello gRNA library (Addgene #73178-LV) with 8ug/ml polybrene (MOI=0.3) the next day. After 24 hours, cells would undergo 1ug/ml puromycin selection. Selected cells were replated at a density of 6.4*10^5 cell/ml after 96 hours of selection and replaced with fresh puromycin. 2 days later, harvest 1/5 of the cell (~20 million) (untreated group, for library representation) and seeded the rest with 10 nM αS -PFF. The seeded

cells were collected the same as normal αS FRET assay as described above after 24 hours and sorted by Sony SY3200 cell sorter. DNA extraction was performed via QIAamp DNA Blood Midi on FRET positive and negative cells, as well as unsorted cells, which were separately amplified by PCR and deep sequenced by Illumina NovaSeq. The FRET positive and negative groups were compared with the untreated total population group separately via Megack RRA. For pathway enrichment, 154 hits were input to g:profiler and plot via Cytoscape as described before.

αS, Tau and TDP-43 Fibril preparation

αS PFF and monomer are generated as described before[217,218]. Briefly, purified human recombinant WT αS monomer (2 mg/ml) was incubated in 20 mM Tris-HCl, pH 8.0, 100 mM NaCl for 72 h at 37°C with shaking at 1000 rpm in an Eppendorf Thermomixer. To determine the concentration of fibrils, the fibril reaction mix was centrifuged at 18,000×g for 15 min to separate fibrils from the monomer. The concentration of αS monomer in the supernatant was determined in a BCA protein assay according to the manufacturer's instructions, using the bovine serum albumin (BSA) standard curve. The measured decrease in αS monomer concentration was used to determine the concentration of fibrils in the 72 h fibril reaction mixture. To isolate preformed fibrils (PFF) from the monomer, centrifuge the αS mix at 18,000×g for 15 min to separate fibrils from the monomer. Resuspend fibril pellet in the buffer containing 20 mM Tris-HCl, 100 mM NaCl, pH 8.0. αS PFF was always freshly sonicated right before seeding.

Fluorescently labeled fibrils of αS were generated as previously described[219]. αS (1 mg/mL) was dissolved in 100 mM NaHCO3, sonicated for 15 min, and spun through a 50 kD filter (Amicon UFC5050) at 16,100 ×g for 15min. Alexa Fluor 647 NHS Ester (Thermo Fisher A20006) was dissolved in DMSO to 10 mg/ml. Dye solution (molar ratio of dye: αS = 2.1:1) was pipetted into monomerized αS during stirring, and the mixture was stirred on bench for ~1h. The mixture was then loaded onto a size exclusion column (Superdex 75 10/300 GL) and eluted with 5mM NaOH. The peak containing monomeric, labeled αS was collected, aliquoted, and kept frozen until use. For aggregation assays, αS was dissolved in 10 mM NaOH at 1 mg/mL. αS-647 was added at a 5% labeling ratio. Then the solution was sonicated for 20 minutes, filtered through a 100 kD membrane filter (Amicon Ultra, 540655) at 16,100 × g for 15 min at 4°C. The protein and dye concentrations were measured by absorption at 280 nm, and 647 nm, respectively, and the labeling ratio was determined to be 4.9%. To prepare labeled αS fibrils, monomer solution (5% α-syn-AF647) and solutions were incubated in 100 mM NaP, pH 7.4, 10 mM NaCl for 120 h aggregated in a non-binding 96-well plate (Corning, #3651) at a concentration of 30 μM with intermittent shaking in aggregation buffer (100 mM NaP, pH 7.4, 10 mM NaCl). A 2 mm diameter glass bead was added to each well to accelerate the aggregation through stirring. The plate was kept at 37°C and agitated by orbital shaking once every 1 minute for 5 seconds.

Tau PFF and monomer are generated as described before[242]. Briefly, purified recombinant tau monomer (300 μg/ml) was incubated in the buffer containing 20 mM Tris-HCl pH 8.0, 100

mM NaCl, 25 μM low molecular weight heparin, 0.5 mM DTT for 48 h at 37°C with shaking at 1000 rpm in an Eppendorf Thermomixer. To determine the concentration of fibrils, the fibril reaction mixer was centrifuged at 18,000×g for 15 min to separate fibrils from monomer. The concentration of tau monomer in the supernatant was determined in a BCA protein assay along with a BSA standard curve. The measured decrease in monomer concentration was used to determine the concentration of tau fibrils in the 48 h fibril reaction mixture. Tau fibrils is resuspended from the pellet with the same Tris buffer at desired concentration.

Recombinant TDP-43 (rTDP-43) was generated in *Escherichia coli* and purified as previously described[216]. Briefly, rTDP-43 was bound to nickel–nitrilotriacetic acid–agarose and washed with wash buffer 1 (50 mM Tris, pH 8.0, 500 mM NaCl, 10% glycerol, 10% sucrose, 1 mM TCEP), washed with wash buffer 2 (50 mM Tris, pH 8.0, 500 mM NaCl, 10% glycerol, 10% sucrose, 50 mM Ultrol Grade imidazole, pH 8.0, 1 mM TCEP), and finally eluted (50 mM Tris, pH 8.0, 500 mM NaCl, 10% glycerol, 10% sucrose, 300 mM Ultrol Grade imidazole, pH 8.0, 1 mM TCEP). Then, rTDP-43 was ultracentrifuged in a Beckman Coulter Optima MAX-XP Ultracentrifuge at 40,000 rpm for 30 min at 4 °C to remove any pre-existing aggregates. Soluble protein was diluted to 4uM in the reaction buffer (50 mM Tris, pH 8.0, 250 mM NaCl, 5% glycerol, 5% sucrose, 150 mM Ultrol Grade imidazole, pH 8.0, 0.5mM TCEP). rTDP-43 aggregation was started by shaking at 1,000 rpm at 22 °C for 30 min with an Eppendorf ThermoMixer C. Samples were incubated at 22 °C and collected after one to ten days. Full-length TDP-43 recombinant protein is produced as previously described[216]. To obtain the TDP-

43 monomer, TDP-43 protein was ultracentrifuge 40,000g 30 mins at 4 °C. The supernatant was collected and freshly used.

Primary neuronal culture

WT hippocampal neurons were obtained from E17-18 mice (Charles River). Hippocampi are dissected in calcium- and magnesium-free Hanks' Balanced Salt solution (HBSS) and dissociated by 0.05% Trypsin-EDTA at 37°C for 5-10 mins followed by 1% Dnase I for 2 mins[220]. The cells are then resuspended with plating media to the concentration of 125k/ml and plated on Poly-D-lysine coated plates or coverslips. The media is changed to neurobasal media (neurobasal plus + B27 + 5mM L-Glutamine) after 2-4 hours. The culture was treated with 1mM Ara-C to inhibit the growth of glia at DIV3. The αS PFF is sonicated and added directly to the cell at DIV10.

VCP and UBXD1 shRNA is delivered via lentivirus. Lentivirus were added to the neurons at DIV5 with MOI≥1. For LLoMe or VCP inhibitors experiments, drug or vehicle control was added simultaneously with αS PFF or monomer (30nM) for 4 hours. Then the media is fully exchanged to the conditioned neurobasal media without drug and αS PFF or monomer. The neurons were harvested at DIV15.

R155H/WT neurons were cultured from embryos from R155H/WT intercross. The hippocampus from each embryo was dissected and cultured separately and then plated at the same density. The genotypes were examined by PCR (Transnetyx) (Forward Primer:

CCTCTAATTGCACTTGTATTGCTTTGT; Reverse Primer:

CTGGGATCTGTCTCTACAACTTTGA).

Immunohistochemistry

Cells were fixed in 4% PFA for 10 mins and permeabilized with 0.1% Triton X-100 in PBS for 10 mins. Then the cells were blocked with 2% BSA in PBS at RT for 1 hour. Cells were stained with primary antibody at 4 °C overnight, followed by three washes with PBS. Cells were then incubated with the Alexa 488 555 or 647 tagged secondary antibody in 1:500 dilution for 1 hour at RT. The nucleus was stained with DAPI (1:1000) for 10 min at RT. After three wash with PBS, the cells are mounted by Mowiol. Pictures were taken by Nikon Eclipse 80i fluorescence microscope and processed via ImageJ.

The FRET images were taken under Olympus FluoView1200 confocal microscope. The laser and band filters were set as listed:

Channel	Excitation wavelength (nm)	Band filter (nm)
αS Biosensor line		
CFP	440	425-475
YFP	488	500-550
FRET	440	500-550
TDP-43 Biosensor line		
Clover	488	500-550
Ruby	559	605-625
FRET	488	605-625

Immunoblot

Mouse cortex or cells are lysed in RIPA buffer with protease inhibitor cocktails (PMSF and PIC) followed by two 30 sec on and 30 off sonication cycles at 50% power. The protein

concentration is normalized by the BCA assay. Samples were loaded into 10 to 15% gel and transferred into nitrocellulose or PVDF membrane. The membranes were blocked by 5% milk in PBS-0.2% Tween20 and incubated with the primary antibody in blocking solution overnight at 4 °C degree. The membrane was then washed three times with PBS-0.2% Tween20 and incubated with secondary goat anti- rabbit or mouse HRP antibody (1:5000) for 1 hour. Blot was rinsed three times with PBS-0.2% Tween20 and probed by a fresh mixture of ECL reagents at dark and then exposed by SYNGENE.

To fractionate the insoluble portion of αS, we performed sequential extraction as described[221]. Briefly, neurons were first dissolved in TBS-1%Tx-100, and sonicated for ten cycles of the 30s on, 30s off with 50% power. The lysate would incubate on ice for 30 mins. 1/10 of the lysate was saved as total protein, while the remains were ultracentrifuged 100,000g 4 °C for 30 mins. The supernatant was collected as Tx- 100 soluble fraction. The pellet was washed with TBS-1%Tx-100, sonicated, and ultracentrifuged. Ultimately, the pellet was resuspended with TBS-2%SDS and sonicated for 15 cycles of 30s on, 30s off. Soluble and insoluble fraction were run by western blot as usual. The loading amount was determined by the concentration of total protein measured by BCA.

TPD-43 soluble and insoluble extraction is done as our previous method. Briefly, neurons from one 35mm dish were first lysed with RIPA buffer with protease inhibitor cocktails (RIPA buffer) on ice. The lysate was then sonicated with QSONICA sonicator for ten cycles of 30s on, 30s off with 50% power. 1/10 of the lysate was saved as total protein. The rest was

ultracentrifuged at 100,000g 4 °C for 30 mins. The supernatant was kept as RIPA soluble fraction. The pellet was then washed with RIPA buffer once, resonicated, and ultracentrifuged with the same condition. The pellet was finally resuspended with the same amount of UREA buffer (30 mM Tris, pH 8.8, 7M urea, 2M thiourea, and 4% CHAPS) as an insoluble fraction. Soluble and insoluble fraction were run by western blot as normal. The loading amount was determined by the concentration of total protein measured by BCA.

Animals

C57BL/6 (stock No.: 000664) and $VCP^{R155H/WT}$ (B6;129S-Vcptm1Itl/J, Stock No: 021968) were purchased from Jackson Laboratory. To obtain VCP cKO (VCPR155C/FL; Rosa26-CRE^{ERT2}), we first crossed VCP $^{flox;flox}$ with Rosa26-CRE^{ERT2} (B6.129-Gt(ROSA)26Sortm1(cre/ERT2)Tyj/J , Stock No: 008463) to get VCP $^{flox;wt;}$ Rosa26-CRE^{ERT2}. Then we bred those mice with $VCP^{R155C/WT}$ reported previously for VCP cKO[222]. All mice utilized in the study and breeding were on a C57BL/6 background. Both male and female mice were used in this study. Animal procedures were performed in accordance with protocols approved by the Animal Studies Committee at Washington University School of Medicine.

Intrastriatal injection and mouse brain harvest

Both mice are Intraperitoneal injected with 75 mg tamoxifen/kg body weight at ten weeks of age and wait one month for gene knockdown. The R155C mutation allele and the sufficiency of VCP flop knockdown were confirmed by PCR. The primers are listed in Appendix. Intrastriatial injection is performed as described. αS PFF is prepared as described above and

diluted in sterile PBS. αS PFF is sonicated 10 mins before injection. The mouse is anesthetized and injected at the dorsal striatum (Bregma=0.2mm, midline=2.0mm, depth=-3.2mm) of the left hemisphere. The same amount of PBS is used as vehicle control. The recovery of mice is monitored in the following week and sacrificed after 90 days. The mouse was first anesthetized in the Isofluorane chamber and perfused with PBS containing heparin. The whole brains were removed from the skull and fixed in 4% PFA overnight at 4 °C degree and cut coronally into 40micrometer sections and stored in cryoprotectant solution at 4 °C degree for staining. Sections were first rinsed three times with TBS and then blocked with blocking solution for 30 minutes (5% normal goat serum with 0.1% Triton X-100 in TBS). Sections were stained with the primary antibody in TBS-0.1% Triton X-100 plus 2% normal goat serum at 4 °C overnight, followed by three washes with TBS. Sections were then incubated with the Alexa 488 555 tagged secondary antibody in 1:1000 dilution for 2 hours at RT. The nucleus was stained with DAPI (1:1000) for 20 min at RT. After three wash with TBS, the sections were mounted on the glass slides. True black (cat: NC1125051) was incubated with the sections for 5 minutes to quench the auto-fluorescence. Finally, slides were coverslipped using Prolong Gold mounting medium. Pictures were taken by a Hamamatsu NanoZoomer or Nikon Eclipse 80i fluorescence microscope. The images were processed, and fluorescence intensity was calculated via ImageJ. The antibody is listed in Appendix.

Antibodies

All antibodies used in this study are listed in supplemental Table 2.

Table 2. 2: Antibody used in the experiments.

Antibody name	manufacturer	catalog number	clone name	WB	IF
Alpha Tubulin	Abcam	ab52866	EP1332Y	1:1000	
Alpha-synuclein [PHOS]/phosho ser 129	Biolegend	825701	P-syn/81A		1:200
ATG5	Cell Signaling	12994	D5F5U	1:500	
biotinylated Alpha-synuclein [PHOS]/phosho ser 129	Biolegend	825704	P-syn/81A		1:2000
BIP/GRP78 (purified)	BD Transduction Labs	610979	Clone 40	1:1000	
FK-2	Enzo	pw8810-050	UBCJ2	1:500	
Galectin 3	santa cruz	sc-32790	B2C10	1:500	
Galectin 8	Abcam	ab109519			1:100
GAPDH	Cell Signaling	2118	14C10	1:1000	
Hsp90	Abcam	13492	AC88	1:1000	
LAMP1	Santa Cruz	sc-20011	H4A3	1:200	
LC-3	nanoTools	0231-100	5F10	1:1000	
mCherry	Abcam	ab167453		1:1000	
NPL4	santa cruz	sc-134746	H-300	1:500	
p62/SQSTM1	Proteintech	18420-1-AP		1:1000	1:100
PAN 14-3-3	Santa Cruz	sc-1657	H-8	1:1000	
PLAA	Proteintech	12529-1-AP		1:500	
syn-1	BD Transduction Labs	610787	Clone 42	1:1000	
TDP43 (TARDBP)	Proteintech	10782-2-AP		1:1000	
TDP43 [PHOSPHO]	Proteintech	22309-1-AP			1:250
TIA1	Santa Cruz	sc-1751	C-20		1:200
Tuj1 (beta III tubulin)	Abcam	ab18207			1:400
Tuj1 (beta III tubulin)	R & D	MAB1195	TuJ-1		1:50
Tyrosine Hydroxylase	Millipore	ab152		1:4000	
UBXD1	Abcam	ab80659		1:500	
UFD1	santa cruz	sc377222	E-9	1:500	
VCP p97 ATPase	Fitzgerald	10R-P104A		1:500	

Statistical Analysis

The data (except CRISPR screening) is analyzed by GraphPad Prism 9. Statistical tests included unpaired t-test, one-way ANOVA, multiple t-test, linear interpolation (95% confidence), and two-way ANOVA. Data were displayed as mean ± SEM. Two-stage step-up methods of Benjamini Krieger and Yekutieli, Dunnett, Sidak correction were used to minimize false alarm from multiple comparisons.

2.4 Results

2. 4. 1 Genome-wide CRISPR knockout screen identifies genes protective against αS seeding

To identify genes that regulate αS seeding, we utilized a previously described HEK293 αS CFP/YFP biosensor cell line (αS biosensor) (Figure 2.1)[101]. These cells stably co-express two αS constructs. One tagged with CFP (donor) and another with YFP (acceptor). We exogenously applied human WT αS PFF or monomer with Lipofectamine for 24 hours to the αS biosensor line. Only αS PFF treated, but not monomer or empty Lipofectamine treated cells, induce new aggregation of soluble intracellular αS, as shown by CFP and YFP positive aggregates. This PFF-dependent process is referred to as a seeding activity. Finally, those CFP/YFP positive aggregates can be visualized by FRET under confocal microscopy (excitation = 440nm, emission= 500-550nm) (Figure 2.1A, lower panel). Quantitation of the percent of FRET+ cells and FRET intensity can be detected using flow cytometry (Figure 2.1B)[223]. The FRET efficiency, measured as $\%_{(FRET+cells)}$ * Median Fluorescent Intensity(MFI) $_{(FRET+cells)}$, was significantly higher in αS PFF treated group as compared with Lipofectamine control and αS monomer controls (mean= 67.55 vs. 0.96 vs. 0.30) (Figure 2.1C). In addition, αS PFF induced FRET efficiency is sensitive and quantitative in a concentration-dependent manner (Figure 2.1D).

To perform our screen, we clonally expressed spCAS9 in the αS biosensor line and then infected with a pooled Brunello gRNA library covering 19114 different genes/ 4 gRNA each and 1000 non-targeting controls at a low MOI (<0.3) for seven days with puromycin selection

(Figure 2.2A). The pooled knockdown αS- spCAS9 biosensor maintained αS seeding capacity in a concentration-dependent manner (Figure S2. 1). These biosensors were treated with 10nM αS PFF and flow-sorted into FRET positive and FRET negative groups. DNA was isolated from FRET positive, FRET negative, and the unseeded total cell population. Then deep sequencing was performed to identify the guide RNAs represented in each group (Figure 2.2A). This sequence data was analyzed via the MegaCK algorithm in both the FRET positive and negative populations compared with untreated control. 111 genes were enriched in the FRET positive population as compared to the total population, and 43 genes were underrepresented in the FRET negative group versus total population (FDR<0.05 and fold change >2 or <0.5) (Figure 2.2B). These 154 genes (red dots) were considered "protective" or suppressors of αS seeding in the biosensor line (Figure 2.2B-C; Appendix).

The screen identified genes and pathways previously identified in other αS screens for αS toxicity. Notably, we identified 15 genes associated with ER-Golgi-endosome trafficking. These included VPS51 and VPS52, which are components of the Golgi-associated retrograde protein (GARP) complex. The GARP complex interacts with PD-associated protein, LRRK2, and deletion of either VPS51 or VPS52 homologs in yeast increases αS accumulation and toxicity[224]. Other modifiers not previously identified in screens include ATP6V0B, ATP6V0C, and ATP6V1A that encode subunits of Vacuolar-type ATPase (V-ATPase). ATP6V0B KD inhibits autophagic degradation and increases αS aggregation[225] and is downregulated in patients with αS inclusions[226]. Pathway analysis identified an enrichment in genes associated with the cellular

stress response, such as VCP, SEC61B, and KDELR1. Notably, the ER stress response is upregulated in PD brains and correlates with αS toxicity in multiple model systems[227].

We validated nine candidate suppressors from both FRET positive and negative selections (ATP6V0C, KDELR1, LAMTOR5, RAB35, RABAC1, SEC61B, TMEM147, VCP, and VPS51) using siRNA knockdown in αS biosensors. Following 48 hours of siRNA treatment, αS PFF (10nM) was added with Lipofectamine, and FRET efficiency was measured 24 hours later. Six candidate suppressors, when knocked down, increased FRET efficiency and included ATP6V0C, VPS51, KDELR1, SEC61B, LAMTOR5, and VCP (Figure 2.2D). To further confirm our findings with VCP, we generated a lentiviral vector expressing a VCP specific or control gRNA, infected spCAS9 αS biosensors for seven days and treated with αS PFF. Similar to that seen with VCP siRNA, FRET efficiency was increased in VCP CRISPR KO αS biosensors (Figure 2.2E-F).

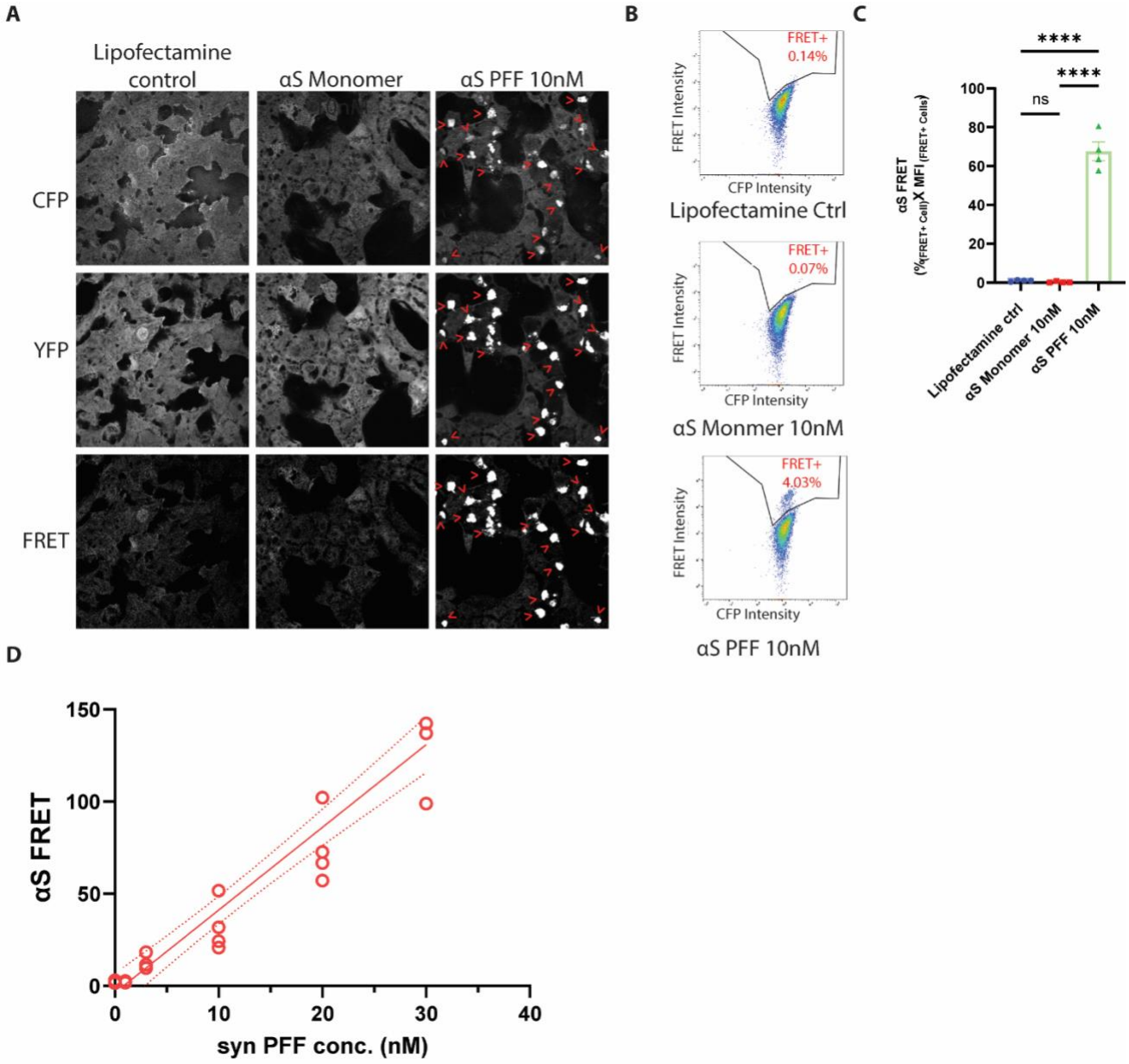

Figure 2. 1: <u>αS seeding can be sensitively detected by FRET in the αS biosensor line.</u>
(A) Representative FRET confocal microscopy images of αS biosensor line (αS CFP/YFP) treated with Lipofectamine (left, ctrl), 10nM αS monomer (center) and αS PFF (right) after 24 hours. Scale bar= 10μm **(B)** Flow cytometry tracing of FRET signal from αS biosensors. FRET+ gate (CFP vs FRET) was drawn from empty Lipofectamine treated cells with no aggregation. **(C)** Quantitation of integrated FRET signal from FRET-flow cytometry is calculated as % FRET+ cell * Median (FRET+ Intensity). **** $p < 0.0001$,n.s., no significance by one-way ANOVA. error bars are ± S.E.M. **(D)** Quantitation of cells treated with increasing concentrations of αS PFF for 24 hours. Cells are harvested after 24 hours and analyzed the same as 1C. Each dot represents an independent experiment.

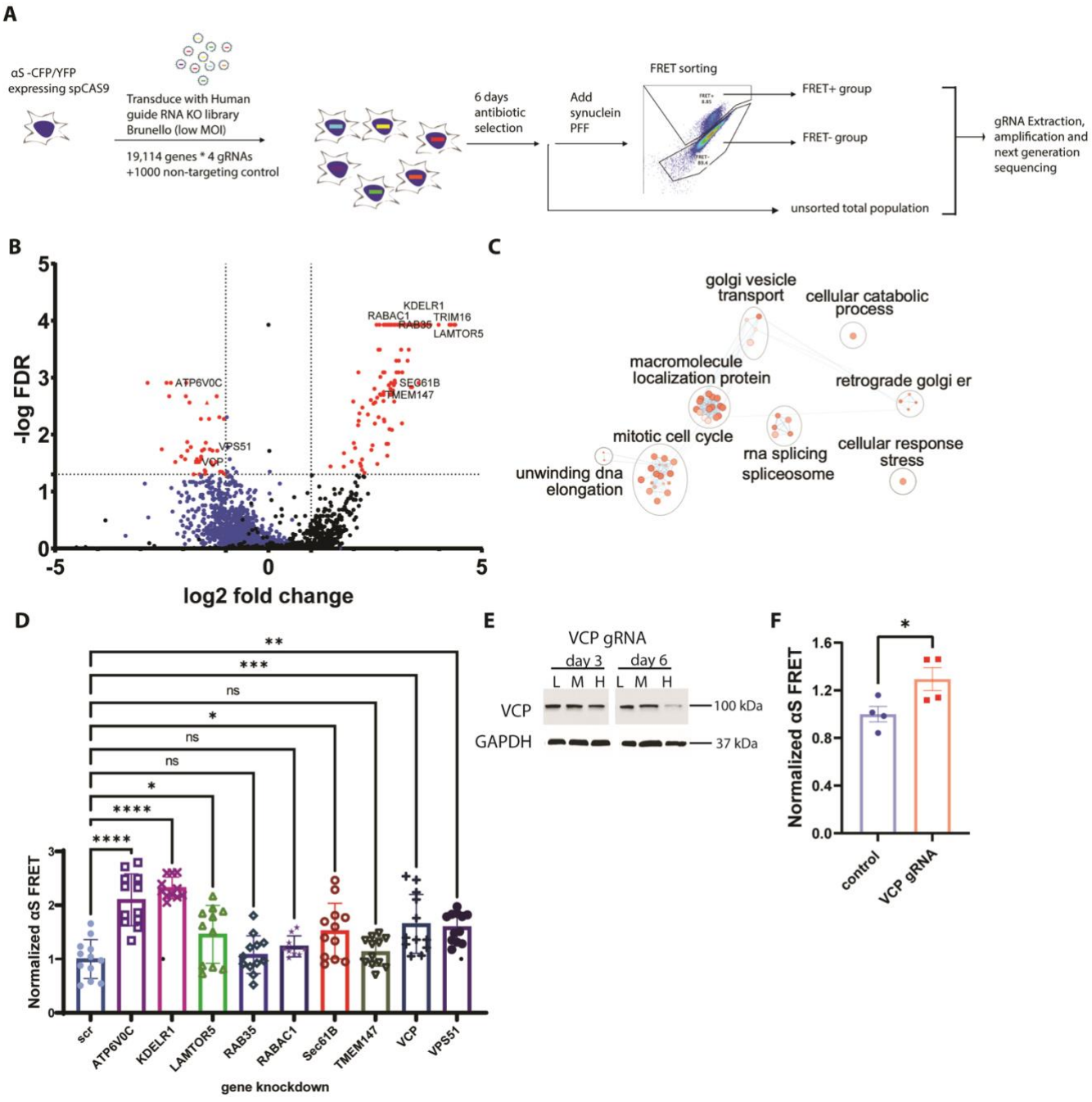
A
αS -CFP/YFP
expressing spCAS9
Transduce with Human
guide RNA KO library
Brunello (low MOI)
19,114 genes * 4 gRNAs
+1000 non-targeting control
6 days
antibiotic
selection
Add
synuclein
PFF
FRET sorting
FRET+ group
FRET- group
unsorted total population
gRNA Extraction,
amplification and
next generation
sequencing
B
-log FDR
log2 fold change
KDELR1
RABAC1
RAB35
TRIM16
LAMTOR5
ATP6V0C
SEC61B
TMEM147
VPS51
VCP
C
golgi vesicle
transport
cellular catabolic
process
macromolecule
localization protein
retrograde golgi er
mitotic cell cycle
rna splicing
spliceosome
cellular response
stress
unwinding dna
elongation
D
Normalized αS FRET
scr
ATP6V0C
KDELR1
LAMTOR5
RAB35
RABAC1
Sec61B
TMEM147
VCP
VPS51
gene knockdown
E
VCP gRNA
day 3
day 6
L M H L M H
VCP
GAPDH
100 kDa
37 kDa
F
Normalized αS FRET
control
VCP gRNA

Figure 2. 2: A genome-wide CRISPR/Cas9 screen identifies genes protective to αS seeding. **(A)** αS biosensor line stably expressing spCAS9 was transduced with sgRNA lentiviral library (Brunello). Following antibiotic selection, biosensors were seeded with αS PFF (10nM) and flow sorted 24 hours later. Genomic DNA from positive and negative groups as well as unsorted total population were collected and decoded by NGS. **(B)** Volcano plot of genes identified in the screen. Colored in blue are all the genes plotted from FRET- group, while colored in black are those plotted from FRET+. Red dots are protective hits from both groups (5% FDR), specifically genes with a fold change <0.5 that were underrepresented in FRET- cells and genes >2 that were overrepresented in the FRET+ cells. **(C)** Pathway analysis of 153 protective genes via g:profiler. The enriched pathway is visualized by cytoscape. **(D)** Normalized FRET from αS biosensors following siRNA knockdown of 9 genes identified in the screen and αS PFF treatment. ($n \geq 9$ repeats ; *** $p < 0.001$, ** $p < 0.01$ and * $p < 0.05$ by one-way ANOVA. error bars are ± S.E.M.) **(E)** Immunoblot with anti-VCP and anti-GAPDH of cell lysates from αS biosensors/spCas9 cells treated with a VCP gRNAs at low (L) medium (M) and high (H) concentration and harvest at 3 and 6 days after transduction. **(F)** Normalized FRET of αS biosensors/spCas9 cells treated with a VCP gRNA or scrambled control gRNA following 24-hour application of αS PFF. ($P = 0.0439$ by a two-tailed student's t-test). $n = 4$ biologically independent FRET assay. Data presents as mean ± S.E.M.

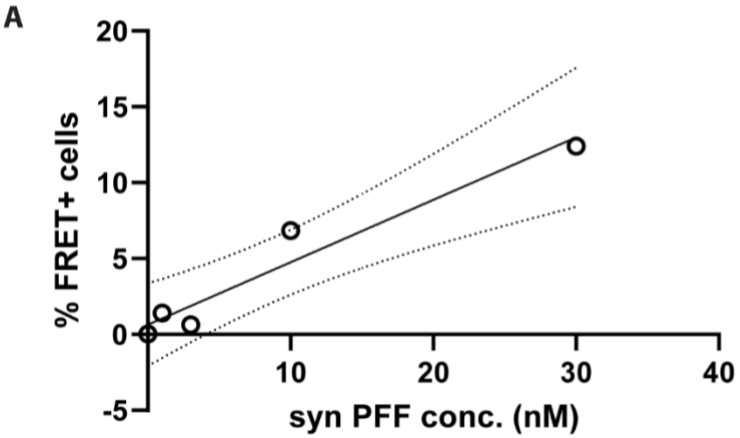

Figure S2. 1: spCas9-gRNA αS biosensor maintain seeding capacity.
spCas9 αS biosensor was treated with pooled library and maintained as described in Fig 2.2A, followed by αS seeding at different concentration. After 24hours, cells are harvested and the percentage of FRET is measured by flow cytometry

2. 4. 2 VCP inhibition increases α-synuclein seeding efficiency

As shown in Figure 2.1, αS seeding as measured by FRET is not seen with the application of monomeric αS[101]. Consistent with this, VCP siRNA treated αS biosensors showed no increase in FRET signal when treated with αS monomer (10nM) as compared with control siRNA treated (Figure 2.3A). Moreover, Lipofectamine is necessary for efficient FRET in this assay ("Lipo" seeding). The application of αS PFF (10nM) directly to the media ("naked" seeding) fails to induce robust aggregation and FRET signal after 24 and 48 hours, with less than 0.2% of cells being FRET positive (data not shown), suggesting that Lipofectamine facilitates entry into the endolysosomal pathway[101]. Notably, VCP KD did not increase "naked' seeding and only augmented "Lipo" seeding when compared with scrambled control KD (Figure 2.3A). To verify αS PFF entry through the endocytic pathway with "Lipo seeding", we pre-treated cells with Dynogo-4a (10μM), a dynamin I/II inhibitor, for one hour before αS PFF with Lipofectamine application for 24 hours. Consistent with previous studies showing that αS PFF internalization is dynamin-dependent[228], we found a decrease in FRET with Dynogo-4a (Figure 2. 3B). Subsequent studies using the αS biosensor line are performed using "Lipo" seeding (Figure 2.3B-E; 2.7A).

In order to probe the role of VCP specifically at the time of endocytic entry into the cytosol, we modified our seeding protocol to a four-hour application of αS with Lipofectamine and subsequent washout of αS PFF from the media. Seeding activity is quantified via FRET-Flow after 20 hours. This four-hour application was sufficient to seed αS aggregation as measured by

FRET in a concentration-dependent manner (Figure 2.3C). A four-hour treatment at the time of αS PFF application with the lysosomal permeabilizing agent (LLoMe, 1μM, 4hr) significantly increased FRET (Figure 2.3D). Treatment of αS biosensors with the VCP inhibitor NMS-873[229] for four hours at the time of αS PFF application similarly increased seeding efficiency as measured by FRET (Figure 2.3D).

We further validated the effect of VCP inhibition with two additional VCP inhibitors, CB-5083[230] and Eeyarestatin I (Eer1)[231]. Continuous application of either inhibitor with αS PFF increased the seeding efficiency as measured by FRET (Figure 2.3F). VCP inhibition has been show to effect both the autophagic and proteasomal pathways. 24-hour application of the proteasome inhibitor Bortezomib or autophagy modulators (100nM Rapamycin and 1μM 3-methyladenine (3-MA)) with αS PFF did not affect seeding efficiency (Figure 2.3F). Finally, both VCP inhibition and knockdown can induce ER stress and activate the unfolded protein response (UPR)[232,233]. Treatment of αS biosensors with the ER stress inducing agents dithiothreitol (DTT, 1mM, 24hr), thapsigargin (0.3μM; 24hr), and tunicamycin (2.5μg/mL, 24hr) with αS PFF (10nM) for 24 hours had no effect or decreased FRET efficiency as compared to vehicle controls. This suggested that the effect of VCP inhibition on seeding is ER stress independent (Figure 2.3E). Notably, no treatment significantly altered FRET efficiency compared with vehicle control when αS monomer was added (blue and red bars, Fig 3E), indicating that these effects are αS PFF dependent.

To see whether the increased seeding efficiency with VCP inhibition was due to an increase in αS PFF uptake, we employed a fluorescently conjugated αS PFF (αS-PFF 647). αS-PFF 647 retains seeding capacity in αS biosensors (Figure S2.2). Four-hour αS biosensor treatment with αS-PFF 647 in the presence of LLoMe or NMS-873 did not increase the amount of internalized αS PFF 647, as quantified by the percentage of Alexa 647 positive cells via flow cytometry (Figure 2.4A-B). Uptake was also unchanged when comparing scrambled and VCP siRNA KD cells (Figure 2.4C). In contrast, the dynamin I/II inhibitor Dynogo-4a significantly decreased αS PFF 647 uptake when measured at 4 hours post seed application (Figure 2.4D). In addition, the increased seeding efficiency with VCP chemical inhibition or VCP siRNA knockdown was not due to an increase in the steady-state levels of soluble αS, as determined by immunoblot against total αS and αS fluorescence intensity as measured by CFP median fluorescent intensity via flow cytometry (Figure 2.4E-K). Notably, VCP siRNA KD was >75% and a four hour treatment with NMS-873 was sufficient to increase the level of high molecular weight (HMW) ubiquitin conjugates consistent with VCP inhibition (Figure 2.4E-H).

To explore the role of VCP in a more relevant system of αS seeding that does not require the use of the carrier Lipofectamine, we adapted a previously described assay that adds αS PFF to primary cultured hippocampal neurons (HNs)[23]. Previous studies show that exogenously applied αS PFF can induce endogenous αS aggregates in HNs that are hyperphosphorylated and Tx-100 insoluble. To avoid continuous αS PFF application, we added αS PFF to the media of HNs for only four hours, followed by washout with conditioned media. A four hour application

of αS PFF versus αS monomer was sufficient to generate detergent-insoluble, high molecular weight αS, and phospho-αS after five days, shown by fractionation immunoblot or via immunofluorescence using a phospho-αS (phospho Ser129/81A) antibody in HNs (Figure 2.5A-B). This four-hour treatment allows us to manipulate the effect of VCP inhibition at the time of seed uptake. We then co-treated HNs with LLoMe (1uM) and αS PFF (1μg/ml) for 4 hours followed by washout, which further increased the amount of phospho-αS as compared with the application of αS PFF and vehicle (Ethanol) after five days (Figure 2.4C-D). These results were αS PFF dependent since treating HNs with LLoMe, and monomeric αS (1μg/ml) failed to generate phospho-αS aggregates (Figure 2.4C). We performed a similar assay and treated HNs for four hours with the reversible VCP inhibitor ML240[234](100nM) and αS PFF (1μg/ml). Notably, the application of ML240 for four hours at the time of αS PFF application increased the level of phospho-αS as compared with vehicle-treated control, while ML240-treated HNs with αS monomers show no phospho-αS signal (Figure 2.4E-F). We further validated the role of VCP with two different shRNAs against VCP. Primary HNs were treated with lentiviral shRNA (at DIV5) for five days prior to a five-day continuous application of αS PFF or monomer treatment (at DIV10). Both VCP shRNAs decreased VCP protein levels and demonstrated an increase in an αS PFF-dependent increase in phospho-αS staining compared with scrambled shRNA control (Figure 2.6). Treatment with LLoMe, ML240, or shRNA-VCP treatment did not alter cell viability as measured by MTT assay after 10 and 15 days in culture (Figure S2. 3).

Several studies support that αS PFFs enter the endocytic pathway and permeabilize the late endosome resulting in seed escape to the cytoplasm235,236. Once damaged, cytosolic galectins (e.g., Gal3 and Gal8) bind to exposed intraluminal carbohydrates tagging the permeabilized late endosome. This damaged galectin-positive late endosomes are then cleared via lysophagy. Indeed treatment of U20S cells with "naked" αS PFF-647 for four hours demonstrates internalized αS PFF in Gal8 and Lamp1 positive structures (Figure S2.4E). Blocking the lysophagic clearance of Gal8 puncta with bafilomycin increases the number of cells with damaged late endosomes with αS PFF treatment (Figure S2.4A-B). This increase returns to baseline following removal of bafilomycin and αS PFF from the media (Figure S2.4C-D). Furthermore, Gal8 positive puncta were retained in VCP knockdown cells (Figure S2.4F-G).

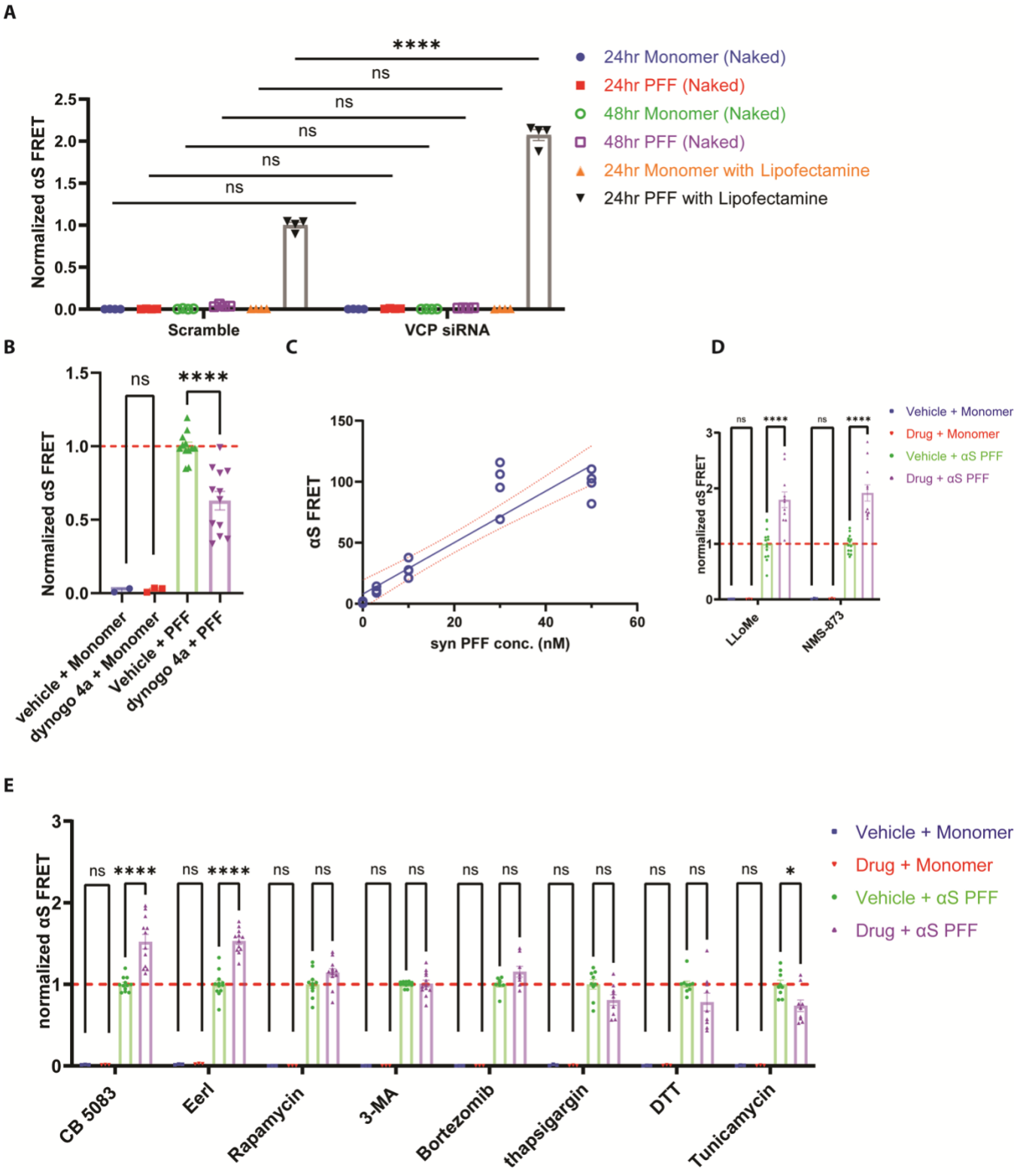
A
Normalized αS FRET
Scramble
VCP siRNA
****
ns
24hr Monomer (Naked)
24hr PFF (Naked)
48hr Monomer (Naked)
48hr PFF (Naked)
24hr Monomer with Lipofectamine
24hr PFF with Lipofectamine
B
Normalized αS FRET
vehicle + Monomer
dynogo 4a + Monomer
Vehicle + PFF
dynogo 4a + PFF
C
αS FRET
syn PFF conc. (nM)
D
normalized αS FRET
LLoMe
NMS-873
Vehicle + Monomer
Drug + Monomer
Vehicle + αS PFF
Drug + αS PFF
E
normalized αS FRET
CB 5083
Eerl
Rapamycin
3-MA
Bortezomib
thapsigargin
DTT
Tunicamycin

Figure 2. 3: VCP inhibition enhances αS seeding.

(A) αS biosensors were treated with scrambled control siRNA or VCP siRNA for 48 hours prior the application of αS monomer or PFF (10nM) with or without Lipofectamine and measured for FRET efficiency at 24 and/or 48 hours. N=4 for each groups. ; n.s.= no significant, **** $p < 0.0001$ by two-way ANOVA compared with scramble siRNA in each conditions. Error bars are ± S.E.M.). **(B)** αS biosensors were treated with Dynogo 4a for one hour prior to αS PFF or monomer (10nM) treatment with Lipofectamine. n =12 repeats for PFF treated conditions. **** $p < 0.0001$; n.s. for monomer treated pairs by two-way ANOVA. **(C)** αS biosensors treated with αS PFF for 4 hours followed by media exchange and washout. FRET signal was measured the same as in 3A, 20 hours after washout. n.s. no significant and **** $p < 0.0001$ compared to vehicle washout at different concentrations. Each dot represents an independent experiment. **(D)** Normalized FRET of αS biosensors co-treated with αS monomer or PFF (30nM) with the indicated chemical compound or vehicle for four hours followed by washout and FRET measurement 20 hours later. (n =14 repeats for each PFF treated conditions; n.s. for all monomer treated pairs; **** $p < 0.0001$ by two-way ANOVA in some PFF treated pairs as indicated. error bars are ± S.E.M.). **(E)** Normalized FRET of αS biosensors co-treated with αS monomer or PFF (10nM) with the indicated chemical compound or vehicle for 24 hours. FRET signal was obtained same as 3A ($n \geq 8$ repeats for each PFF treated conditions; n.s. for all monomer treated pairs; **** $p < 0.0001$ and * $p < 0.05$ by two-way ANOVA in some PFF treated pairs as indicated. error bars are ± S.E.M.).

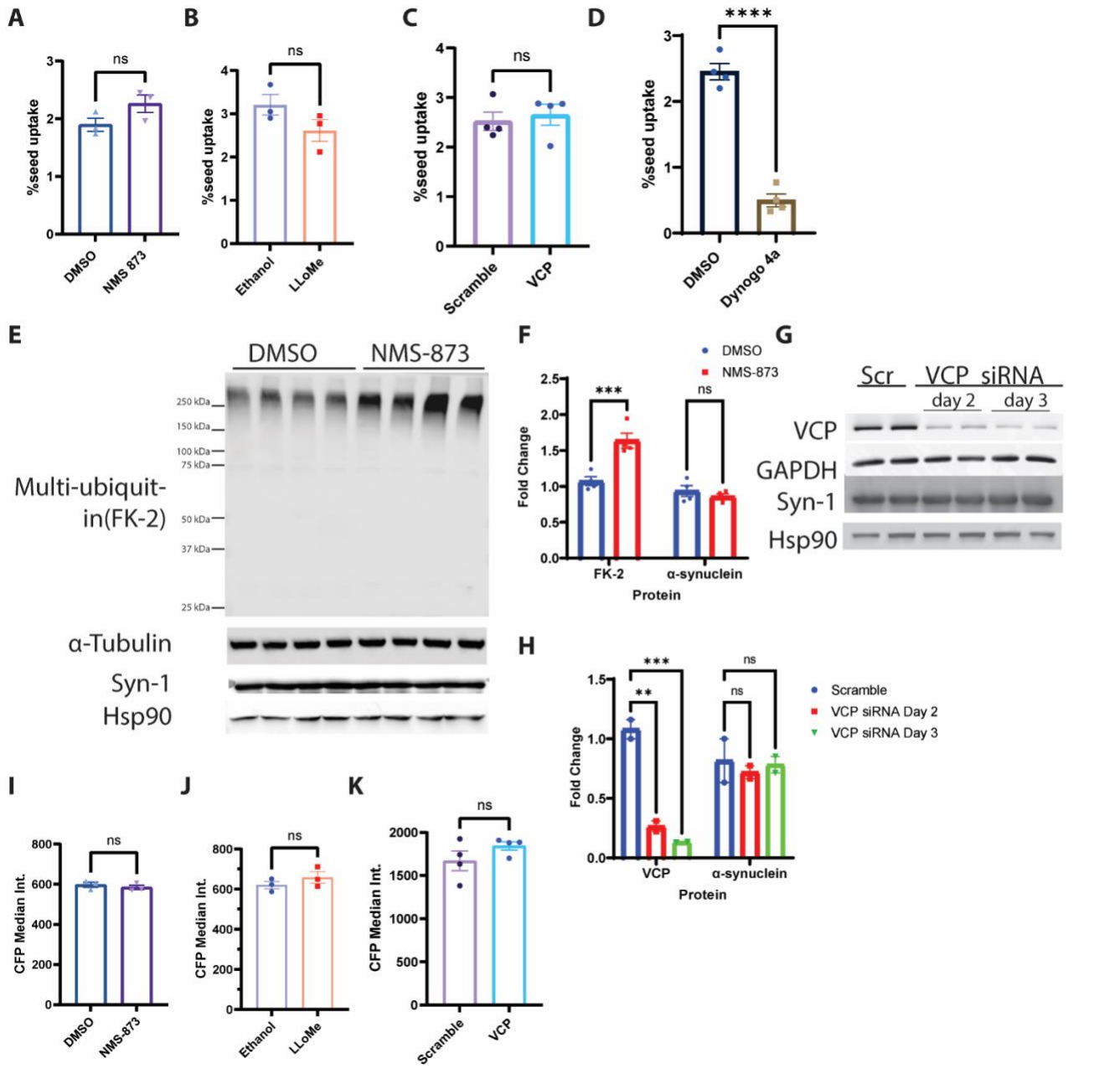
A
B
C
D
%seed uptake
ns
****
DMSO
NMS 873
Ethanol
LLoMe
Scramble
VCP
Dynogo 4a
E
DMSO
NMS-873
Multi-ubiquit-in(FK-2)
250 kDa
150 kDa
100 kDa
75 kDa
50 kDa
37 kDa
25 kDa
α-Tubulin
Syn-1
Hsp90
F
DMSO
NMS-873
Fold Change
***
FK-2
α-synuclein
Protein
G
Scr
VCP siRNA
day 2
day 3
VCP
GAPDH
Syn-1
Hsp90
H
**
Scramble
VCP siRNA Day 2
VCP siRNA Day 3
I
J
K
CFP Median Int.

Figure 2. 4: VCP inhibition does not affect seed uptake or αS protein levels.
(A) Quantification of percentage of Alexa- 647 positive cells (seed uptake) from αS biosensors co-treated with Alexa-647 tagged αS PFF together with vehicle or NMS-873 (1μM) for 4 hours. n=3 biological repeat. Data is Mean ± S.E.M. n.s. no significant from student's t test **(B)** Quantification of seed uptake from αS biosensors co-treated with Alexa-647 tagged αS PFF and LLoMe or vehicle for 4 hours. n=3 biological repeat. Data is mean ± S.E.M. n.s. no significant from student's t test. **(C)** Quantification of seed uptake from VCP or scramble siRNA treated cells with 4-hour Alexa-647 tagged αS PFF application. n=4 biological repeat. Data is mean ± S.E.M. n.s. no significant from student's t test. **(D)** Quantification of seed uptake from αS biosensors treated with Dynogo-4a or DMSO for one hour and then Alexa-647 tagged αS PFF for four hours. n=4 biological repeat. Data is mean ± S.E.M. ****$p < 0.0001$ from student's t test. (**E)** Immunoblot of anti-Ubiquitin (FK-2), and total α-synuclein (syn-1) from αS biosensors treated for four-hours with NMS-873 (5μM) or DMSO. α-tubulin and HSP90 are loading controls. **(F)** Quantitation of band intensities of VCP and α-synuclein in E. *** $p < 0.001$ and n.s.=no significant by two-way ANOVA. **(G)** Immunoblot of anti-VCP, and α-synuclein (syn-1) from αS biosensors treated with scrambled or VCP siRNA for 48 and 72 hours. GAPDH and HSP90 are loading controls. **(H)** Quantitation of band intensities of VCP and α-synuclein in G. ** $p < 0.01$ *** $p < 0.001$ and n.s.=no significant by two-way ANOVA. **(I)** Quantification of CFP fluorescent intensity of NMS-873 treated cells. Drug treatment and timeline were the same as 3D. n=3 biological repeat. Data is mean ± S.E.M n.s. no significant from student's t test. **(J)** Quantification of CFP fluorescent intensity of LLoMe treated cells. Drug treatment and timeline were the same as 3D. n=3 biological repeat. Data is mean ± S.E.M. n.s. no significant from student's t test. **(K)** CFP fluorescent intensity of αS biosensors treated with scrambled or VCP siRNA. n=4 biological repeat. Data is mean ± S.E.M.

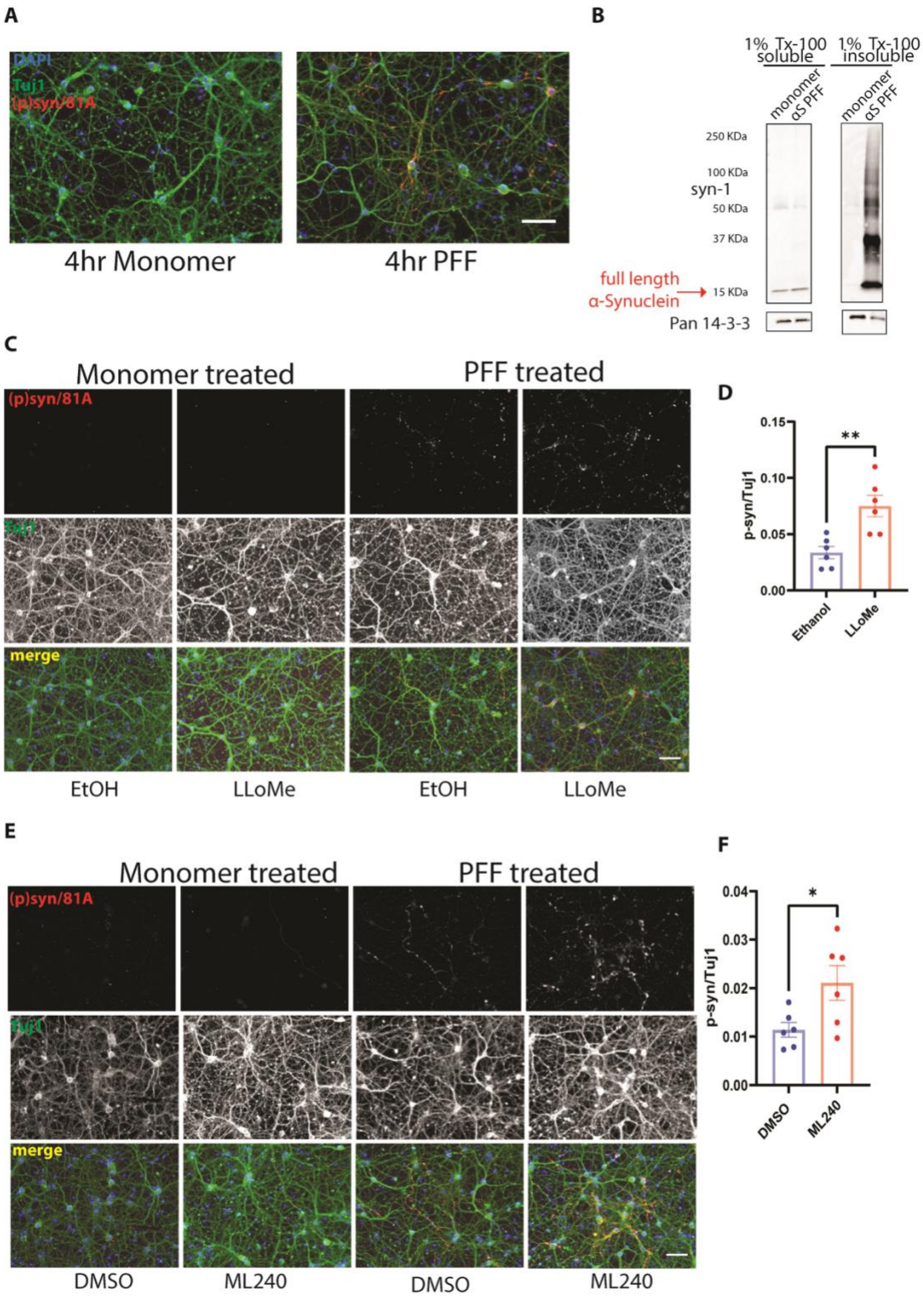
A
DAPI
Tuj1
(p)syn/81A
4hr Monomer
4hr PFF
B
1% Tx-100 soluble
1% Tx-100 insoluble
monomer αS PFF
monomer αS PFF
250 KDa
100 KDa
syn-1
50 KDa
37 KDa
full length α-Synuclein
15 KDa
Pan 14-3-3
C
Monomer treated
PFF treated
(p)syn/81A
Tuj1
merge
EtOH
LLoMe
EtOH
LLoMe
D
p-syn/Tuj1
0.15
0.10
0.05
0.00
**
Ethanol
LLoMe
E
Monomer treated
PFF treated
(p)syn/81A
Tuj1
merge
DMSO
ML240
DMSO
ML240
F
p-syn/Tuj1
0.04
0.03
0.02
0.01
0.00
*
DMSO
ML240

Figure 2. 5: VCP inhibition enhances αS seeding in neurons.
(A) Immunofluorescence for phospho-αS and Tuj1 (neurite marker) in HNs treated for 4 hours with αS PFF or monomer (1μg/ml) followed by washout and harvest 5 days later. **(B)** Immunoblot for αS from detergent soluble and insoluble lysates of HNs treated for 4 hours with αS PFF or monomer (1μg/ml) and then harvested 5 days later. Note that the 2%SDS insoluble fraction has high molecular weight αS positive multimers. PAN 14-3-3 is the loading control. **(C)** Immunofluorescence for phospho-αS and Tuj1 in HNs co-treated with αS PFF or monomer (1μg/ml) and LLoMe (1uM) or vehicle for 4 hours. Immunostaining was performed after 5 days. Scale bar =20μm. **(D)** Quantitation of phospho-αS/Tuj1 staining as in 3C. Quantitation in 3C and subsequent HN studies were performed using the average intensity of multiple fields from individual coverslips. Each coverslip was treated as an independent experiment. n=6 for ethanol and LLoMe groups respectively. Experiments were repeated from 3 different cultures. **$p < 0.01$ by student's t-test. Error bars are ± S.E.M. **(E)** Immunofluorescence for phospho-αS and Tuj1 in HNs co-treated with αS PFF or monomer (1μg/ml) and ML240 (100nM) or DMSO control for 4 hours and harvested after 5 days. Scale bar =20μm **(F)** Quantitation of phospho-αS/Tuj1 staining as in 3D. n=6 for DMSO and ML240 group. Experiments were repeated from 3 different cultures. *$p < 0.05$ by student's t-test. Error bars are ± S.E.M.).

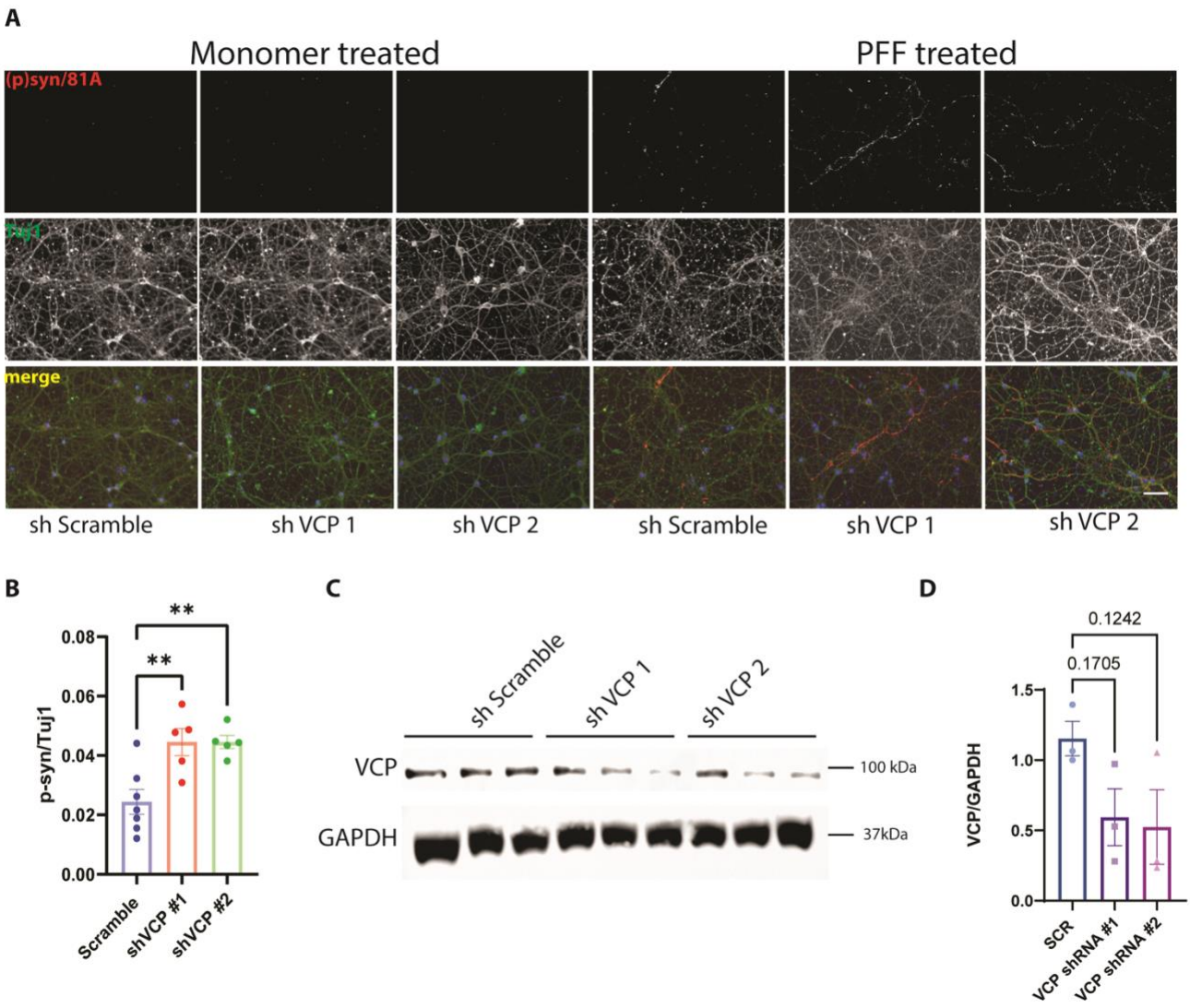

Figure 2. 6: VCP knockdown enhances αS seeding in neurons.
(A) Immunofluorescence for phospho-αS and Tuj1 in HNs infected with lentiviral vectors expressing scrambled or one of two different shRNAs targeting VCP for 5 days and then treated with αS PFF or monomer (1μg/ml) for 5 days. Scale bar =20μm **(B)** Quantitation of phospho-αS/Tuj1 staining as in 3F. Experiments were repeated from 3 different cultures. N=7,5 and 5 for scramble and VCP shRNA 1 and 2 respectively. **p < 0.01 one-way ANOVA with Dunnett correction. Error bars are ± S.E.M. **(C)** Representative immunoblot from independent HN lysates treated with scramble or VCP shRNAs for anti-VCP and GAPDH. **(D)** Quantitation of band intensities of VCP over GAPDH control.

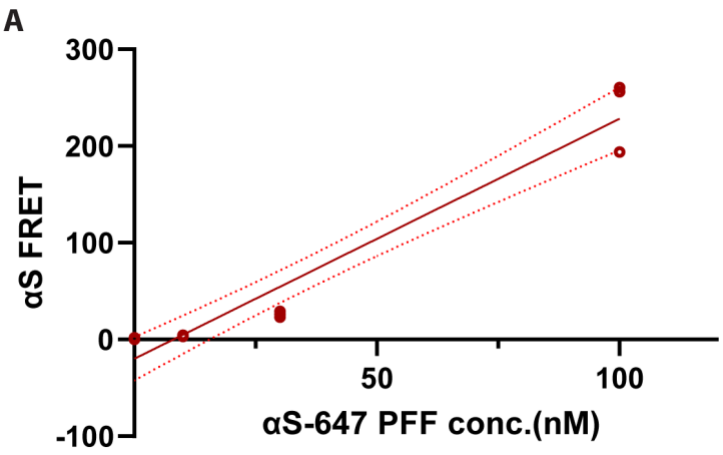

Figure S2. 2: αS biosensor shows seeding activities in a concentration dependent manner. Alexa647 tagged αS PFF show moderate seeding capacity according to FRET assay.

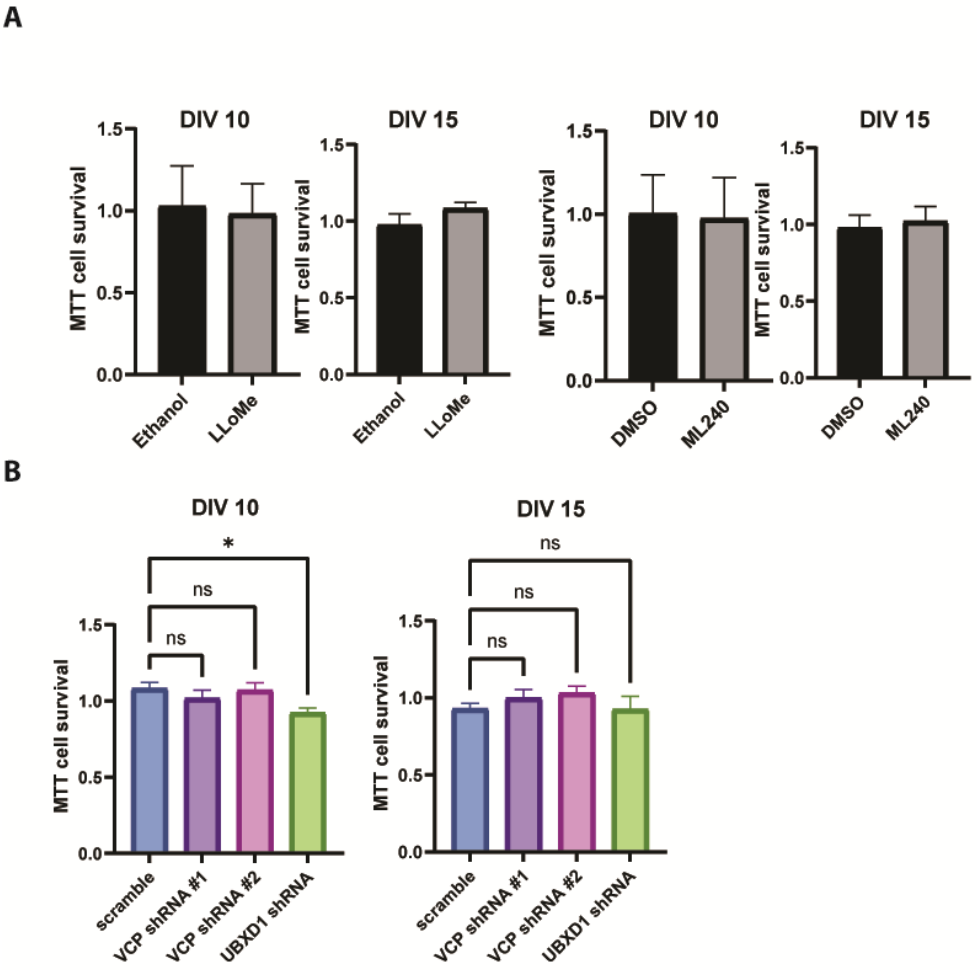

Figure S2. 3: Cell viability in HNs with treatment.

(A) HNs are treated with LLoMe (1uM) or ML240 (100nM) for 4 hours at DIV10. Cell are tested by MTT assay right after the temporal treatment (DIV10) or at the time we harvest the cell for staining (DIV15). **(B)** HNs are transduced with lentivirus shRNA targeting genes as indicated at DIV4 (MOI=10). Cell viabilities are tested by MTT assay at DIV10 and DIV15 respectively. $p<0.05$ and n.s. = no significant by one-way ANOVA.

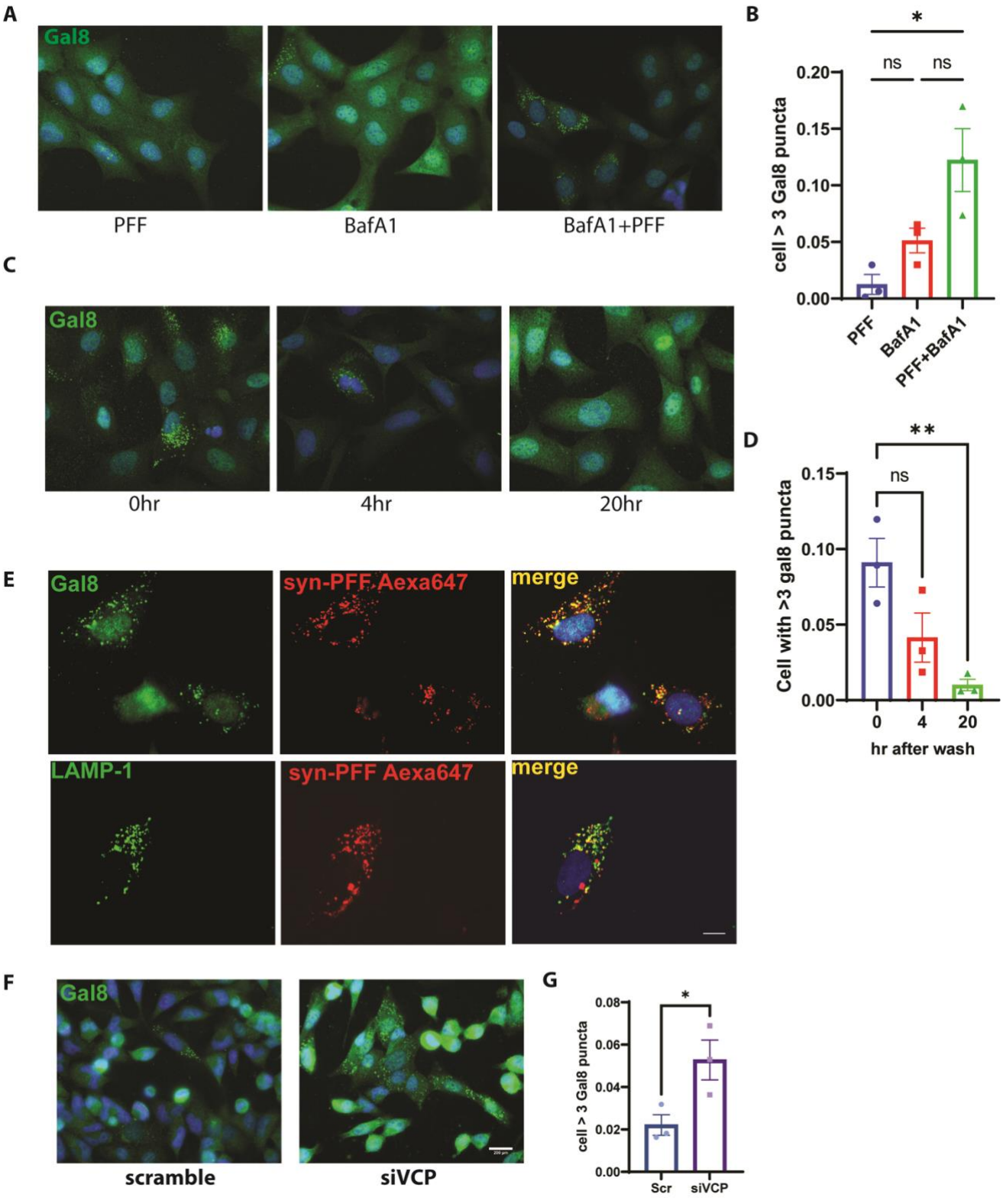
A
Gal8
PFF
BafA1
BafA1+PFF
B
*
ns
ns
cell > 3 Gal8 puncta
0.20
0.15
0.10
0.05
0.00
PFF
BafA1
PFF+BafA1
C
Gal8
0hr
4hr
20hr
D
**
ns
Cell with >3 gal8 puncta
0.15
0.10
0.05
0.00
0
4
20
hr after wash
E
Gal8
syn-PFF Aexa647
merge
LAMP-1
syn-PFF Aexa647
merge
F
Gal8
scramble
siVCP
G
*
cell > 3 Gal8 puncta
0.08
0.06
0.04
0.02
0.00
Scr
siVCP

Figure S2. 4: αS fibrils induce reversible endolysosomal damages.
(A) U2OS cells are treated αS PFF (100nM) with or without BafA1 (100nM). Cells are harvested after 24hrs and stained by Galectin-8. Cells with only BafA1 is considered as baseline control. **(B)** Quantification of images in A. αS PFF treated Cells with more than 3 Gal8 puncta are counted, and normalized by number of nucleus (DAPI) in a double-blind analysis. **(C)** U2OS cells treated αS PFF and BafA1 (100nM) for 4 hours and chased for indicated time. **(D)** Quantification of images in C. **(E)** Co-localization of exogenous Alexa647 tagged αS PFF (100nM) after 24hours with LAMP1 and Gal8. **(F)** U2OS cells with VCP siRNA KD or scramble are treated with BafA1 (100nM) and αS PFF (100nM). Cells are harvested after 24hrs and stained by Galectin-8. **(G)** Quantification of images in F.

2. 4. 3 VCP disease mutations increase αS seeding both *in vitro*

VCP disease mutations affect a subset of VCP dependent cellular processes such as endocytic trafficking, nutrient sensing, autophagosome maturation, and, more recently, lysophagy[133,206]. This is due to an impairment in VCP mutant association with the adaptor UBXD1[235]. We performed siRNA knockdown of VCP and the VCP adaptors UFD1, NPL4, UBXD1, and PLAA and the autophagy proteins ATG5 and SQSTM1 along with a scrambled control in αS biosensors (Figure S 2.4A). Following 48 hours of knockdown, αS biosensors were treated with αS PFF or monomer (10nM), and FRET was measured 24 hours later. Knockdown of the VCP adaptor UBXD1 significantly increased FRET efficiency compared with scramble siRNA control, whereas application of monomeric αS did not alter the FRET signal (Figure 2.7A). To confirm UBXD1 is an essential VCP cofactor for seeding, we knocked down UBXD1 using shRNA in primary HNs five days prior to αS PFF application. UBXD1 KD also increased phospho-αS staining compared with scrambled shRNA control (Figure 2.7B-D). The increase in phospho-αS staining was not associated with a minor change in cell viability that was measured by MTT assay after 10 (1.08 vs. 0.92 0, p= 0.0329) and 15 days (p= >0.9999) in culture (Figure S2.3).

To understand if VCP disease mutations augment αS seeding activity, we first evaluated αS seeding in the setting of mutant VCP overexpression. αS biosensors were transfected with mCherry-tagged VCP-WT or one of three different mCherry-tagged VCP disease mutations (R95G, R155H, and A232E) for 24 hours then treated with αS PFF (10nM) and quantified for

FRET efficiency 24 hours later. Transfected cells are selected for mCherry signal via flow cytometry simultaneously with FRET. Whereas cells not expressing mCherry were unchanged and cells expressed similarly level of tagged VCP(Figure 2.8A and S2.5B). To evaluate this in primary HNs, we transduced neurons with lentiviral constructs (CCIV) expressing wild-type VCP-myc or one of two different VCP disease mutations (VCP^{R155H}-myc and VCP^{A232E}-myc) or empty vector (CCIV), five days prior to αS PFF application. Lysates from similarly treated HNs demonstrated comparable levels of myc-tagged VCP-WT or mutant expression. Following five days, VCP-R155H and VCP-A232E expressing neuronal cultures had an increase in phospho-αS staining compared with control and VCP-WT expressing cultures (Figure 2.8B-D).

In order to explore αS PFF seeding in a non-overexpressed neuronal system, we cultured primary HNs from $VCP^{WT/WT}$ and $VCP^{RH/WT}$ embryos, treated them with αS PFF, and then immunostained for phospho-αS five days later. VCP-R155H mutation knockin mice have been previously generated and characterized . $VCP^{RH/WT}$ HNs had a significant increase in phospho-αS staining compared with $VCP^{WT/WT}$ HNs controls (Figure 2.8E-F). Notably, the phospho-αS staining in $VCP^{RH/WT}$ treated HNs was less filamentous and predominantly perinuclear compared to $VCP^{WT/WT}$ HNs. The perinuclear phospho-αS aggregates co-localized with p62/SQSTM1 and LAMP1 suggesting an alteration in aggregate trafficking (Figure 2.8G).

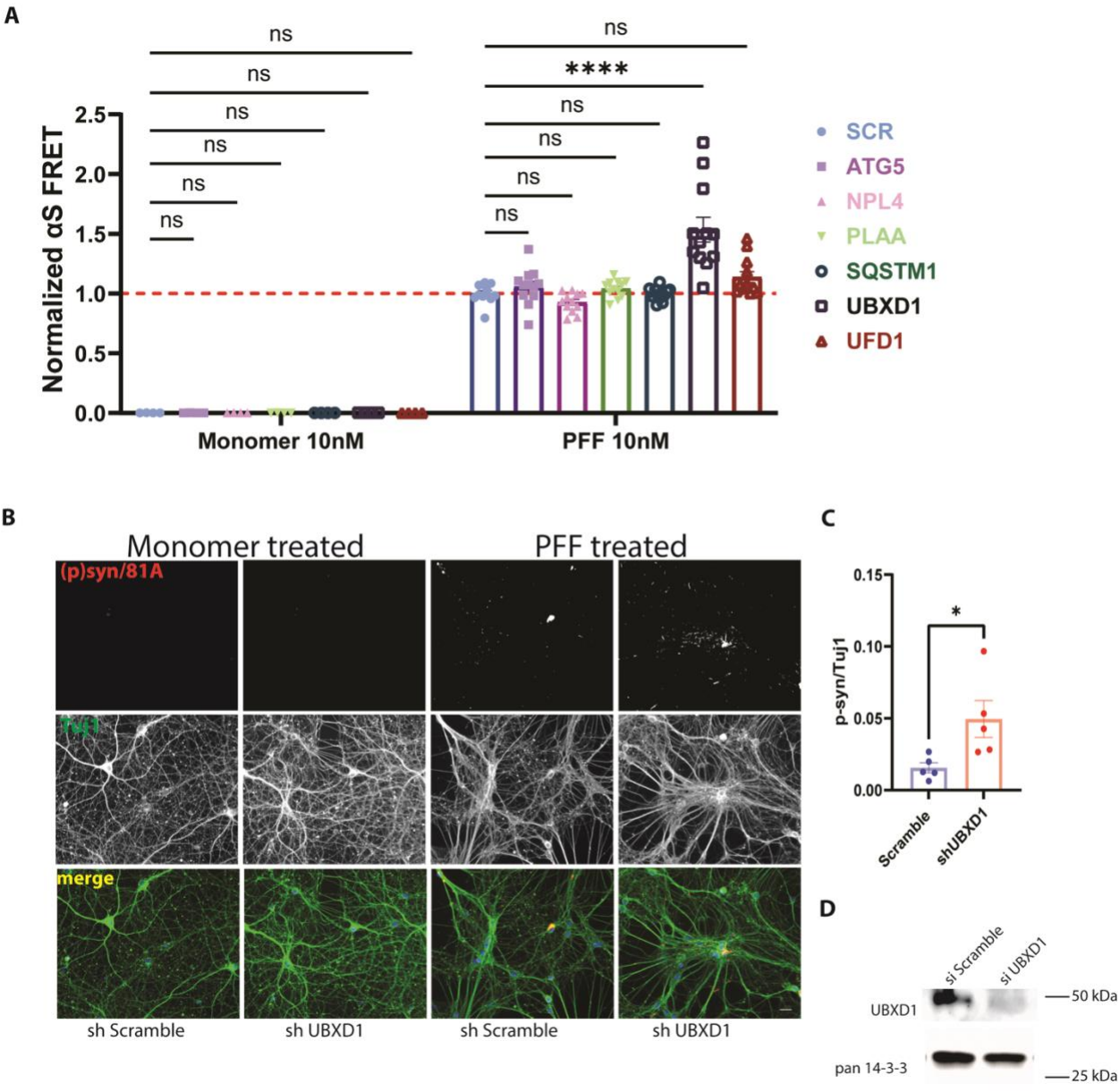
A
ns
ns
ns
ns
ns
ns
ns
****
ns
ns
ns
ns
Normalized αS FRET
2.5
2.0
1.5
1.0
0.5
0.0
Monomer 10nM
PFF 10nM
SCR
ATG5
NPL4
PLAA
SQSTM1
UBXD1
UFD1
B
Monomer treated
PFF treated
(p)syn/81A
Tuj1
merge
sh Scramble
sh UBXD1
sh Scramble
sh UBXD1
C
0.15
0.10
0.05
0.00
p-syn/Tuj1
*
Scramble
shUBXD1
D
si Scramble
si UBXD1
UBXD1
50 kDa
pan 14-3-3
25 kDa

Figure 2. 7: VCP cofactor UBXD1 knockdown augments αS seeding.
(A) αS biosensors were treated with scrambled control siRNA or siRNAs targeting the indicated genes for 48 hours prior to the application of αS PFF or monomer (10nM) and harvested for FRET efficiency at 24 hours. n =4 and 12 for the monomer and PFF treated group respectively for each KD. Adjusted p ****p < 0.0001 for UBXD1 by two-way ANOVA with Šidák correction n.s. = no significance. Error bars are ± S.E.M. **(B)** Immunofluorescence for phospho-αS and Tuj1 in HNs infected with lentiviral vectors expressing scrambled or a shRNA targeting UBXD1 for 5 days and then treated with αS PFF or monomer (1μg/ml) for 5 days Scale bar =20μm. **(C)** Quantitation of phospho-αS/Tuj1 staining from PFF treated HNs infected with scramble or control UBXD1 shRNAs. Experiments were repeated from 3 different cultures. N= 5 for each groups.. * p<0.05 by Student's t test). **(D)** Representative immunoblot from HN lysates treated with scramble or UBXD1 shRNAs for anti-UBXD1 and α-tubulin

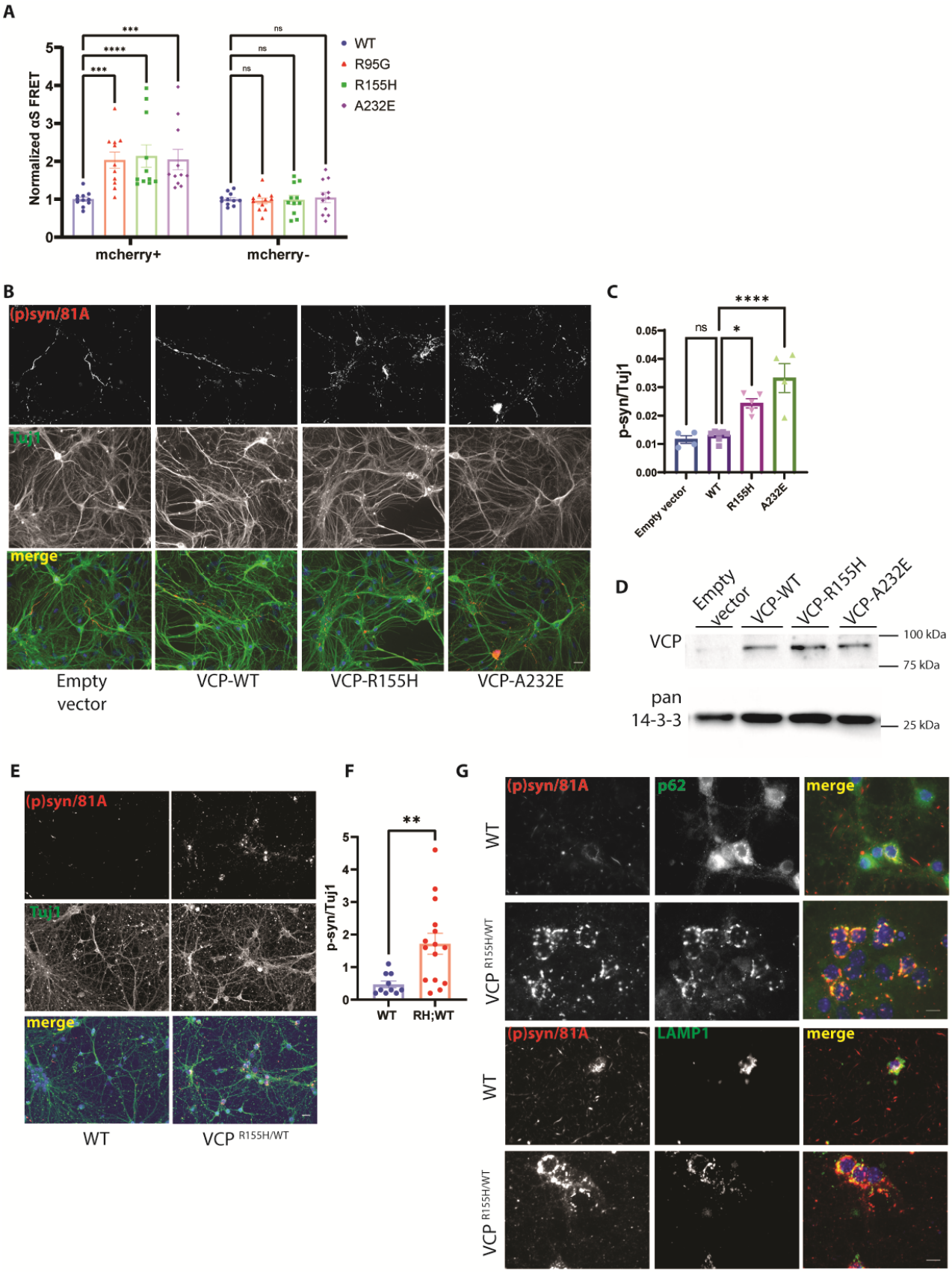
A
Normalized αS FRET
mcherry+
mcherry-
WT
R95G
R155H
A232E
B
(p)syn/81A
Tuj1
merge
Empty vector
VCP-WT
VCP-R155H
VCP-A232E
C
p-syn/Tuj1
Empty vector
WT
R155H
A232E
D
Empty vector
VCP-WT
VCP-R155H
VCP-A232E
VCP
pan 14-3-3
100 kDa
75 kDa
25 kDa
E
(p)syn/81A
Tuj1
merge
WT
VCP R155H/WT
F
p-syn/Tuj1
WT
RH;WT
G
(p)syn/81A
p62
merge
WT
VCP R155H/WT
(p)syn/81A
LAMP1
merge
WT
VCP R155H/WT

Figure 2. 8: VCP disease mutation expression enhances αS seeding.
(A) αS biosensors were transfected with plasmids expressing VCP-WT, or one of three disease mutations (R95G, R155H and A232E) fused to an mcherry tag for 24 hours and then treated with αS PFF (10nM). FRET efficiency is quantified in mCherry+ and mCherry- cells separately and all normalized to VCP-WT (n=11 repeats for each group. ***p < 0.001; ****p < 0.0001; ns, no significance; two-way ANOVA with Dunnett's correction) **(B)** Immunofluorescence for phospho-αS and Tuj1 in HNs treated with empty control lentiviral vector, VCP-WT-myc or one of two myc tagged VCP disease mutations (R155H or A232E). HNs were transduced with lentivirus as indicated for 5 days before 10nM αS PFF treatment. HNs were harvested after another 5 days. Scale bar =20μm. **(C)** Quantitation of phospho-αS/Tuj1 staining as in 8C. Experiments were repeated from 3 different cultures. *p < 0.05; ****p < 0.0001; ns, no significance compared with the VCP-WT group by one-way ANOVA. **(D)** Immunoblot of lysates from HNs overexpressing lentiviruses expressing empty vector, VCP-WT-myc, VCP-R155H-myc or VCP-A232E-myc using an anti-myc antibody or pan 14-3-3 as a loading control. **(E)** Immunofluorescence for phospho-αS and Tuj1 in HNs from wild-type mice or mice carrying a VCP-R155H knock-in allele ($VCP^{R155H/WT}$) treated with αS PFF (1μg/ml) for 5 days. **(F)** Quantitation of phospho-αS/Tuj1 staining as in 8F. Neurons came from 10 and 15 independent cultures from WT and $VCP^{R155H/WT}$ embryos. Outlier is removed by ROUT method, Q=1%, followed by Student's t test. p<0.0001), Scale bar =20μm. **(G)** Immunofluorescence of WT or $VCP^{R155H/WT}$ HNs treated with αS PFF (1μg/ml) and harvested 5 days later with anti-phospho-αS (red) and p62 (green) (upper panels) or anti-phospho-αS (red) LAMP1 (green) (lower panels). Scale bar =10μm.

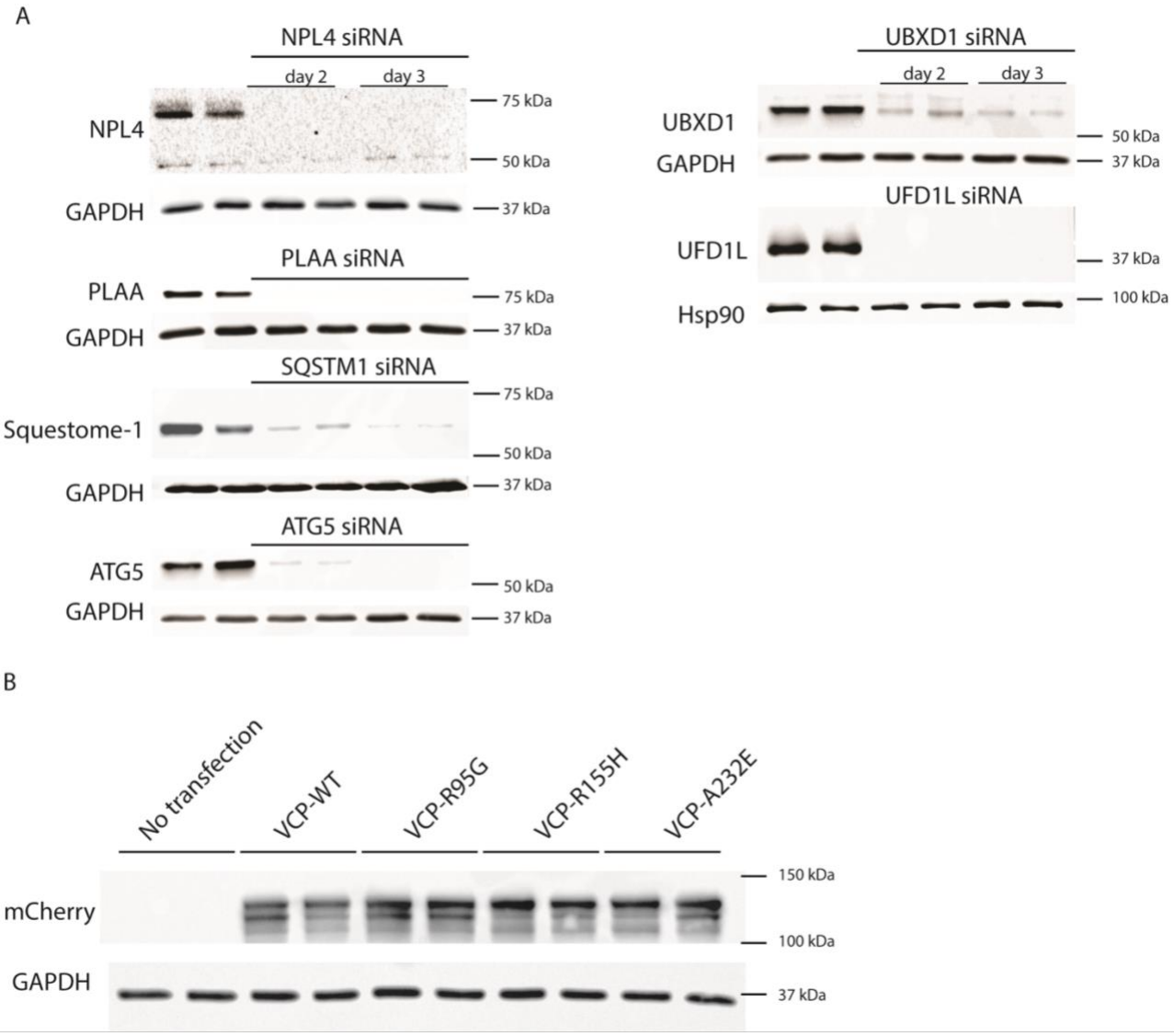

Figure S2. 5: Gene knockdown efficiency and VCP vector transfection.
(A) αS biosensor is reverse transfected with siRNA (6pmol). Cell lysis are saved at 48 and 72 hours after transfection. Immunoblot is performed on each KD for protein level change. **(B)** Immunoblot with anti-mCherry of αS biosensor lysate with overexpression of different VCP vectors.

2. 4. 4 VCP disease mutations increase αS seeding *in vivo*

We next examined the effect of pathogenic VCP mutations on αS seeding *in vivo*. $VCP^{RH/WT}$ mice display no neuronal loss, TDP-43 inclusions, or pathologic features consistent with autophago-lysosomal dysfunction up to 13 months old[145]. To explore an additional VCP mouse model that only expresses a VCP disease mutant allele, we also used a mouse line that deletes the VCP-WT allele and only allows expression of a single VCP-R155C mutant allele following tamoxifen treatment ($VCP^{RC/FL}$; Rosa26-Cre ERT2 (cVCP-RC) (Figure 2.S5). Similar to our previous study, lysates from the cortex of $VCP^{RH/WT}$ mice have no changes in the levels of autophagic proteins (Sequestosome-1/p62), ER stress (BiP/GRP78), or ubiquitinated proteins (Figure 2.S5B-C)[145]. Following five days i.p. tamoxifen treatment, cortical lysates from cVCP-RC mice have a 41% reduction in total VCP protein level but no changes in autophagic levels (Sequestosome-1/p62), ER stress (BIP/GRP78), or ubiquitinated proteins (Figure 2.S5B-C). However, high molecular weight ubiquitinated proteins, and SQSTM1 levels increase with age, as demonstrated by immunoblot of cortical lysates at six months after tamoxifen, supporting that VCP dysfunction is present (Figure 2.S5D-E). We have previously demonstrated that an increase in Gal3 levels occurs early, before autophagic dysfunction in $VCP^{RH/WT}$ mouse muscle[212]. Similar to skeletal muscle, Gal3 and LAMP1 levels are increased in both $VCP^{RH/WT}$ and cVCP-RC mouse cortical lysates suggesting an accumulation of damaged late endosomes (Figure 2.S5B-C)[133,212].

We injected 5ug αS PFF or PBS into the striatum of 4-month-old C57 control, $VCP^{RH/WT}$, or cVCP-RC mice and harvested the brain after three months (Figure 2.9A). Age-matched untreated control, $VCP^{RH/WT}$, cVCP-RC, C57 mice, or mice treated with PBS had no phospho-αS staining in any brain regions (Figure 2.9A-E). In contrast, C57 control mice injected with αS PFF had a significant increase of phospho-αS in multiple brain regions (Figure 2.9A-E). We found phospho-αS staining was significantly increased in the anterior and posterior cortices of $VCP^{RH/WT,}$ and cVCP-RC injected with αS PFF compared with that of C57 (Figure 2.9A-E). Other brain regions such as the amygdala and substantia nigra trended toward an increase in phospho-αS staining but did not reach statistical significance (Figure 2.9F-G).

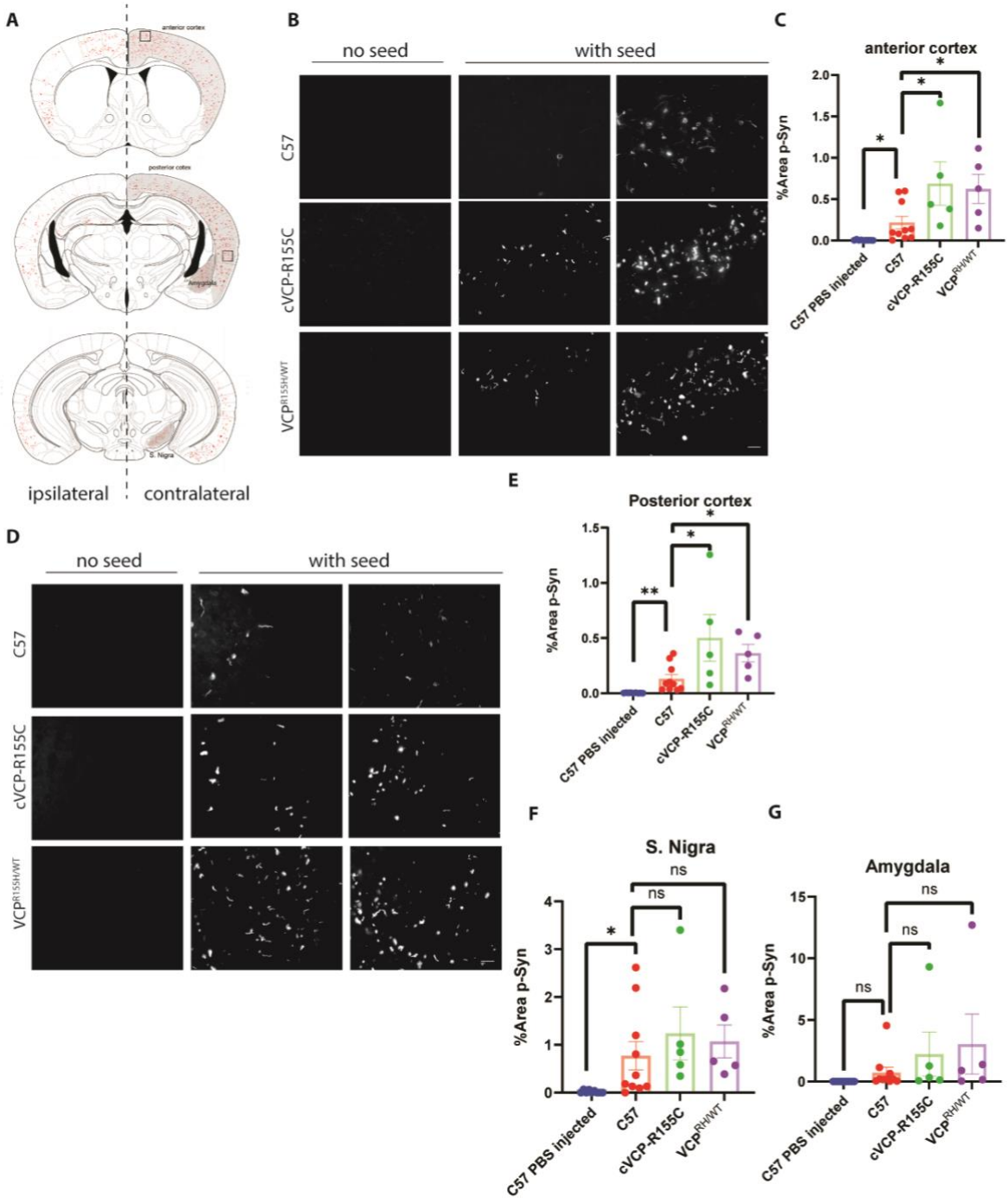
A
anterior cortex
posterior cotex
Amygdala
S. Nigra
ipsilateral
contralateral
B
no seed
with seed
C57
cVCP-R155C
VCP R155H/WT
C
anterior cortex
%Area p-Syn
C57 PBS injected
C57
cVCP-R155C
VCP RH/WT
D
no seed
with seed
C57
cVCP-R155C
VCP R155H/WT
E
Posterior cortex
%Area p-Syn
C57 PBS injected
C57
cVCP-R155C
VCP RH/WT
F
S. Nigra
%Area p-Syn
ns
C57 PBS injected
C57
cVCP-R155C
VCP RH/WT
G
Amygdala
%Area p-Syn
ns
C57 PBS injected
C57
cVCP-R155C
VCP RH/WT

Figure 2. 9: VCP disease mutations enhance αS seeding *in vivo*.
(A) Drawing of coronal sections through mouse brains. Shaded regions indicate areas utilized for quantitation and boxes denote regions corresponding to images in B and D. **(B)** Representative immunofluorescence images with pSer129-syn antibody of anterior cortices from C57, cVCP-R155C, and $VCP^{R155H/WT}$ mice injected unilaterally into the striatum with 5ug αS PFF after 90 days. 4 month aged C57 (n=10), VCP R155H/WT (n=5) and VCP R155C/FL; Rosa26-Cre ERT2 (cVCP-R155C) (n=5). Scale bar=25 μm. **(C)** Quantitation of the percentage of p-syn in entire anterior cortices (* $P<0.05$ by student's t-test). **(D)** Representative immunofluorescence images with pSer129-syn antibody of posterior cortices from C57, cVCP-R155C, and $VCP^{R155H/WT}$ mice as described in A. scale bar=25 μm. **(E)** Quantitation of the percentage of p-syn in posterior cortices (* $P<0.05$, ** $P<0.01$(* $P<0.05$ by student's t-test). **(F-G)** Quantitation of p-syn in Amygdala and substantia Nigra. (* $P<0.05$, ns, no significance student's t-test)

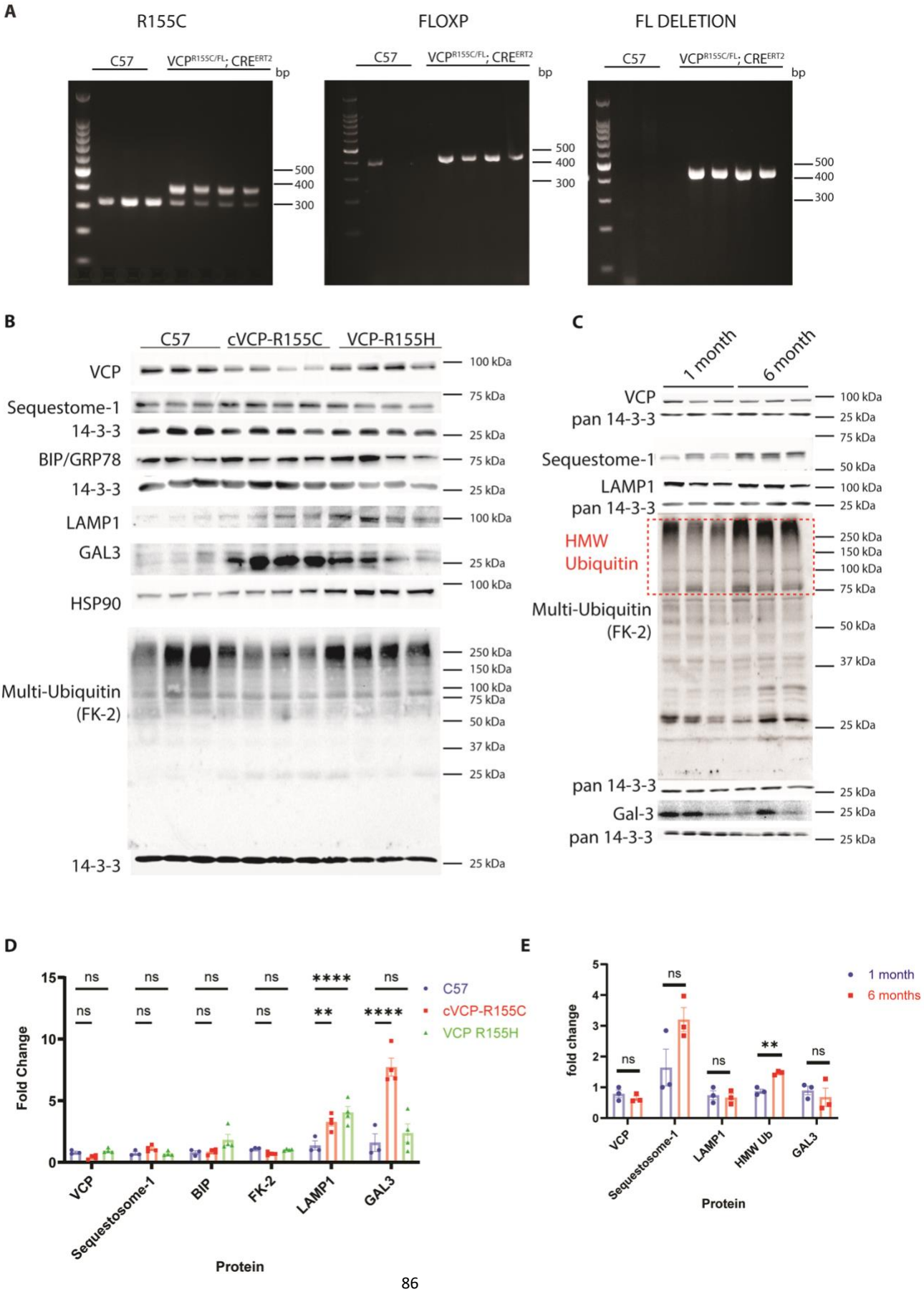
A
R155C
FLOXP
FL DELETION
C57
VCP R155C/FL; CRE ERT2
bp
500
400
300
B
C57
cVCP-R155C
VCP-R155H
VCP
Sequestome-1
14-3-3
BIP/GRP78
LAMP1
GAL3
HSP90
Multi-Ubiquitin (FK-2)
100 kDa
75 kDa
25 kDa
250 kDa
150 kDa
50 kDa
37 kDa
C
1 month
6 month
pan 14-3-3
HMW Ubiquitin
Gal-3
D
Fold Change
C57
cVCP-R155C
VCP R155H
ns
**
****
Protein
E
fold change
1 month
6 months

Figure S2. 6: VCP disease mutant mice accumulate Galectin-3.
(A) Genotyping of cVCP-R155C mice. Cortical tissues from 4-month-old cVCP-R155C and C57 are genotyped. cVCP-R155C mice are i.p. injected with Tamoxifen in 5 continuous day and harvested after one month for genotyping. **(B)** Representative immunoblot for VCP, p62, pan 14-3-3, BiP/GRP78, Lamp1, Galectin-3, HSP90, and ubiquitin (FK2) from cortical brain lysates of 4-month-old C57 (n=3), $VCP^{R155H/WT}$ (n=4) and cVCP-R155C (n=4) mice. In the case of cVCP-R155C mice, they are intraperitoneally injected with tamoxifen at 90 days of age and the brain was collected after one month. **(C)** Quantification of band intensities of VCP, p62, Bip/GRP78, LC3, FK2, Lamp1 and Gal3. **(D)** Representative immunoblot for VCP, p62, 14-3-3, Lamp1, Galectin-3, and ubiquitin (FK2) from cortical brain lysates of cVCP-R155C mice following one month or six months of i.p. tamoxifen treatment. **(E)** Quantitation of band intensities of VCP, p62, Lamp1, FK2 and Gal3 (n=3 for both groups, multiple t test, p=0.001516, n.s.= no significance).

2.4.5 VCP disease mutations enhance other proteopathic seeding

A subset of VCP patients have Parkinsonism and post-mortem evidence of αS pathology. However, most VCP patients have TDP-43 inclusions in the CNS and muscle[207–209]. To evaluate the role of VCP in the seeding of TDP-43, we utilized a HEK TDP-43 FRET biosensor that expresses both a Clover tagged-TDP-43 CTF and Ruby tagged-TDP-43 C-Terminal Fragment (CTF) (aa 262-414) (TDP biosensors). Exogenously applied preformed fibrillar TDP-43 (TDP-43 PFF 50nM) with Lipofectamine, but not monomeric TDP-43 (50nM), recruited the aggregation of soluble intracellular TDP-43 CTF after 48 hours. This resulted in Clover and Ruby positive aggregation as visualized by fluorescence (Figure 2.10A). Similar to the αS biosensor line, these TDP-43 PFF-dependent aggregates can also be detected by FRET under confocal microscopy (excitation=488nM and emission=605-625nM) (Figure 2.10A). Cells with FRET were quantified using a Clover vs. FRET plot with flow cytometry and selected against empty Lipofectamine treated control with no aggregates (black polygon gates in Figure 2.10B). FRET efficiency is calculated as a percentage $_{\text{(FRET positive cell)}}$* MFI $_{\text{(FRET positive cell)}}$[223]. The TDP-43 FRET signal is TDP-43 PFF-dependent since little signal was captured in monomer and empty Lipofectamine treated groups (Figure 2.10A-C). In addition, this FRET signal is sensitive and quantitative in a concentration-dependent manner (Figure 2.10D). To biochemically confirm that the FRET signal corresponded to TDP-43 CTF aggregation, we analyzed the cell lysates by fractionation immunoblot. An anti-GFP antibody was used to detect Clover- and Ruby-tagged

TDP-43 CTF (~40kDa). Only TDP-43 PFF treated TDP biosensor lines generated detergent-insoluble and high molecular weight TDP-43 CTFs (Figure 2.10E).

As with αS-biosensors, co-application of the VCP inhibitor NMS-873 (5uM) for four hours at the time of seed application (50 and 100nM) to TDP biosensors followed by washout significantly increased FRET as compared with DMSO treated control cells two days later (Figure 2.10F). This phenomenon is seed-dependent since NMS-873 failed to increase FRET in TDP-43 biosensors when TDP-43 monomer treatment was used. To explore the role of VCP disease mutations on TDP-43 seeding, we transfected TDP biosensors with myc tagged-VCP-WT or one of two different VCP disease mutations (R155H and A232E) for 24 hours, followed by TDP-43 PFF application. Cells expressing either VCP disease mutants exhibited an increase in FRET efficiency 48 hours later compared with VCP-WT control (Figure 2.10G & S2.7). Meanwhile, a recent studies demonstrated an VCP disease mutation in Alzheimer patients (D395G) increase tau seeding efficiency[140]. The similar effect was showed in tau seeding with mcherry tagged VCP- R95G, R155H and A232E (Figure S 2.8).

To further explore the effect of TDP-43 seeding in a more relevant system, we developed a TDP-43 seeding assay in primary hippocampal neurons. The addition of TDP-43 PFF (10nM) to HNs resulted in the appearance of phosphorylated TDP-43 Ser409/410 (pTDP) positive puncta in TDP-43 PFF treated group (Figure 2.11A; S2.9). Fractionation of lysates from HNs one or five days post-treatment with buffer, monomeric TDP-43 (10nM), or TDP-43 PFF (10nM) and subsequent immunoblot for TDP-43 revealed an increase in high molecular weight TDP-43 in

the RIPA insoluble fraction of TDP-43 PFF treated HNs (Figure 2.11B). The pTDP staining was not present immediately after the addition of TDP-43 PFF since no increase in pTDP above that seen prior to seed application. In contrast there was a significant increase in pTDP staining when TDP-43 PFF treated HNs were stained after 5 days (Figure 2.11C). Moreover, the amount of pTDP staining post-TDP-43 PFF treatment correlated with the concentration of TDP-43 PFF seed used. In addition, TDP-43 PFF induced cytosolic pTDP-43 puncta co-localized with TIA1 and p62/SQSTM1 similar to pathologic TDP-43 inclusions in patients (Figure 2.11E)[237]. As seen with VCP mutant expression in TDP-43 biosensors, treatment of primary HNs from $VCP^{WT/WT}$ and $VCP^{RH/WT}$ embryos with TDP-43 PFF (10 nM) revealed an increase pTDP-43 puncta in $VCP^{RH/WT}$ HNs compared with $VCP^{WT/WT}$ HNs (Figure 2.11F-G).

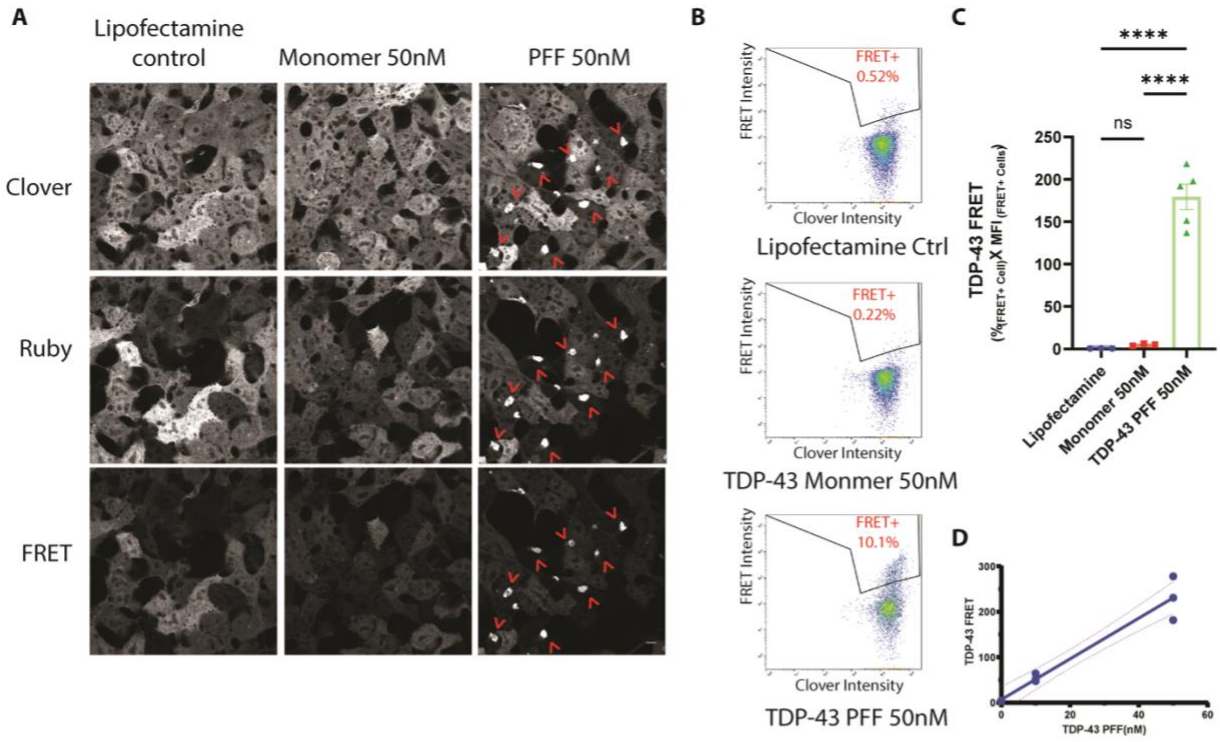
A
Lipofectamine control
Monomer 50nM
PFF 50nM
Clover
Ruby
FRET
B
FRET+ 0.52%
FRET Intensity
Clover Intensity
Lipofectamine Ctrl
FRET+ 0.22%
TDP-43 Monmer 50nM
FRET+ 10.1%
TDP-43 PFF 50nM
C
****
****
ns
TDP-43 FRET
(%FRET+ Cell) X MFI (FRET+ Cells)
Lipofectamine
Monomer 50nM
TDP-43 PFF 50nM
D
TDP-43 FRET
TDP-43 PFF(nM)

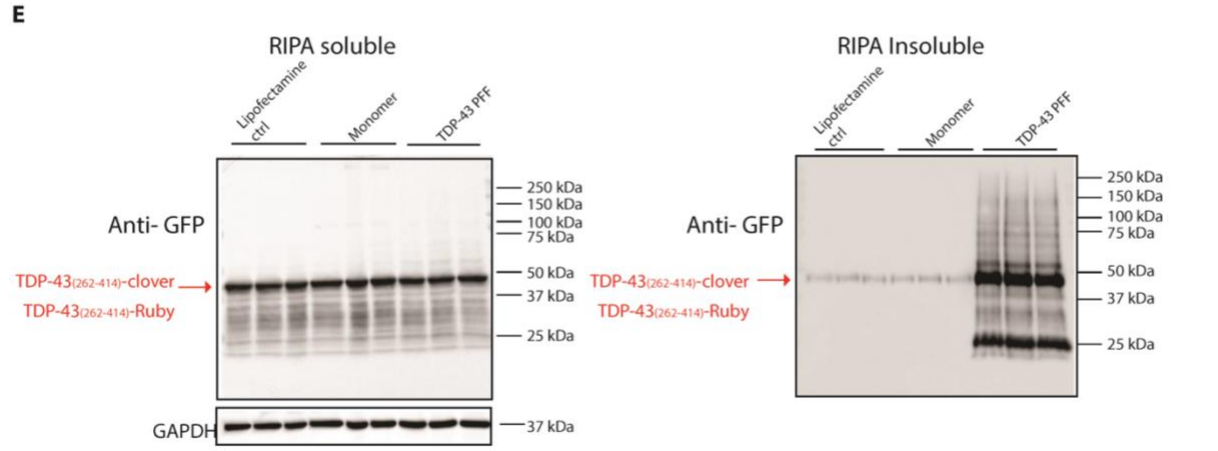
E
RIPA soluble
Lipofectamine ctrl
Monomer
TDP-43 PFF
Anti- GFP
TDP-43(262-414)-clover
TDP-43(262-414)-Ruby
250 kDa
150 kDa
100 kDa
75 kDa
50 kDa
37 kDa
25 kDa
GAPDH
37 kDa
RIPA Insoluble
Lipofectamine ctrl
Monomer
TDP-43 PFF
Anti- GFP
TDP-43(262-414)-clover
TDP-43(262-414)-Ruby
250 kDa
150 kDa
100 kDa
75 kDa
50 kDa
37 kDa
25 kDa

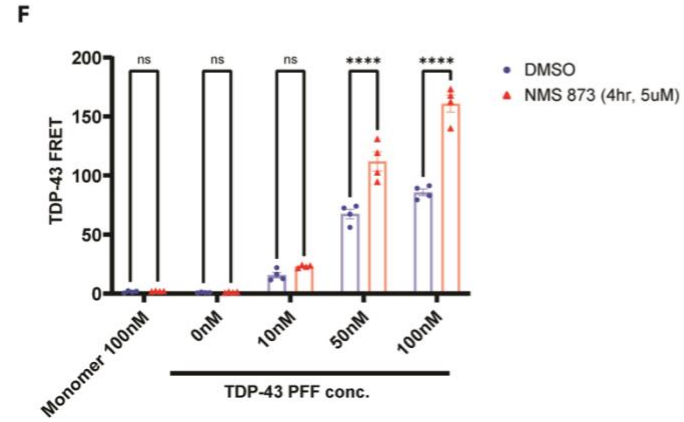
F
TDP-43 FRET
ns
ns
ns
****
****
DMSO
NMS 873 (4hr, 5uM)
Monomer 100nM
0nM
10nM
50nM
100nM
TDP-43 PFF conc.

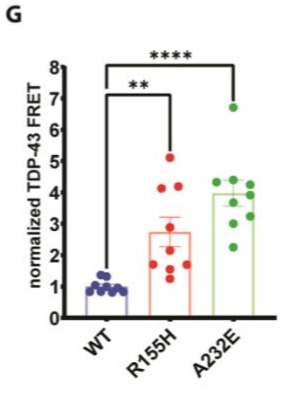
G
****
**
normalized TDP-43 FRET
WT
R155H
A232E

Figure 2. 10: VCP inhibition or VCP disease mutations enhance TDP-43 seeding in cells.
(A) Representative FRET confocal microscopy images of TDP-43 biosensor line (TDP-43 Clover/Ruby) treated with empty Lipofectamine (left, ctrl), 50nM TDP-43 monomer (middle) and 50nM TDP-43 PFF (right) after 48 hours. Scale bar= 10μm **(B)** Tracing of FRET signal via flow cytometry. FRET+ gate (Clover vs FRET) was drawn from empty Lipofectamine treated cells with no aggregation. **(C)** Quantitation of integrated FRET signal is measured by % FRET+ cell * Median Fluorescent Intensity (FRET+ cells). **** $p < 0.0001$,n.s., no significance by one-way ANOVA. Error bars are ± S.E.M. **(D)** Graph of FRET efficiency from TDP-43 biosensors were treated with TDP-43 PFF at different concentration and harvested after 48 hours (each dot represents triplicates in each condition). **(E)** Immunoblot for TDP-43 CTF (anti-GFP) from detergent soluble and insoluble lysates of TDP-43 biosensor cells treated with TDP-43 monomer or PFF and then harvested after 48 hours. Note that the RIPA insoluble fraction accumulated high molecular weight TDP-43 positive multimers. GAPDH is a loading control. **(F)** Normalized FRET from TDP-43 biosensors co-treated with TDP-43 monomer or PFF and NMS-873 (5μm) or DMSO vehicle control for four hours followed by washout. Cells were harvested at 48 hours after the treatment, and analyzed the same as 10C. FRET signal is normalized to DMSO 100nM PFF treated group. ($n>4$ repeats for each group. ****$p < 0.0001$;n.s. no significance, two-way ANOVA with Šidák correction) **(G)** TDP-43 biosensors were transfected with plasmids expressing VCP-WT, or one of two disease mutations (R155H and A232E) for 24 hours and then treated with TDP-43 PFF (10nM) for 48 hours. FRET efficiency is all normalized by VCP^{WT}. ($n=9$ repeats for each group. *$p < 0.05$, **$p < 0.01$; ****$p < 0.0001$; one-way ANOVA with Dunnett's correction)

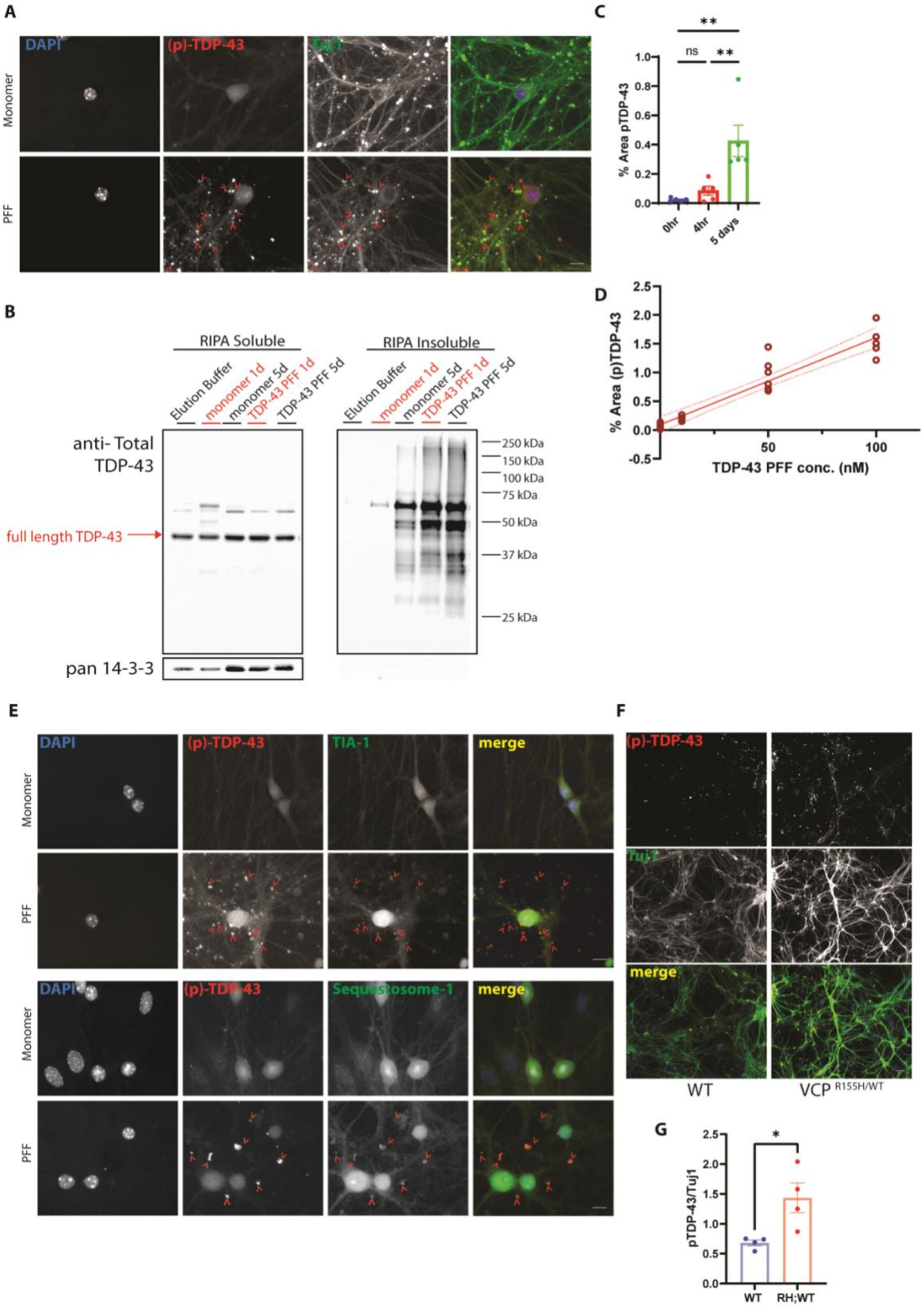
A
DAPI
(p)-TDP-43
Tuj1
Monomer
PFF
C
**
ns
**
% Area pTDP-43
1.0
0.8
0.6
0.4
0.2
0.0
0hr
4hr
5 days
B
RIPA Soluble
RIPA Insoluble
Elution Buffer
monomer 1d
monomer 5d
TDP-43 PFF 1d
TDP-43 PFF 5d
anti- Total TDP-43
full length TDP-43
pan 14-3-3
250 kDa
150 kDa
100 kDa
75 kDa
50 kDa
37 kDa
25 kDa
D
% Area (p)TDP-43
2.5
2.0
1.5
1.0
0.5
0.0
-0.5
50
100
TDP-43 PFF conc. (nM)
E
DAPI
(p)-TDP-43
TIA-1
merge
Monomer
PFF
DAPI
(p)-TDP-43
Sequestosome-1
merge
Monomer
PFF
F
(p)-TDP-43
Tuj1
merge
WT
VCP R155H/WT
G
*
pTDP-43/Tuj1
2.5
2.0
1.5
1.0
0.5
0.0
WT
RH;WT

Figure 2. 11: VCP disease mutations increase TDP-43 seeding in neurons.
(A) Immunofluorescent staining for pTDP-43 (red), Tuj1 (green), and nuclei (blue) in primary hippocampal neurons treated with 10nM TDP-43 monomer or 10nM TDP-43 PFF for 5 days. Scare bar= 10μm **(B)** Immunoblot for TDP-43 from detergent soluble and insoluble lysates of HNs treated with 10nM TDP-43 monomer or 10 nM PFF and then harvested after 1 or 5 days. Note that the RIPA insoluble fraction has high molecular weight TDP-43 positive multimers. 14-3-3 is a loading control. **(C)** Quantitation of area of pTDP-43 immunofluorescence in HNs after 4 hours or 5 days after 10nM TDP-43 PFF treatment. **(D)** Quantitation of area of pTDP-43 immunofluorescence treated with the indicated concentrations of TDP-43 PFF and harvested at 5 days. **(E)** Immunofluorescent images for pTDP-43, SQSTM1, and TIA-1 from neurons treated with TDP-43 monomer or TDP-43 PFF for five days. Scare bar= 10 μm. **(F)** Immunofluorescence for phospho-TDP-43 (red) and Tuj1 (green) in HNs from wild-type mice or mice carrying a VCP-R155H knockin allele (VCPR155H/WT) treated with TDP-43 for PFF for 5 days. (Scare bar= 20μm). **(G)** Quantitation of phospho-TDP/Tuj1 staining (Neurons coming from 3 and 4 independent cultures from WT and $VCP^{R155H/WT}$ embryos. Outlier is removed by ROUT method, Q=1%, followed by Student's t test. n=4, WT and $VCP^{R155H/WT}$ group respectively. *$p<0.05$.)

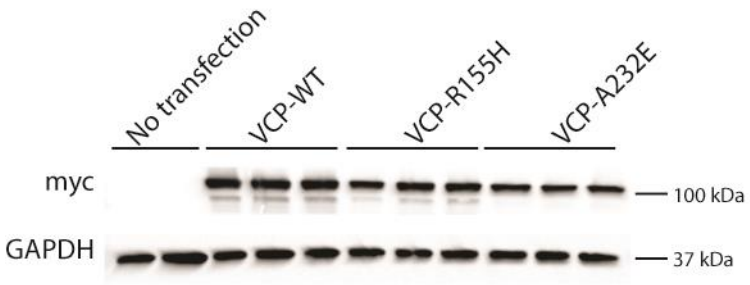

Figure S2. 7: Immunoblot of VCP overexpression in TDP biosensor line.
Immunoblot of lysates from TDP biosensor overexpressing empty vector, VCP-WT-myc, VCP-R155H-myc or VCP-A232E-myc using an anti-myc antibody or GAPDH as a loading control.

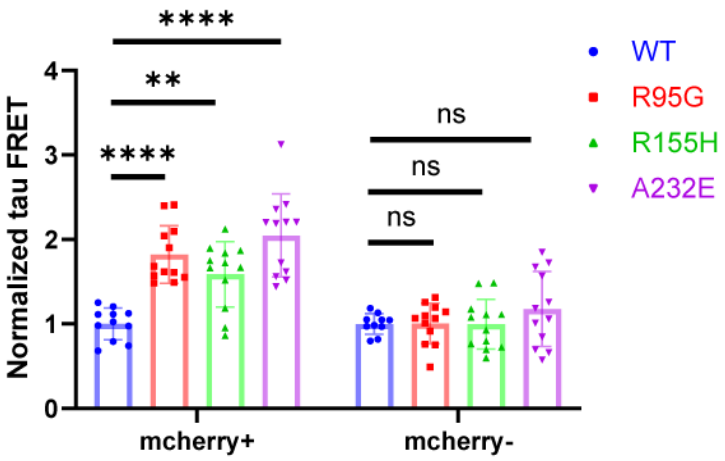

Figure S2. 8: VCP disease mutations elevate Tau seeding.
Tau biosensors were transfected with plasmids expressing VCP-WT, or one of three disease mutations (R95G, R155H and A232E) fused to a mcherry tag for 24 hours and then treated with tau PFF (2nM). FRET efficiency is quantified in mCherry+ and mCherry- cells separately and all normalized to VCP-WT (n=11 repeats for each group. ***p < 0.001; ****p < 0.0001; ns, no significance; two-way ANOVA with Dunnett's correction)

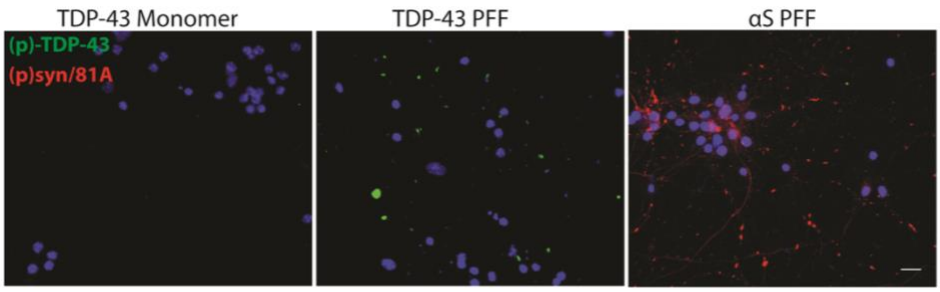

Figure S2. 9: pTDP-43 is TDP-43 PFF specific in hippocampal neurons.
10nM TDP4-43 monomer, TDP-43 PFF or αS PFF is added to DIV10 HNs as indicated. After 5 days, HNs are harvested and stained with both (p)TDP-43 and (p)syn(81A).

2.5 Discussion

Functional genomic screens utilizing CRISPR knockout approaches are an invaluable tool to elucidate proteins related to distinct cellular pathways. Here, we employed a CRISPR whole-genome KO screen to identify modifiers of αS seeding using an αS biosensor cell line. αS seeding spans many cellular processes that include endocytic uptake, vesicular trafficking, templated aggregate conversion, and protein degradation by both the proteasome and autophagy. Our screen identified proteins associated with vesicular trafficking between the ER, Golgi and endosome, and the cellular stress response. Notably, these pathways have been identified as modifiers of αS toxicity and stability in yeast and cell models[238,239]. Vesicular trafficking may have been particularly enriched since our screen and the αS biosensor cell line required αS PFFs to be applied with the carrier, Lipofectamine, as a means of facilitating endocytic uptake.

Our further studies expanded upon the role of VCP in αS seeding. VCP is a multifunctional protein necessary for many ubiquitin-dependent processes, including protein degradation, vesicle trafficking, cell division, and organelle clearance[206]. Recently, we identified a role for VCP in recognition of permeabilized late endosomes and their subsequent lysophagic degradation[133]. Endocytosed proteopathic seeds such as αS and Tau enter the cytoplasm, where templated aggregate conversion of soluble monomer occurs by damaging the endosomal membrane[133,240,241]. The fate of permeabilized late endosomes depends upon the degree of membrane damage. For example, some damaged endosomes are rapidly repaired by ESCRT proteins[242]. In contrast, endosomes damaged beyond repair are tagged by intracellular galectins

such as galectin-3[133]. Galectin positive endosomes recruit the ubiquitin ligase, Trim16, which ubiquitinates endosomal membrane proteins[243]. Notably, only lysine-63 linked ubiquitin chains on the endosome surface are targeted for lysophagy[133]. VCP, in association with UBXD1, PLAA, and the deubiquitinase YOD1 recognize and cleave lysine-48 linked ubiquitin chains on damaged late endosomes, leaving lysine-63 linked ubiquitin chains allowing lysophagic degradation[133]. Loss of VCP or VCP disease mutant expression leads to the persistence of galectin-3 positive damaged late endosomes in cells, mouse models, and patient tissue[133,212].

A previous genomic screen using a Tau biosensor line identified several components of the ESCRT machinery as suppressors of Tau seeding[244]. Our screen identified VCP and Trim16 as suppressors of αS seeding. Further experiments found that knockdown of the VCP adaptor, UBXD1 that is necessary for lysophagy, and VCP disease mutations defective in lysophagy also increase αS seeding. One distinction between these two screens is the use of Lipofectamine to facilitate entry into the endocytic pathway of αS. Lipofectamine is known to damage endosomal membranes and may allow αS to generate larger "holes" that are not repaired by ESCRTS[242]. However, VCP's role in seeding was not exclusively Lipofectamine dependent since VCP inhibition, knockdown, or VCP mutant expression facilitated "naked" αS PFF seeding in HNs and *in vivo*.

VCP disease mutations cause multisystem proteinopathy (MSP)[245]. MSP is a late-onset degenerative disorder with varied phenotypes and pathologies. These include inclusion body myopathy, ALS, and FTD[213]. While the predominant aggregate pathology in the brain is reported

to be TDP-43, several studies support the identification of αS positive aggregates in the brain[207,208,246]. Indeed, ~5% of MSP patients have coincident Parkinsonism[214]. Notably, two recently identified families with a VCP-D395G mutation were found to have distinctive tau pathology leading to the description of a vacuolar tauopathy in the CNS[140]. Aggregate pathology in the skeletal muscle can be varied and include TDP-43, hnRNPA1/A2B1, SQSTM1, β-amyloid, desmin, and VCP[74,247,248] Weakness typically precedes the onset of neurodegenerative features such as dementia by ten years suggesting that pathology begins in peripheral tissue such as skeletal muscle[214]. Whether protein aggregates from skeletal can seed the aggregate process in motor neurons or cortical neurons, remain speculative. It is noteworthy that mice carrying the D395G missense mutation in VCP had an increase in Tau seeding, supporting that VCP disease mutations can facilitate the propagation of different aggregate species[214].

TDP-43 inclusions are a prominent feature in affected VCP disease tissue [74,208]. Our data further support that TDP-43 PFF similar to αS-PFF can seed pathologic TDP-43 inclusions in HNs. TDP-43 seeding in HNs recapitulates several features of TDP-43 pathology such as phosphorylation, cytoplasmic redistribution, and co-localization with stress granule markers and SQSTM1[249]. VCP disease mutation expression increases seeding associated pathologic TDP-43 inclusions as measured by increased phospho-TDP-43 immunostaining in HNs. This process is TDP-43 PFF dependent since monomeric TDP-43 fails to have the same effect. Whether the accumulation of TDP-43 inclusions is also affected by an additional role for VCP in stress granule clearance remains to be determined[158].

Halting or mitigating the pathologic spread of protein inclusions in neurodegenerative disorders such as Parkinson's disease, ALS and fronto-temporal dementia has potential therapeutic implications. Our study identifies a VCP dependent endocytic pathway that suppresses the proteopathic spread of αS *in vivo* and TDP-43 *in vitro*. Future studies aimed at defining the molecular components and mechanism related to VCP associated aggregate seeding may lead to therapies targeting multiple proteinopathies and degenerative diseases.

Chapter 3 Discussion and future direction

3.1 protective role of VCP in protopathic seeding

NDDs become more predominant as we step into an aging society. The early symptoms of NDDs are confusing with normal aging. Therefore, blocking the disease progression is an attractive alternative. Proteopathic inclusion is a hallmark of NDDs, and its spreading can correspond to neuronal loss and function loss. Because of that, it is important to understand the mechanism of proteopathic seeding.

In this dissertation, we demonstrated the role of VCP in proteopathic seeding. In intracellular αS seeding, VCP inhibition or knockdown or VCP disease mutations can enhance seeding efficiency in αS biosensors and hippocampal neurons. This effect is independent of VCP's established roles in ER stress, autophagy, the ubiquitin-proteasome system, and αS fibril uptake or expression. Previous studies suggested that αS fibril is mainly taken up by the endosome and merges into the lysosome for degradation. However, about half αS fibril integrated cannot be cleaned after 24 hours[250]. This implied that the classical lysosomal pathway is insufficient for αS fibril degradation. Jiang et al., and Flavin et al., found that the fibril but not oligomer or monomer form of αS can permeabilize the endolysosome membrane, marked by galectin protein[240,251]. Here, we demonstrated that VCP inhibition could aggravate the endolysosome integrity. Our lab previously characterized VCP on lyosophagic degradation of permeabilized late endosomes. In this work, enhancing lysosomal membrane permeability with

the small molecule, LLoMe, or inhibiting VCP dependent-lysosome surveillance with UBXD1 knockdown or expression of VCP disease mutations also increases αS seeding.

We propose VCP mediated αS seeding via lysopahgy, a conserved mechanism when cells are challenged by large molecules or pathogen invasion. Upon αS fibril uptake, αS fibril will accumulate at the endolysosome vesicle. Some αS fibrils will be degraded via lysosome. At the same time, some might damage the endolysosome and escape to the cytoplasm, where the αS fibril will recruit αS monomers and template new fibril formation. This seeding process is deleterious to the cell. However, the damaged endolysosome can be labeled by galectin protein and recruit VCP and its cofactors UBXD1, which modulate damaged endolysosome to autophagy degradation. In contrast, VCP mutations, with reduced binding to UBXD1, showed impaired lysosphagy, failed to clean up αS fibril embedding damaged endolysosome, and, in turn, have higher seeding efficiency.

This study also suggested a unified model of proteopathic seeding mediated by VCP. Although the distinct inclusion is a pathological hallmark for NDDs, emerging evidence suggests the interconnection between proteopathic seeding. For example, TDP-43 inclusions are identified in a wide range of NDDs[3] and myopathy[252]; APOE4 has been a genetic risk factor for Aβ pathology (AD and DLB) for a long time. However, recent studies by Davis et al., and Zhao et al., show that APOE4 has a detrimental effect on synucleinopathy and motor performance independent of Aβ and tau pathology[253,254]. VCP mutations can also cause different types of

NDDs, containing TDP-43, αS, or tau inclusions exclusively. This evidence indicates a shared pathway in proteopathic seeding. Our works demonstrate that VCP mutations similarly affect αS, tau, and TDP-43 seeding, further supporting it. Both tau and TDP-43 fibril can also be taken up by endocytosis. Tau fibril can also induce endolysosome damage, facilitating tau seeding in vitro[241]. This VCP mediated lysophagy might share in common for proteopathic seeding in general. To test this hypothesis, we can conduct a genomic-wide screen or a targeted screen on the seeding of other proteopathic proteins like tau and TDP-43for lysophagy components.

Besides, VCP mutations also impair mitochondria function and morphology[152,153]. VCP-UBXD1 responds to mitophagy when mitochondria are disordered. Mitochondria dysfunction is strongly associated with Parkinson's disease, and αS PFF is preferentially bound to the mitochondrial membrane and destroys its respiration function[255]. Although no current evidence supports mitochondria dysfunction towards seeding, we cannot exclude other mechanisms that might take place simultaneously.

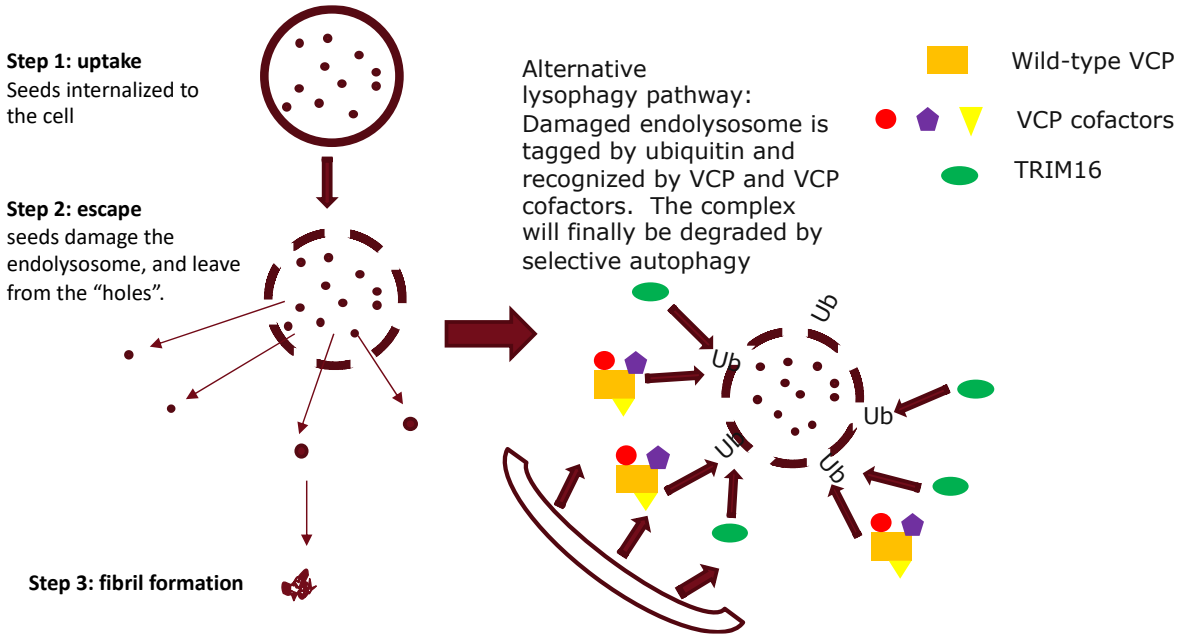

Figure 3. 1: a proposed model of VCP roles on seeding

3.2 New modifiers and pathways in α-synuclein seeding

In this dissertation, we used CRISPR KO screening to identify gene modifiers for αS seeding. Even though some screens had been done on α-synuclein, we are the first group to look at αS seeding. Our subsequent work focus on VCP, one of the genes cause of MSP1. However, there are other genes and pathways that might be important. First, to further support our hypothesis, we can test other lysophagy genes in our list, such as TRIM16. TRIM16 might have a dual function in seeding. On the one hand, TRIM16 binds to galectin-3 upon damaged endolysosome, adds autophagy targeted tag K63, and promotes lysophagy by interacting with autophagy factors ULK1, beclin-1, and ATG16L[243]. On the other hand, TRIM16 can interact with NRF2 and SQSTM1 and assist aggregates degradation via autophagy[256]. Furthermore, a recent study that used lysosome immunoprecipitation and proximity assays followed by mass spectrometry identified protein possibly participating in lysophagy after LLOMe treatment[257]. Seven genes in our αS seeding hits (ATP6V1A, ATP6V1G1, NAPA, UBE2C, YKT6, LAMTOR5, and NPC2) might also involve in lysophagy and exhibit a similar effect as VCP.

Of note, vesicle and membrane trafficking pathway is enriched in αS induced toxicity screens on yeast[172,173]. Particularly, in a *C elegans* screening, a homolog of vesicle trafficking genes VPS41 and SEC22 was identified, modifying αS aggregation in the worm and protecting DA neurons loss. In our screen, vesicle transport and trafficking are enriched. For example, VPS51 and another hit VPS52 are components of GARP/EARP complexes, which play a role in

endosome cargo sorting and retrograde transport to trans-Golgi. Loss-of-function mutations of VPS51 can lead to a rare neurological disorder[258]. We can further test the effect of those trafficking genes in our screen on seeding by traditional neuronal culture or on propagation via microfluidic devices. Beyond that, we validated hits ATP6V0C, KDELR1, LAMTOR5, and SEC61B suggested novel pathways, including ER stress response, might contribute to αS seeding, which has not been documented.

Furthermore, 35 out of 154 hits from the primary CRISPR KO screen are druggable at different degrees, leading to > 100 different drug candidates. For example, Acetaminophen, a drug target to co-chaperone PTGES3, decreases αS oligomerization and alleviates dopaminergic neurons loss in worm PD models[259,260]. Insofar, the effect of those druggable hits should be validated and followed by a drug screen to find a therapeutic target for αS.

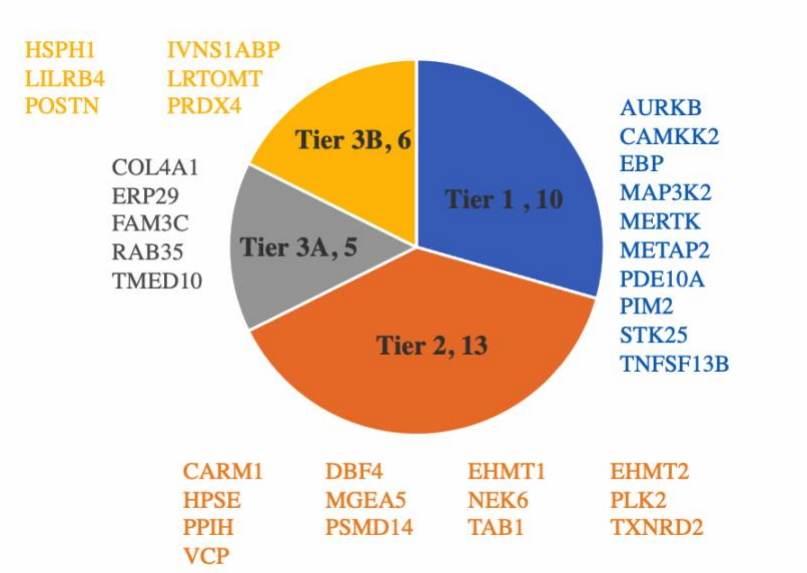

Figure 3. 2: identified druggable genes from primary hits.

3.3 TDP-43 seeding in ALS-FTD

In this dissertation, we illustrated two TDP-43 seeding models *in vitro*. Compared with the existing TDP-43 model, The TDP-43 biosensor is more sensitive, quantitively, and seeding specific. Our data further support that similar to αS-PFF, TDP-43 PFF can seed pathologic TDP-43 inclusions in HNs. TDP-43 seeding in HNs phenocopies several features of TDP-43 pathology such as hyperphosphorylation, cytoplasmic redistribution, and co-localization with stress granule markers and SQSTM1[249]. Lastly, this work demonstrates the effect of VCP on TDP-43 seeding. VCP disease mutation expression increases seeding associated pathologic TDP-43 inclusions in both TDP-43 biosensor and HNs.

A future application is to test the TDP-43 seeding capacity of variants in TDP-43 positive FTD-ALS, including GRN, TMEM106B, CHMP2B, UBQLN2, OPTN, MATR3, hnRNPA1/A2b1, TBK1, ATXN2, UBQLN2, SQSTM1, etc. Many gene variants are linked with TDP-43 inclusion or solubility, but their effect on TDP-43 seeding has not been characterized. Double knockdown of CHMP2A and CHMP2B showed increasing tau seeding activities[261]. OPTN and SQSTM1 are both autophagy receptors[262]; UBQLN2 promotes proteasome degradation of polyubiquitinated proteins[262] and recently found to play a role in autophagy as well[263]. The seeding essay can help us to understand the mechanism of TDP-43 pathology in those patients.

Furthermore, TDP biosensor lines may apply to diagnosis. This line is at least 250 more sensitive than commercial TDP-43 ELISA kits. TDP-43 can be secreted extracellularly via exosome[47,264]. The plasma TDP-43 level is significantly higher in FTD-TDP groups than that in AD and healthy control. The finding in CSF is ambiguous. Although one group showed a comparable level of TDP-43 of FTD-TDP, FTD-tau in CSF[265], most studies suggested the CSF TDP-43 level raised in ALS and FTD-TDP patients compared with either healthy control or TDP-43 negative NDDs[266]. TDP-43 level in CSF is also correlated with ALS patients' survival time[267]. This discrepancy may be due to the detection methods and different sub-types of patients. Moreover, incubating ALS-FTD CSF with cells induced cytoplasmic TDP-43 aggregates after 21 days, suggesting the existence of TDP-43 seeds in those fluids[47]. Hence, the seeding capable TDP-43 may be used as a diagnostic biomarker or prognosis for TDP-43 pathologies.

In addition, those TDP-43 seeding platform allows us to perform other assays, including CRISPR genomic widescreen on TDP-43 seeding, microRNA arrays, or bulk RNA sequencing. TDP-43 contains two RRMs and selectively regulate more than hundreds of mRNA and microRNA level. Particularly, selective miRNAs are dysregulated in ALS patients with TDP-43 inclusion[268,269]. We found that rescue mir-34a, a spinal cord neuronal enriched microRNA that decreased in ALS patients, in the TDP-43 biosensor line significantly decreased seeding

efficiency. Given the reversible effect, small size, and abundant miRNA targets, understanding the TDP-43 seeding modifiers will help us discover new clinical targets for TDP-43 pathology.

3.4 peripheral seeding of TDP-43

MSP can affect multiple tissues, including muscle, bone, and nervous system. In VCP patients, myopathy is usually the first call, which onset precedes FTD-ALS (it happens) about 13 years on average, even though in some cases FTD-ALS can occur independently[270]. This clinical data agrees with VCP mouse models, including ours, in which muscles developed MSP-like phenotypes and accumulated insoluble TDP-43 prior to brain dysfunction[236]. Additionally, protein aggregate is a common feature of multiple myopathies, and some proteins like desmin own prion-like properties. Muscles, excised in our daily life, are more exposed and susceptible to injury and environmental stress. A recent study found TDP-43 accumulated as amyloid in myo-granule when muscle regenerates after injury[271]. Additionally, this aggregation is more frequent in muscles with VCP mutation[272]. One future direction is to test if TDP-43 inclusion from patients' muscle seeding is capable of seeding. If so, are they behave the same as the one in CNS?

Finally, whether TDP-43 can spread within the muscle or from muscle to the brain has not been proven in cell or mouse models. Although no evidence showed it happened with TDP-43, peripheral seeding is observed in other proteopathic seeds. The prions can spread from different

peripheral routes to the brains in prion diseases[273]. Intraperitoneal administration of Aβ-rich brain extracts to young APP mice can induce β-amyloidosis in the cortices, although less efficient and more delayed than direction intracerebral injection[274]. Although αS is most abundant in the brain, αS is found in the plasma and CSF of patients and healthy control. Several clinical studies found αS inclusion in peripheral tissues such as stomach, colon, and rectum in PD patient[275], and αS fibril can retrogradely transport via the vagal nerve to the dorsal motor nucleus in the brainstem[276]. Either intramuscular (from hind-leg muscle or gut muscle wall), intravenous or intraperitoneal injection of αS fibril could induce phosphorylated αS aggregates in the brains, bring to PD like symptoms, such as loss of dopaminergic neurons, motor, and cognitive deficits, even though those seedings are slower and less efficient than intracerebral injection[277–279].

To test the TDP-43 peripheral seeding hypothesis, we can inject seeding capable TDP-43 fibril or brain lysate into the skeletal muscles at one leg, harvest both muscle, spinal cord, and brain at different time points, and test the transmission and seeding event retrogradely in TDP-43 transgenic mice.

References

1. Gooch CL, Pracht E, Borenstein AR. The burden of neurological disease in the United States: A summary report and call to action. *Ann Neurol*. 2017;81(4):479-484. doi:10.1002/ana.24897

2. Bräuer S, Zimyanin V, Hermann A. Prion-like properties of disease-relevant proteins in amyotrophic lateral sclerosis. *J Neural Transm*. 2018;125(4):591-613. doi:10.1007/s00702-018-1851-y

3. Kawakami I, Arai T, Hasegawa M. The basis of clinicopathological heterogeneity in TDP-43 proteinopathy. *Acta Neuropathol (Berl)*. 2019;138(5):751-770. doi:10.1007/s00401-019-02077-x

4. Brettschneider J, Tredici KD, Lee VMY, Trojanowski JQ. Spreading of pathology in neurodegenerative diseases: a focus on human studies. *Nat Rev Neurosci*. 2015;16(2):109-120. doi:10.1038/nrn3887

5. Li JY, Englund E, Holton JL, et al. Lewy bodies in grafted neurons in subjects with Parkinson's disease suggest host-to-graft disease propagation. *Nat Med*. 2008;14(5):501-503. doi:10.1038/nm1746

6. Hasegawa M, Nonaka T, Masuda-Suzukake M. Prion-like mechanisms and potential therapeutic targets in neurodegenerative disorders. *Pharmacol Ther*. 2017;172:22-33. doi:10.1016/j.pharmthera.2016.11.010

7. Nonaka T, Masuda-Suzukake M, Arai T, et al. Prion-like Properties of Pathological TDP-43 Aggregates from Diseased Brains. *Cell Rep*. 2013;4(1):124-134. doi:10.1016/j.celrep.2013.06.007

8. Cremades N, Cohen SIA, Deas E, et al. Direct observation of the interconversion of normal and toxic forms of α-synuclein. *Cell*. 2012;149(5):1048-1059. doi:10.1016/j.cell.2012.03.037

9. Roberts HL, Brown DR. Seeking a mechanism for the toxicity of oligomeric α-synuclein. *Biomolecules*. 2015;5(2):282-305. doi:10.3390/biom5020282

10. Cowan CM, Mudher A. Are tau aggregates toxic or protective in tauopathies? *Front Neurol*. 2013;4 AUG(August):1-13. doi:10.3389/fneur.2013.00114

11. Goedert M, Masuda-Suzukake M, Falcon B. Like prions: The propagation of aggregated tau and α-synuclein in neurodegeneration. *Brain*. 2017;140(2):266-278. doi:10.1093/brain/aww230

12. Arnsten AFT, Datta D, Del Tredici K, Braak H. Hypothesis: Tau pathology is an initiating factor in sporadic Alzheimer's disease. *Alzheimers Dement*. 2021;17(1):115-124. doi:10.1002/alz.12192

13. Taguchi YV, Gorenberg EL, Nagy M, et al. Hsp110 mitigates α-synuclein pathology in vivo. *Proc Natl Acad Sci*. 2019;116(48):24310-24316. doi:10.1073/pnas.1903268116

14. Mao X, Ou MT, Karuppagounder SS, et al. Pathological -synuclein transmission initiated by binding lymphocyte-activation gene 3. *Science*. 2016;353(6307):aah3374-aah3374. doi:10.1126/science.aah3374

15. Guzman-Martinez L, Maccioni RB, Andrade V, Navarrete LP, Pastor MG, Ramos-Escobar N. Neuroinflammation as a Common Feature of Neurodegenerative Disorders. *Front Pharmacol*. 2019;10. Accessed January 23, 2022. https://www.frontiersin.org/article/10.3389/fphar.2019.01008

16. Islam MdT. Oxidative stress and mitochondrial dysfunction-linked neurodegenerative disorders. *Neurol Res*. 2017;39(1):73-82. doi:10.1080/01616412.2016.1251711

17. Laferrière F, Maniecka Z, Pérez-Berlanga M, et al. TDP-43 extracted from frontotemporal lobar degeneration subject brains displays distinct aggregate assemblies and neurotoxic effects reflecting disease progression rates. *Nat Neurosci*. 2019;22(1):65-77. doi:10.1038/s41593-018-0294-y

18. Mahul-Mellier AL, Burtscher J, Maharjan N, et al. The process of Lewy body formation, rather than simply α-synuclein fibrillization, is one of the major drivers of neurodegeneration. *Proc Natl Acad Sci*. 2020;117(9):4971-4982. doi:10.1073/pnas.1913904117

19. Mavroeidi P, Xilouri M. Neurons and Glia Interplay in α-Synucleinopathies. *Int J Mol Sci*. 2021;22(9):4994. doi:10.3390/ijms22094994

20. Cabin DE, Shimazu K, Murphy D, et al. Synaptic Vesicle Depletion Correlates with Attenuated Synaptic Responses to Prolonged Repetitive Stimulation in Mice Lacking. :11.

21. Villar-Piqué A, Lopes da Fonseca T, Outeiro TF. Structure, function and toxicity of alpha-synuclein: the Bermuda triangle in synucleinopathies. *J Neurochem*. 2016;139:240-255. doi:10.1111/jnc.13249

22. Yamasaki TR, Holmes BB, Furman JL, et al. Parkinson's disease and multiple system atrophy have distinct α-synuclein seed characteristics. *J Biol Chem*. 2019;294(3):1045-1058. doi:10.1074/jbc.RA118.004471

23. Volpicelli-Daley LA, Luk KC, Patel TP, et al. Exogenous α-Synuclein Fibrils Induce Lewy Body Pathology Leading to Synaptic Dysfunction and Neuron Death. *Neuron*. 2011;72(1):57-71. doi:10.1016/j.neuron.2011.08.033

24. Peng C, Gathagan RJ, Covell DJ, et al. Cellular Milieu Imparts Distinct Pathological α-Synuclein Strains in α-Synucleinopathies. *Nature*. 2018;557(7706):558-563. doi:10.1038/s41586-018-0104-4

25. Volpicelli-Daley LA, Luk KC, Patel TP, et al. Exogenous α-Synuclein Fibrils Induce Lewy Body Pathology Leading to Synaptic Dysfunction and Neuron Death. *Neuron*. 2011;72(1):57-71. doi:10.1016/j.neuron.2011.08.033

26. Rey NL, George S, Steiner JA, et al. Spread of aggregates after olfactory bulb injection of α-synuclein fibrils is associated with early neuronal loss and is reduced long term. *Acta Neuropathol (Berl)*. 2018;135(1):65-83. doi:10.1007/s00401-017-1792-9

27. Luk KC, Kehm VM, Zhang B, O'Brien P, Trojanowski JQ, Lee VMY. Intracerebral inoculation of pathological α-synuclein initiates a rapidly progressive neurodegenerative α-synucleinopathy in mice. *J Exp Med*. 2012;209(5):975-986. doi:10.1084/jem.20112457

28. Luk KC, Kehm V, Carroll J, et al. Pathological α-Synuclein Transmission Initiates Parkinson-like Neurodegeneration in Nontransgenic Mice. *Science*. 2012;338(6109):949-953. doi:10.1126/science.1227157

29. Recasens A, Ulusoy A, Kahle PJ, Di Monte DA, Dehay B. In vivo models of alpha-synuclein transmission and propagation. *Cell Tissue Res*. 2018;373(1):183-193. doi:10.1007/s00441-017-2730-9

30. Lee HJ, Suk JE, Bae EJ, Lee JH, Paik SR, Lee SJ. Assembly-dependent endocytosis and clearance of extracellular a-synuclein. *Int J Biochem Cell Biol*. 2008;40(9):1835-1849. doi:10.1016/j.biocel.2008.01.017

31. Stopschinski BE, Holmes BB, Miller GM, et al. Specific glycosaminoglycan chain length and sulfation patterns are required for cell uptake of tau versus α-synuclein and β-amyloid aggregates. *J Biol Chem*. 2018;293(27):10826-10840. doi:10.1074/jbc.RA117.000378

32. Mao X, Ou MT, Karuppagounder SS, et al. Pathological α-synuclein transmission initiated by binding lymphocyte-activation gene 3. *Science*. 2016;353(6307):aah3374. doi:10.1126/science.aah3374

33. Lee HJ, Suk JE, Bae EJ, Lee JH, Paik SR, Lee SJ. Assembly-dependent endocytosis and clearance of extracellular a-synuclein. *Int J Biochem Cell Biol*. 2008;40(9):1835-1849.

doi:10.1016/j.biocel.2008.01.017

34. Karpowicz RJ, Haney CM, Mihaila TS, Sandler RM, Petersson EJ, Lee VMY. Selective imaging of internalized proteopathic α-synuclein seeds in primary neurons reveals mechanistic insight into transmission of synucleinopathies. *J Biol Chem*. 2017;292(32):13482-13497. doi:10.1074/jbc.M117.780296

35. Jinn S, Drolet RE, Cramer PE, et al. TMEM175 deficiency impairs lysosomal and mitochondrial function and increases α-synuclein aggregation. *Proc Natl Acad Sci*. 2017;114(9):2389-2394. doi:10.1073/pnas.1616332114

36. Jiang P, Gan M, Yen SH, McLean PJ, Dickson DW. Impaired endo-lysosomal membrane integrity accelerates the seeding progression of α-synuclein aggregates. *Sci Rep*. 2017;7(1):7690. doi:10.1038/s41598-017-08149-w

37. Tsujimura A, Taguchi K, Watanabe Y, et al. Lysosomal enzyme cathepsin B enhances the aggregate forming activity of exogenous α-synuclein fibrils. *Neurobiol Dis*. 2015;73:244-253. doi:10.1016/j.nbd.2014.10.011

38. Ono K, Tsuji M, Yamasaki TR, Pasinetti GM. Anti-aggregation Effects of Phenolic Compounds on α-synuclein. *Molecules*. 2020;25(10):2444. doi:10.3390/molecules25102444

39. Nahass GR, Sun Y, Xu Y, et al. Brazilin Removes Toxic Alpha-Synuclein and Seeding Competent Assemblies from Parkinson Brain by Altering Conformational Equilibrium. *J Mol Biol*. 2021;433(8):166878. doi:10.1016/j.jmb.2021.166878

40. Deshayes N, Arkan S, Hansen C. The Molecular Chaperone DNAJB6, but Not DNAJB1, Suppresses the Seeded Aggregation of Alpha-Synuclein in Cells. *Int J Mol Sci*. 2019;20(18):4495. doi:10.3390/ijms20184495

41. Gao X, Carroni M, Nussbaum-Krammer C, et al. Human Hsp70 Disaggregase Reverses Parkinson's-Linked α-Synuclein Amyloid Fibrils. *Mol Cell*. 2015;59(5):781-793. doi:10.1016/j.molcel.2015.07.012

42. Ulusoy A, Musgrove RE, Rusconi R, et al. Neuron-to-neuron α-synuclein propagation in vivo is independent of neuronal injury. *Acta Neuropathol Commun*. 2015;3(1):13. doi:10.1186/s40478-015-0198-y

43. Grozdanov V, Danzer KM. Release and uptake of pathologic alpha-synuclein. *Cell Tissue Res*. 2018;373(1):175-182. doi:10.1007/s00441-017-2775-9

44. Danzer KM, Kranich LR, Ruf WP, et al. Exosomal cell-to-cell transmission of alpha

synuclein oligomers. *Mol Neurodegener*. 2012;7(1):42. doi:10.1186/1750-1326-7-42

45. Ngolab J, Trinh I, Rockenstein E, et al. Brain-derived exosomes from dementia with Lewy bodies propagate α-synuclein pathology. *Acta Neuropathol Commun*. 2017;5(1):46. doi:10.1186/s40478-017-0445-5

46. Abounit S, Bousset L, Loria F, et al. Tunneling nanotubes spread fibrillar α-synuclein by intercellular trafficking of lysosomes. *EMBO J*. 2016;35(19):2120-2138. doi:10.15252/embj.201593411

47. Ding X, Ma M, Teng J, et al. Exposure to ALS-FTD-CSF generates TDP-43 aggregates in glioblastoma cells through exosomes and TNTs-like structure. *Oncotarget*. 2015;6(27):24178-24191. doi:10.18632/oncotarget.4680

48. Zhao HT, John N, Delic V, et al. LRRK2 Antisense Oligonucleotides Ameliorate α-Synuclein Inclusion Formation in a Parkinson's Disease Mouse Model. *Mol Ther - Nucleic Acids*. 2017;8:508-519. doi:10.1016/j.omtn.2017.08.002

49. Bieri G, Brahic M, Bousset L, et al. LRRK2 modifies α-syn pathology and spread in mouse models and human neurons. *Acta Neuropathol (Berl)*. 2019;137(6):961-980. doi:10.1007/s00401-019-01995-0

50. Davis AA, Inman CE, Wargel ZM, et al. *APOE* genotype regulates pathology and disease progression in synucleinopathy. *Sci Transl Med*. 2020;12(529):eaay3069. doi:10.1126/scitranslmed.aay3069

51. Madureira M, Connor-Robson N, Wade-Martins R. "LRRK2: Autophagy and Lysosomal Activity." *Front Neurosci*. 2020;14. Accessed January 23, 2022. https://www.frontiersin.org/article/10.3389/fnins.2020.00498

52. Pankratz N, Byder L, Halter C, et al. Presence of an APOE4 allele results in significantly earlier onset of Parkinson's disease and a higher risk with dementia. *Mov Disord*. 2006;21(1):45-49. doi:10.1002/mds.20663

53. Prasad A, Bharathi V, Sivalingam V, Girdhar A, Patel BK. Molecular Mechanisms of TDP-43 Misfolding and Pathology in Amyotrophic Lateral Sclerosis. *Front Mol Neurosci*. 2019;12:25. doi:10.3389/fnmol.2019.00025

54. Porta S, Xu Y, Lehr T, et al. Distinct brain-derived TDP-43 strains from FTLD-TDP subtypes induce diverse morphological TDP-43 aggregates and spreading patterns in vitro and in vivo. *Neuropathol Appl Neurobiol*. 2021;47(7):1033-1049. doi:10.1111/nan.12732

55. Iguchi Y, Katsuno M, Niwa J ichi, et al. TDP-43 Depletion Induces Neuronal Cell Damage through Dysregulation of Rho Family GTPases. *J Biol Chem*. 2009;284(33):22059-22066. doi:10.1074/jbc.M109.012195

56. Kraemer BC, Schuck T, Wheeler JM, et al. Loss of murine TDP-43 disrupts motor function and plays an essential role in embryogenesis. *Acta Neuropathol (Berl)*. 2010;119(4):409-419. doi:10.1007/s00401-010-0659-0

57. Shimonaka S, Nonaka T, Suzuki G, Hisanaga S ichi, Hasegawa M. Templated Aggregation of TAR DNA-binding Protein of 43 kDa (TDP-43) by Seeding with TDP-43 Peptide Fibrils. *J Biol Chem*. 2016;291(17):8896-8907. doi:10.1074/jbc.M115.713552

58. Prasad A, Bharathi V, Sivalingam V, Girdhar A, Patel BK. Molecular Mechanisms of TDP-43 Misfolding and Pathology in Amyotrophic Lateral Sclerosis. *Front Mol Neurosci*. 2019;12:25. doi:10.3389/fnmol.2019.00025

59. Guo W, Chen Y, Zhou X, et al. An ALS-associated mutation affecting TDP-43 enhances protein aggregation, fibril formation and neurotoxicity. *Nat Struct Mol Biol*. 2011;18(7):822-830. doi:10.1038/nsmb.2053

60. Johnson BS, Snead D, Lee JJ, McCaffery JM, Shorter J, Gitler AD. TDP-43 Is Intrinsically Aggregation-prone, and Amyotrophic Lateral Sclerosis-linked Mutations Accelerate Aggregation and Increase Toxicity. *J Biol Chem*. 2009;284(30):20329-20339. doi:10.1074/jbc.M109.010264

61. Fang YS, Tsai KJ, Chang YJ, et al. Full-length TDP-43 forms toxic amyloid oligomers that are present in frontotemporal lobar dementia-TDP patients. *Nat Commun*. 2014;5(1):4824. doi:10.1038/ncomms5824

62. Chen AKH, Lin RYY, Hsieh EZJ, et al. Induction of Amyloid Fibrils by the C-Terminal Fragments of TDP-43 in Amyotrophic Lateral Sclerosis. *J Am Chem Soc*. 2010;132(4):1186-1187. doi:10.1021/ja9066207

63. Furukawa Y, Kaneko K, Watanabe S, Yamanaka K, Nukina N. A Seeding Reaction Recapitulates Intracellular Formation of Sarkosyl-insoluble Transactivation Response Element (TAR) DNA-binding Protein-43 Inclusions. *J Biol Chem*. 2011;286(21):18664-18672. doi:10.1074/jbc.M111.231209

64. Nonaka T, Masuda-Suzukake M, Arai T, et al. Prion-like Properties of Pathological TDP-43 Aggregates from Diseased Brains. *Cell Rep*. 2013;4(1):124-134. doi:10.1016/j.celrep.2013.06.007

65. Ishii T, Kawakami E, Endo K, Misawa H, Watabe K. Formation and spreading of TDP-43 aggregates in cultured neuronal and glial cells demonstrated by time-lapse imaging. Raoul C, ed. *PLOS ONE*. 2017;12(6):e0179375. doi:10.1371/journal.pone.0179375

66. Porta S, Xu Y, Restrepo CR, et al. Patient-derived frontotemporal lobar degeneration brain extracts induce formation and spreading of TDP-43 pathology in vivo. *Nat Commun*. 2018;9(1):4220. doi:10.1038/s41467-018-06548-9

67. Ding X, Xiang Z, Qin C, et al. Spreading of TDP-43 pathology via pyramidal tract induces ALS-like phenotypes in TDP-43 transgenic mice. *Acta Neuropathol Commun*. 2021;9(1):15. doi:10.1186/s40478-020-01112-3

68. Wils H, Kleinberger G, Janssens J, et al. TDP-43 transgenic mice develop spastic paralysis and neuronal inclusions characteristic of ALS and frontotemporal lobar degeneration. *Proc Natl Acad Sci*. 2010;107(8):3858-3863. doi:10.1073/pnas.0912417107

69. Tsai KJ, Yang CH, Fang YH, et al. Elevated expression of TDP-43 in the forebrain of mice is sufficient to cause neurological and pathological phenotypes mimicking FTLD-U. *J Exp Med*. 2010;207(8):1661-1673. doi:10.1084/jem.20092164

70. Nonaka T, Masuda-Suzukake M, Arai T, et al. Prion-like Properties of Pathological TDP-43 Aggregates from Diseased Brains. *Cell Rep*. 2013;4(1):124-134. doi:10.1016/j.celrep.2013.06.007

71. Jo M, Lee S, Jeon YM, Kim S, Kwon Y, Kim HJ. The role of TDP-43 propagation in neurodegenerative diseases: integrating insights from clinical and experimental studies. *Exp Mol Med*. 2020;52(10):1652-1662. doi:10.1038/s12276-020-00513-7

72. Josephs KA, Whitwell JL, Weigand SD, et al. TDP-43 is a key player in the clinical features associated with Alzheimer's disease. *Acta Neuropathol (Berl)*. 2014;127(6):811-824. doi:10.1007/s00401-014-1269-z

73. Jo M, Lee S, Jeon YM, Kim S, Kwon Y, Kim HJ. The role of TDP-43 propagation in neurodegenerative diseases: integrating insights from clinical and experimental studies. *Exp Mol Med*. 2020;52(10):1652-1662. doi:10.1038/s12276-020-00513-7

74. Weihl CC, Temiz P, Miller SE, et al. TDP-43 accumulation in inclusion body myopathy muscle suggests a common pathogenic mechanism with frontotemporal dementia. *J Neurol Neurosurg Psychiatry*. 2008;79(10):1186-1189. doi:10.1136/jnnp.2007.131334

75. Singh S, Kadioglu H, Patel K, Carrier L, Agnetti G. Is Desmin Propensity to Aggregate Part of its Protective Function? *Cells*. 2020;9(2):491. doi:10.3390/cells9020491

76. Kedia N, Arhzaouy K, Pittman SK, et al. Desmin forms toxic, seeding-competent amyloid aggregates that persist in muscle fibers. *Proc Natl Acad Sci*. 2019;116(34):16835-16840. doi:10.1073/pnas.1908263116

77. Hu X, Crick SL, Bu G, Frieden C, Pappu RV, Lee JM. Amyloid seeds formed by cellular uptake, concentration, and aggregation of the amyloid-beta peptide. *Proc Natl Acad Sci*. 2009;106(48):20324-20329. doi:10.1073/pnas.0911281106

78. Nath S, Agholme L, Kurudenkandy FR, Granseth B, Marcusson J, Hallbeck M. Spreading of Neurodegenerative Pathology via Neuron-to-Neuron Transmission of -Amyloid. *J Neurosci*. 2012;32(26):8767-8777. doi:10.1523/JNEUROSCI.0615-12.2012

79. Domert J, Rao SB, Agholme L, et al. Spreading of amyloid-β peptides via neuritic cell-to-cell transfer is dependent on insufficient cellular clearance. *Neurobiol Dis*. 2014;65:82-92. doi:10.1016/j.nbd.2013.12.019

80. Baker HF. Induction of ~(A4)-Amyloid in Primates by Injection of Alzheimer's Disease Brain Homogenate. *Mol Neurobiol*. 1994;8:15.

81. Meyer-Luehmann M, Coomaraswamy J, Bolmont T, et al. Exogenous Induction of Cerebral ß-Amyloidogenesis Is Governed by Agent and Host. *Science*. 2006;313(5794):1781-1784. doi:10.1126/science.1131864

82. Eisele YS, Obermüller U, Heilbronner G, et al. Peripherally Applied Aβ-Containing Inoculates Induce Cerebral β-Amyloidosis. *Science*. 2010;330(6006):980-982. doi:10.1126/science.1194516

83. He B, Zheng M, Liu Q, et al. Injected Amyloid Beta in the Olfactory Bulb Transfers to Other Brain Regions via Neural Connections in Mice. *Mol Neurobiol*. 2018;55(2):1703-1713. doi:10.1007/s12035-017-0446-1

84. Song HL, Shim S, Kim DH, et al. β-Amyloid is transmitted via neuronal connections along axonal membranes: β-Amyloid Transmission. *Ann Neurol*. 2014;75(1):88-97. doi:10.1002/ana.24029

85. Watts JC, Condello C, Stohr J, et al. Serial propagation of distinct strains of A prions from Alzheimer's disease patients. *Proc Natl Acad Sci*. 2014;111(28):10323-10328. doi:10.1073/pnas.1408900111

86. Self-Propagating, Molecular-Level Polymorphism in Alzheimer's β-Amyloid Fibrils. 2005;307:5.

87. Frost B, Jacks RL, Diamond MI. Propagation of Tau Misfolding from the Outside to the Inside of a Cell. *J Biol Chem*. 2009;284(19):12845-12852. doi:10.1074/jbc.M808759200

88. Nonaka T, Watanabe ST, Iwatsubo T, Hasegawa M. Seeded Aggregation and Toxicity of α-Synuclein and Tau. *J Biol Chem*. 2010;285(45):34885-34898. doi:10.1074/jbc.M110.148460

89. Guo JL, Lee VMY. Seeding of Normal Tau by Pathological Tau Conformers Drives Pathogenesis of Alzheimer-like Tangles. *J Biol Chem*. 2011;286(17):15317-15331. doi:10.1074/jbc.M110.209296

90. Wu JW, Herman M, Liu L, et al. Small Misfolded Tau Species Are Internalized via Bulk Endocytosis and Anterogradely and Retrogradely Transported in Neurons. *J Biol Chem*. 2013;288(3):1856-1870. doi:10.1074/jbc.M112.394528

91. Iba M, Guo JL, McBride JD, Zhang B, Trojanowski JQ, Lee VMY. Synthetic Tau Fibrils Mediate Transmission of Neurofibrillary Tangles in a Transgenic Mouse Model of Alzheimer's-Like Tauopathy. *J Neurosci*. 2013;33(3):1024-1037. doi:10.1523/JNEUROSCI.2642-12.2013

92. Bolmont T, Clavaguera F, Meyer-Luehmann M, et al. Induction of Tau Pathology by Intracerebral Infusion of Amyloid-β-Containing Brain Extract and by Amyloid-β Deposition in APP × Tau Transgenic Mice. *Am J Pathol*. 2007;171(6):2012-2020. doi:10.2353/ajpath.2007.070403

93. Clavaguera F, Bolmont T, Crowther RA, et al. Transmission and spreading of tauopathy in transgenic mouse brain. *Nat Cell Biol*. 2009;11(7):909-913. doi:10.1038/ncb1901

94. Clavaguera F, Akatsu H, Fraser G, et al. Brain homogenates from human tauopathies induce tau inclusions in mouse brain. *Proc Natl Acad Sci*. 2013;110(23):9535-9540. doi:10.1073/pnas.1301175110

95. Ahmed Z, Cooper J, Murray TK, et al. A novel in vivo model of tau propagation with rapid and progressive neurofibrillary tangle pathology: the pattern of spread is determined by connectivity, not proximity. *Acta Neuropathol (Berl)*. 2014;127(5):667-683. doi:10.1007/s00401-014-1254-6

96. Liu L, Drouet V, Wu JW, et al. Trans-Synaptic Spread of Tau Pathology In Vivo. Ikezu T, ed. *PLoS ONE*. 2012;7(2):e31302. doi:10.1371/journal.pone.0031302

97. de Calignon A, Polydoro M, Suárez-Calvet M, et al. Propagation of Tau Pathology in a Model of Early Alzheimer's Disease. *Neuron*. 2012;73(4):685-697.

doi:10.1016/j.neuron.2011.11.033

98. Sanders DW, Kaufman SK, DeVos SL, et al. Distinct Tau Prion Strains Propagate in Cells and Mice and Define Different Tauopathies. *Neuron*. 2014;82(6):1271-1288. doi:10.1016/j.neuron.2014.04.047

99. Shahnawaz M, Mukherjee A, Pritzkow S, et al. Discriminating α-synuclein strains in Parkinson's disease and multiple system atrophy. *Nature*. 2020;578(7794):273-277. doi:10.1038/s41586-020-1984-7

100. Lau A, So RWL, Lau HHC, et al. α-Synuclein strains target distinct brain regions and cell types. *Nat Neurosci*. 2020;23(1):21-31. doi:10.1038/s41593-019-0541-x

101. Yamasaki TR, Holmes BB, Furman JL, et al. Parkinson's disease and multiple system atrophy have distinct α-synuclein seed characteristics. *J Biol Chem*. 2019;294(3):1045-1058. doi:10.1074/jbc.RA118.004471

102. Peng C, Gathagan RJ, Covell DJ, et al. Cellular milieu imparts distinct pathological α-synuclein strains in α-synucleinopathies. *Nature*. 2018;557(7706):558-563. doi:10.1038/s41586-018-0104-4

103. Osterberg VR, Spinelli KJ, Weston LJ, Luk KC, Woltjer RL, Unni VK. Progressive Aggregation of Alpha-Synuclein and Selective Degeneration of Lewy Inclusion-Bearing Neurons in a Mouse Model of Parkinsonism. *Cell Rep*. 2015;10(8):1252-1260. doi:10.1016/j.celrep.2015.01.060

104. Desplats P, Lee HJ, Bae EJ, et al. Inclusion formation and neuronal cell death through neuron-to-neuron transmission of -synuclein. *Proc Natl Acad Sci*. 2009;106(31):13010-13015. doi:10.1073/pnas.0903691106

105. Ren PH, Lauckner JE, Kachirskaia I, Heuser JE, Melki R, Kopito RR. Cytoplasmic penetration and persistent infection of mammalian cells by polyglutamine aggregates. *Nat Cell Biol*. 2009;11(2):219-225. doi:10.1038/ncb1830

106. Herrera F, Tenreiro S, Miller-Fleming L, Outeiro TF. Visualization of cell-to-cell transmission of mutant huntingtin oligomers. *PLoS Curr*. 2011;3:RRN1210. doi:10.1371/currents.RRN1210

107. Furukawa Y, Kaneko K, Watanabe S, Yamanaka K, Nukina N. A Seeding Reaction Recapitulates Intracellular Formation of Sarkosyl-insoluble Transactivation Response Element (TAR) DNA-binding Protein-43 Inclusions. *J Biol Chem*. 2011;286(21):18664-18672. doi:10.1074/jbc.M111.231209

108. Münch C, O'Brien J, Bertolotti A. Prion-like propagation of mutant superoxide dismutase-1 misfolding in neuronal cells. *Proc Natl Acad Sci*. 2011;108(9):3548-3553. doi:10.1073/pnas.1017275108

109. Chia R, Tattum MH, Jones S, Collinge J, Fisher EMC, Jackson GS. Superoxide Dismutase 1 and tgSOD1G93A Mouse Spinal Cord Seed Fibrils, Suggesting a Propagative Cell Death Mechanism in Amyotrophic Lateral Sclerosis. Feany MB, ed. *PLoS ONE*. 2010;5(5):e10627. doi:10.1371/journal.pone.0010627

110. Grad LI, Guest WC, Yanai A, et al. Intermolecular transmission of superoxide dismutase 1 misfolding in living cells. *Proc Natl Acad Sci*. 2011;108(39):16398-16403. doi:10.1073/pnas.1102645108

111. Ogawa M, Furukawa Y. A seeded propagation of Cu, Zn-superoxide dismutase aggregates in amyotrophic lateral sclerosis. *Front Cell Neurosci*. 2014;8. doi:10.3389/fncel.2014.00083

112. Grad LI, Yerbury JJ, Turner BJ, et al. Intercellular propagated misfolding of wild-type Cu/Zn superoxide dismutase occurs via exosome-dependent and -independent mechanisms. *Proc Natl Acad Sci*. 2014;111(9):3620-3625. doi:10.1073/pnas.1312245111

113. Ayers JI, Fromholt S, Koch M, et al. Experimental transmissibility of mutant SOD1 motor neuron disease. *Acta Neuropathol (Berl)*. 2014;128(6):791-803. doi:10.1007/s00401-014-1342-7

114. Nomura T, Watanabe S, Kaneko K, Yamanaka K, Nukina N, Furukawa Y. Intranuclear Aggregation of Mutant FUS/TLS as a Molecular Pathomechanism of Amyotrophic Lateral Sclerosis. *J Biol Chem*. 2014;289(2):1192-1202. doi:10.1074/jbc.M113.516492

115. Zhou Q, Lehmer C, Michaelsen M, et al. Antibodies inhibit transmission and aggregation of *C9orf72* poly- GA dipeptide repeat proteins. *EMBO Mol Med*. 2017;9(5):687-702. doi:10.15252/emmm.201607054

116. Westergard T, Jensen BK, Wen X, et al. Cell-to-Cell Transmission of Dipeptide Repeat Proteins Linked to C9orf72 -ALS/FTD. *Cell Rep*. 2016;17(3):645-652. doi:10.1016/j.celrep.2016.09.032

117. May S, Hornburg D, Schludi MH, et al. C9orf72 FTLD/ALS-associated Gly-Ala dipeptide repeat proteins cause neuronal toxicity and Unc119 sequestration. *Acta Neuropathol (Berl)*. 2014;128(4):485-503. doi:10.1007/s00401-014-1329-4

118. Flores BN, Dulchavsky ME, Krans A, et al. Distinct C9orf72-Associated Dipeptide Repeat Structures Correlate with Neuronal Toxicity. Pandey U, ed. *PLOS ONE*.

2016;11(10):e0165084. doi:10.1371/journal.pone.0165084

119. Meyer H, Weihl CC. The VCP/p97 system at a glance: connecting cellular function to disease pathogenesis. *J Cell Sci*. Published online January 1, 2014:jcs.093831. doi:10.1242/jcs.093831

120. Buchberger A, Schindelin H, Hänzelmann P. Control of p97 function by cofactor binding. *FEBS Lett*. 2015;589(19PartA):2578-2589. doi:10.1016/j.febslet.2015.08.028

121. van den Boom J, Wolf M, Weimann L, et al. VCP/p97 Extracts Sterically Trapped Ku70/80 Rings from DNA in Double-Strand Break Repair. *Mol Cell*. 2016;64(1):189-198. doi:10.1016/j.molcel.2016.08.037

122. Li JM, Wu H, Zhang W, Blackburn MR, Jin J. The p97-UFD1L-NPL4 Protein Complex Mediates Cytokine-Induced IκBα Proteolysis. *Mol Cell Biol*. 2014;34(3):335-347. doi:10.1128/MCB.01190-13

123. Dobrynin G, Popp O, Romer T, et al. Cdc48/p97–Ufd1–Npl4 antagonizes Aurora B during chromosome segregation in HeLa cells. *J Cell Sci*. 2011;124(9):1571-1580. doi:10.1242/jcs.069500

124. Radhakrishnan SK, den Besten W, Deshaies RJ. p97-dependent retrotranslocation and proteolytic processing govern formation of active Nrf1 upon proteasome inhibition. *eLife*. 2014;3:e01856. doi:10.7554/eLife.01856

125. Ramanathan HN, Ye Y. The p97 ATPase associates with EEA1 to regulate the size of early endosomes. *Cell Res*. 2012;22(2):346-359. doi:10.1038/cr.2011.80

126. Ritz D, Vuk M, Kirchner P, et al. Endolysosomal sorting of ubiquitylated caveolin-1 is regulated by VCP and UBXD1 and impaired by VCP disease mutations. *Nat Cell Biol*. 2011;13(9):1116-1123. doi:10.1038/ncb2301

127. Kirchner P, Bug M, Meyer H. Ubiquitination of the N-terminal Region of Caveolin-1 Regulates Endosomal Sorting by the VCP/p97 AAA-ATPase. *J Biol Chem*. 2013;288(10):7363-7372. doi:10.1074/jbc.M112.429076

128. Ju JS, Fuentealba RA, Miller SE, et al. Valosin-containing protein (VCP) is required for autophagy and is disrupted in VCP disease. *J Cell Biol*. 2009;187(6):875-888. doi:10.1083/jcb.200908115

129. Tresse E, Salomons FA, Vesa J, et al. VCP/p97 is essential for maturation of ubiquitin-containing autophagosomes and this function is impaired by mutations that cause IBMPFD.

Autophagy. 2010;6(2):217-227. doi:10.4161/auto.6.2.11014

130. Hill SM, Wrobel L, Ashkenazi A, et al. VCP/p97 regulates Beclin-1-dependent autophagy initiation. *Nat Chem Biol*. 2021;17(4):448-455. doi:10.1038/s41589-020-00726-x

131. Haines DS, Lee JE, Beauparlant SL, et al. Protein Interaction Profiling of the p97 Adaptor UBXD1 Points to a Role for the Complex in Modulating ERGIC-53 Trafficking. *Mol Cell Proteomics*. 2012;11(6):M111.016444. doi:10.1074/mcp.M111.016444

132. Bento AC, Bippes CC, Kohler C, Hemion C, Frank S, Neutzner A. UBXD1 is a mitochondrial recruitment factor for p97/VCP and promotes mitophagy. *Sci Rep*. 2018;8(1):12415. doi:10.1038/s41598-018-30963-z

133. Papadopoulos C, Kirchner P, Bug M, et al. VCP/p97 cooperates with YOD1, UBXD1 and PLAA to drive clearance of ruptured lysosomes by autophagy. *EMBO J*. 2017;36(2):135-150. doi:10.15252/embj.201695148

134. Kovach MJ, Waggoner B, Leal SM, et al. Clinical Delineation and Localization to Chromosome 9p13.3–p12 of a Unique Dominant Disorder in Four Families: Hereditary Inclusion Body Myopathy, Paget Disease of Bone, and Frontotemporal Dementia. *Mol Genet Metab*. 2001;74(4):458-475. doi:10.1006/mgme.2001.3256

135. Kimonis V. Inclusion Body Myopathy with Paget Disease of Bone and/or Frontotemporal Dementia. In: Adam MP, Ardinger HH, Pagon RA, et al., eds. *GeneReviews®*. University of Washington, Seattle; 1993. Accessed January 23, 2022. http://www.ncbi.nlm.nih.gov/books/NBK1476/

136. Neumann M, Mackenzie IR, Cairns NJ, et al. TDP-43 in the Ubiquitin Pathology of Frontotemporal Dementia With VCP Gene Mutations. *J Neuropathol Exp Neurol*. 2007;66(2):6.

137. Spina S, Van Laar AD, Murrell JR, et al. Phenotypic variability in three families with *valosin-containing protein* mutation. *Eur J Neurol*. 2013;20(2):251-258. doi:10.1111/j.1468-1331.2012.03831.x

138. Chan N, Le C, Shieh P, et al. Valosin-containing protein mutation and Parkinson's disease. *Parkinsonism Relat Disord*. 2012;18(1):107-109. doi:10.1016/j.parkreldis.2011.07.006

139. De Ridder W, Azmi A, Clemen CS, et al. Multisystem proteinopathy due to a homozygous p.Arg159His *VCP* mutation: A tale of the unexpected. *Neurology*. 2020;94(8):e785-e796. doi:10.1212/WNL.0000000000008763

140. Darwich NF, Phan JM, Kim B, et al. Autosomal dominant VCP hypomorph mutation impairs disaggregation of PHF-tau. *Science*. Published online October 1, 2020:eaay8826. doi:10.1126/science.aay8826

141. Taylor JP. Multisystem proteinopathy: Table: Intersecting genetics in muscle, bone, and brain degeneration. *Neurology*. 2015;85(8):658-660. doi:10.1212/WNL.0000000000001862

142. Weihl CC, Dalal S, Pestronk A, Hanson PI. Inclusion body myopathy-associated mutations in p97/VCP impair endoplasmic reticulum-associated degradation. *Hum Mol Genet*. 2006;15(2):189-199. doi:10.1093/hmg/ddi426

143. Manno A, Noguchi M, Fukushi J, Motohashi Y, Kakizuka A. Enhanced ATPase activities as a primary defect of mutant valosin-containing proteins that cause inclusion body myopathy associated with Paget disease of bone and frontotemporal dementia. *Genes Cells Devoted Mol Cell Mech*. 2010;15(8):911-922. doi:10.1111/j.1365-2443.2010.01428.x

144. Arhzaouy K, Papadopoulos C, Schulze N, Pittman SK, Meyer H, Weihl CC. VCP maintains lysosomal homeostasis and TFEB activity in differentiated skeletal muscle. *Autophagy*. 2019;15(6):1082-1099. doi:10.1080/15548627.2019.1569933

145. Wani A, Zhu J, Ulrich JD, et al. Neuronal VCP loss of function recapitulates FTLD-TDP pathology. *Cell Rep*. 2021;36(3):109399. doi:10.1016/j.celrep.2021.109399

146. Müller JMM, Deinhardt K, Rosewell I, Warren G, Shima DT. Targeted deletion of p97 (VCP/CDC48) in mouse results in early embryonic lethality. *Biochem Biophys Res Commun*. 2007;354(2):459-465. doi:10.1016/j.bbrc.2006.12.206

147. Zhang T, Mishra P, Hay BA, Chan D, Guo M. Valosin-containing protein (VCP/p97) inhibitors relieve Mitofusin-dependent mitochondrial defects due to VCP disease mutants. *eLife*. 2017;6:e17834. doi:10.7554/eLife.17834

148. Ju JS, Miller SE, Hanson PI, Weihl CC. Impaired Protein Aggregate Handling and Clearance Underlie the Pathogenesis of p97/VCP-associated Disease. *J Biol Chem*. 2008;283(44):30289-30299. doi:10.1074/jbc.M805517200

149. Hubbers CU, Clemen CS, Kesper K, et al. Pathological consequences of VCP mutations on human striated muscle. *Brain*. 2007;130(2):381-393. doi:10.1093/brain/awl238

150. Blythe EE, Gates SN, Deshaies RJ, Martin A. Multisystem proteinopathy (MSP) mutations in VCP/p97 increase NPLOC4·UFD1L binding and substrate processing. Published online 2020:26.

151. Trusch F, Matena A, Vuk M, et al. The N-terminal Region of the Ubiquitin Regulatory X (UBX) Domain-containing Protein 1 (UBXD1) Modulates Interdomain Communication within the Valosin-containing Protein p97. *J Biol Chem*. 2015;290(49):29414-29427. doi:10.1074/jbc.M115.680686

152. Kimura Y, Fukushi J, Hori S, et al. Different dynamic movements of wild-type and pathogenic VCPs and their cofactors to damaged mitochondria in a Parkin-mediated mitochondrial quality control system. *Genes Cells*. 2013;18(12):1131-1143. doi:10.1111/gtc.12103

153. Bartolome F, Wu HC, Burchell VS, et al. Pathogenic VCP Mutations Induce Mitochondrial Uncoupling and Reduced ATP Levels. *Neuron*. 2013;78(1):57. doi:10.1016/j.neuron.2013.02.028

154. Xu S, Peng G, Wang Y, Fang S, Karbowski M. The AAA-ATPase p97 is essential for outer mitochondrial membrane protein turnover. Glick B, ed. *Mol Biol Cell*. 2011;22(3):291-300. doi:10.1091/mbc.e10-09-0748

155. Zhang T, Mishra P, Hay BA, Chan D, Guo M. Valosin-containing protein (VCP/p97) inhibitors relieve Mitofusin-dependent mitochondrial defects due to VCP disease mutants. *eLife*. 2017;6:e17834. doi:10.7554/eLife.17834

156. Bento AC, Bippes CC, Kohler C, Hemion C, Frank S, Neutzner A. UBXD1 is a mitochondrial recruitment factor for p97/VCP and promotes mitophagy. *Sci Rep*. 2018;8(1):12415. doi:10.1038/s41598-018-30963-z

157. McLelland GL, Goiran T, Yi W, et al. Mfn2 ubiquitination by PINK1/parkin gates the p97-dependent release of ER from mitochondria to drive mitophagy. *eLife*. 2018;7:e32866. doi:10.7554/eLife.32866

158. Buchan JR, Kolaitis RM, Taylor JP, Parker R. Eukaryotic Stress Granules Are Cleared by Autophagy and Cdc48/VCP Function. *Cell*. 2013;153(7):1461-1474. doi:10.1016/j.cell.2013.05.037

159. Rodriguez-Ortiz CJ, Flores JC, Valenzuela JA, et al. The Myoblast C2C12 Transfected with Mutant Valosin-Containing Protein Exhibits Delayed Stress Granule Resolution on Oxidative Stress. *Am J Pathol*. 2016;186(6):1623-1634. doi:10.1016/j.ajpath.2016.02.007

160. Yang X, Boehm JS, Yang X, et al. A public genome-scale lentiviral expression library of human ORFs. *Nat Methods*. 2011;8(8):659-661. doi:10.1038/nmeth.1638

161. Rual JF, Hirozane-Kishikawa T, Hao T, et al. Human ORFeome Version 1.1: A Platform

for Reverse Proteomics. *Genome Res*. 2004;14(10b):2128-2135. doi:10.1101/gr.2973604

162. Schuster A, Erasimus H, Fritah S, et al. RNAi/CRISPR Screens: from a Pool to a Valid Hit. *Trends Biotechnol*. 2019;37(1):38-55. doi:10.1016/j.tibtech.2018.08.002

163. Ford K, McDonald D, Mali P. Functional Genomics via CRISPR–Cas. *J Mol Biol*. 2019;431(1):48-65. doi:10.1016/j.jmb.2018.06.034

164. Outeiro TF, Lindquist S. Yeast Cells Provide Insight into Alpha-Synuclein Biology and Pathobiology. *Science*. 2003;302(5651):1772-1775. doi:10.1126/science.1090439

165. Botstein D, Chervitz SA, Cherry M. Yeast as a Model Organism. *Science*. 1997;277(5330):1259-1260. doi:10.1126/science.277.5330.1259

166. Lai CH, Chou CY, Ch'ang LY, Liu CS, Lin W chang. Identification of Novel Human Genes Evolutionarily Conserved in *Caenorhabditis elegans* by Comparative Proteomics. *Genome Res*. 2000;10(5):703-713. doi:10.1101/gr.10.5.703

167. Hamamichi S, Rivas RN, Knight AL, Cao S, Caldwell KA, Caldwell GA. Hypothesis-based RNAi screening identifies neuroprotective genes in a Parkinson's disease model. *Proc Natl Acad Sci*. 2008;105(2):728-733. doi:10.1073/pnas.0711018105

168. Gonçalves SA, Macedo D, Raquel H, et al. shRNA-Based Screen Identifies Endocytic Recycling Pathway Components That Act as Genetic Modifiers of Alpha-Synuclein Aggregation, Secretion and Toxicity. Serio TR, ed. *PLOS Genet*. 2016;12(4):e1005995. doi:10.1371/journal.pgen.1005995

169. Rousseaux MWC, Vázquez-Vélez GE, Al-Ramahi I, et al. A Druggable Genome Screen Identifies Modifiers of α-Synuclein Levels via a Tiered Cross-Species Validation Approach. *J Neurosci*. 2018;38(43):9286-9301. doi:10.1523/JNEUROSCI.0254-18.2018

170. Yuan NN, Cai CZ, Wu MY, et al. Canthin-6-One Accelerates Alpha-Synuclein Degradation by Enhancing UPS Activity: Drug Target Identification by CRISPR-Cas9 Whole Genome-Wide Screening Technology. *Front Pharmacol*. 2019;10:16. doi:10.3389/fphar.2019.00016

171. Willingham S, Outeiro TF, DeVit MJ, Lindquist SL, Muchowski PJ. Yeast Genes That Enhance the Toxicity of a Mutant Huntingtin Fragment or α-Synuclein. *Science*. 2003;302(5651):1769-1772. doi:10.1126/science.1090389

172. Cooper AA, Gitler AD, Cashikar A, et al. a-Synuclein Blocks ER-Golgi Traffic and Rab1 Rescues Neuron Loss in Parkinson's Models. 2006;313:6.

173. Yeger-Lotem E, Riva L, Su LJ, et al. Bridging high-throughput genetic and transcriptional data reveals cellular responses to alpha-synuclein toxicity. *Nat Genet*. 2009;41(3):316-323. doi:10.1038/ng.337

174. Gitler AD, Chesi A, Geddie ML, et al. α-Synuclein is part of a diverse and highly conserved interaction network that includes PARK9 and manganese toxicity. *Nat Genet*. 2009;41(3):308-315. doi:10.1038/ng.300

175. Chen YC, Farzadfard F, Gharaei N, Chen WCW, Cao J, Lu TK. Randomized CRISPR-Cas Transcriptional Perturbation Screening Reveals Protective Genes against Alpha-Synuclein Toxicity. *Mol Cell*. 2017;68(1):247-257.e5. doi:10.1016/j.molcel.2017.09.014

176. Flower TR, Clark-Dixon C, Metoyer C, et al. YGR198w (YPP1) targets A30P α-synuclein to the vacuole for degradation. *J Cell Biol*. 2007;177(6):1091-1104. doi:10.1083/jcb.200610071

177. Liang J, Clark-Dixon C, Wang S, et al. Novel suppressors of α-synuclein toxicity identified using yeast. *Hum Mol Genet*. 2008;17(23):3784-3795. doi:10.1093/hmg/ddn276

178. Doudna JA, Charpentier E. The new frontier of genome engineering with CRISPR-Cas9. *Science*. 2014;346(6213):1258096. doi:10.1126/science.1258096

179. Gasiunas G, Barrangou R, Horvath P, Siksnys V. Cas9-crRNA ribonucleoprotein complex mediates specific DNA cleavage for adaptive immunity in bacteria. *Proc Natl Acad Sci*. 2012;109(39):E2579-E2586. doi:10.1073/pnas.1208507109

180. Mali P, Yang L, Esvelt KM, et al. RNA-Guided Human Genome Engineering via Cas9. *Science*. 2013;339(6121):823-826. doi:10.1126/science.1232033

181. Cong L, Ran FA, Cox D, et al. Multiplex Genome Engineering Using CRISPR/Cas Systems. *Science*. 2013;339(6121):819-823. doi:10.1126/science.1231143

182. Wang T, Wei JJ, Sabatini DM, Lander ES. Genetic Screens in Human Cells Using the CRISPR-Cas9 System. *Science*. 2014;343(6166):80-84. doi:10.1126/science.1246981

183. Shalem O, Sanjana NE, Hartenian E, et al. Genome-Scale CRISPR-Cas9 Knockout Screening in Human Cells. *Science*. 2014;343(6166):84-87. doi:10.1126/science.1247005

184. BioGRID ORCS Database Statistics | BioGRID. Accessed January 23, 2022. https://wiki.thebiogrid.org/doku.php/ORCS:statistics

185. Yu JSL, Yusa K. Genome-wide CRISPR-Cas9 screening in mammalian cells. *Methods*.

2019;164-165:29-35. doi:10.1016/j.ymeth.2019.04.015

186. Momen-Roknabadi A, Oikonomou P, Zegans M, Tavazoie S. An inducible CRISPR interference library for genetic interrogation of Saccharomyces cerevisiae biology. *Commun Biol*. 2020;3(1):723. doi:10.1038/s42003-020-01452-9

187. BioGRID ORCS Database Statistics _ BioGRID.html.

188. Li Q, Li Y, Yang S, et al. CRISPR–Cas9-mediated base-editing screening in mice identifies DND1 amino acids that are critical for primordial germ cell development. *Nat Cell Biol*. 2018;20(11):1315-1325. doi:10.1038/s41556-018-0202-4

189. Tian R, Gachechiladze MA, Ludwig CH, et al. CRISPR Interference-Based Platform for Multimodal Genetic Screens in Human iPSC-Derived Neurons. *Neuron*. 2019;104(2):239-255.e12. doi:10.1016/j.neuron.2019.07.014

190. Genome-wide CRISPR screen for PARKIN regulators reveals transcriptional repression as a determinant of mitophagy | PNAS. Accessed January 23, 2022. https://www.pnas.org/content/115/2/E180

191. Findlay GM, Daza RM, Martin B, et al. Accurate classification of BRCA1 variants with saturation genome editing. *Nature*. 2018;562(7726):217-222. doi:10.1038/s41586-018-0461-z

192. Sanson KR, Hanna RE, Hegde M, et al. Optimized libraries for CRISPR-Cas9 genetic screens with multiple modalities. *Nat Commun*. 2018;9(1):5416. doi:10.1038/s41467-018-07901-8

193. Doench JG, Fusi N, Sullender M, et al. Optimized sgRNA design to maximize activity and minimize off-target effects of CRISPR-Cas9. *Nat Biotechnol*. 2016;34(2):184-191. doi:10.1038/nbt.3437

194. Feldman D, Singh A, Schmid-Burgk JL, et al. Optical Pooled Screens in Human Cells. *Cell*. 2019;179(3):787-799.e17. doi:10.1016/j.cell.2019.09.016

195. Hasle N, Cooke A, Srivatsan S, et al. High-throughput, microscope-based sorting to dissect cellular heterogeneity. *Mol Syst Biol*. 2020;16(6). doi:10.15252/msb.20209442

196. Kanfer G, Sarraf SA, Maman Y, et al. Image-based pooled whole-genome CRISPRi screening for subcellular phenotypes. *J Cell Biol*. 2021;220(2):e202006180. doi:10.1083/jcb.202006180

197. Kramer NJ, Haney MS, Morgens DW, et al. CRISPR–Cas9 screens in human cells and primary neurons identify modifiers of C9ORF72 dipeptide-repeat-protein toxicity. *Nat Genet*. 2018;50(4):603-612. doi:10.1038/s41588-018-0070-7

198. van Ham TJ, Thijssen KL, Breitling R, Hofstra RMW, Plasterk RHA, Nollen EAA. C. elegans Model Identifies Genetic Modifiers of α-Synuclein Inclusion Formation During Aging. Kim SK, ed. *PLoS Genet*. 2008;4(3):e1000027. doi:10.1371/journal.pgen.1000027

199. Höllerhage M, Bickle M, Höglinger GU. Unbiased Screens for Modifiers of Alpha-Synuclein Toxicity. *Curr Neurol Neurosci Rep*. 2019;19(2):8. doi:10.1007/s11910-019-0925-z

200. Goedert M. Alpha-synuclein and neurodegenerative diseases. *Nat Rev Neurosci*. 2001;2(7):492-501. doi:10.1038/35081564

201. Prusiner SB, Woerman AL, Mordes DA, et al. Evidence for α-synuclein prions causing multiple system atrophy in humans with parkinsonism. *Proc Natl Acad Sci*. 2015;112(38):E5308-E5317. doi:10.1073/pnas.1514475112

202. Desplats P, Lee HJ, Bae EJ, et al. Inclusion formation and neuronal cell death through neuron-to-neuron transmission of -synuclein. *Proc Natl Acad Sci*. 2009;106(31):13010-13015. doi:10.1073/pnas.0903691106

203. Volpicelli-Daley LA, Luk KC, Lee VMY. Addition of exogenous α-synuclein preformed fibrils to primary neuronal cultures to seed recruitment of endogenous α-synuclein to Lewy body and Lewy neurite–like aggregates. *Nat Protoc*. 2014;9(9):2135-2146. doi:10.1038/nprot.2014.143

204. Jiang P, Gan M, Yen SH, McLean PJ, Dickson DW. Impaired endo-lysosomal membrane integrity accelerates the seeding progression of α-synuclein aggregates. *Sci Rep*. 2017;7(1):7690. doi:10.1038/s41598-017-08149-w

205. Höllerhage M, Bickle M, Höglinger GU. Unbiased Screens for Modifiers of Alpha-Synuclein Toxicity. *Curr Neurol Neurosci Rep*. 2019;19(2):8. doi:10.1007/s11910-019-0925-z

206. Meyer H, Weihl CC. The VCP/p97 system at a glance: connecting cellular function to disease pathogenesis. *J Cell Sci*. 2014;127(18):3877-3883. doi:10.1242/jcs.093831

207. Spina S, Van Laar AD, Murrell JR, et al. Phenotypic variability in three families with *valosin-containing protein* mutation. *Eur J Neurol*. 2013;20(2):251-258. doi:10.1111/j.1468-1331.2012.03831.x

208. Neumann M, Mackenzie IR, Cairns NJ, et al. TDP-43 in the Ubiquitin Pathology of Frontotemporal Dementia With VCP Gene Mutations. *J Neuropathol Exp Neurol*. 2007;66(2):6.

209. Forman MS, Mackenzie IR, Cairns NJ, et al. Novel Ubiquitin Neuropathology in Frontotemporal Dementia With *Valosin-Containing Protein* Gene Mutations. *J Neuropathol Exp Neurol*. 2006;65(6):571-581. doi:10.1097/00005072-200606000-00005

210. Ju JS, Miller SE, Hanson PI, Weihl CC. Impaired Protein Aggregate Handling and Clearance Underlie the Pathogenesis of p97/VCP-associated Disease. *J Biol Chem*. 2008;283(44):30289-30299. doi:10.1074/jbc.M805517200

211. Blythe EE, Gates SN, Deshaies RJ, Martin A. Multisystem Proteinopathy Mutations in VCP/p97 Increase NPLOC4·UFD1L Binding and Substrate Processing. *Structure*. 2019;27(12):1820-1829.e4. doi:10.1016/j.str.2019.09.011

212. Arhzaouy K, Papadopoulos C, Schulze N, Pittman SK, Meyer H, Weihl CC. VCP maintains lysosomal homeostasis and TFEB activity in differentiated skeletal muscle. *Autophagy*. 2019;15(6):1082-1099. doi:10.1080/15548627.2019.1569933

213. Taylor JP. Multisystem proteinopathy: Table: Intersecting genetics in muscle, bone, and brain degeneration. *Neurology*. 2015;85(8):658-660. doi:10.1212/WNL.0000000000001862

214. Mehta S, Khare M, Ramani R, et al. Genotype-phenotype studies of VCP-associated inclusion body myopathy with Paget disease of bone and/or frontotemporal dementia: Genotype-Phenotype studies of IBMPFD. *Clin Genet*. 2013;83(5):422-431. doi:10.1111/cge.12000

215. Conicella AE, Dignon GL, Zerze GH, et al. TDP-43 α-helical structure tunes liquid–liquid phase separation and function. *Proc Natl Acad Sci*. 2020;117(11):5883-5894. doi:10.1073/pnas.1912055117

216. French RL, Grese ZR, Aligireddy H, et al. Detection of TAR DNA-binding protein 43 (TDP-43) oligomers as initial intermediate species during aggregate formation. *J Biol Chem*. 2019;294(17):6696-6709. doi:10.1074/jbc.RA118.005889

217. Dhavale DD, Tsai C, Bagchi DP, Engel LA, Sarezky J, Kotzbauer PT. A sensitive assay reveals structural requirements for α-synuclein fibril growth. *J Biol Chem*. 2017;292(22):9034-9050. doi:10.1074/jbc.M116.767053

218. Bagchi DP, Yu L, Perlmutter JS, et al. Binding of the Radioligand SIL23 to α-Synuclein Fibrils in Parkinson Disease Brain Tissue Establishes Feasibility and Screening Approaches

for Developing a Parkinson Disease Imaging Agent. Tansey MG, ed. *PLoS ONE*. 2013;8(2):e55031. doi:10.1371/journal.pone.0055031

219. Nahass GR, Sun Y, Xu Y, et al. Brazilin Removes Toxic Alpha-Synuclein and Seeding Competent Assemblies from Parkinson Brain by Altering Conformational Equilibrium. *J Mol Biol*. 2021;433(8):166878. doi:10.1016/j.jmb.2021.166878

220. Kaech S, Banker G. Culturing hippocampal neurons. *Nat Protoc*. 2006;1(5):2406-2415. doi:10.1038/nprot.2006.356

221. Volpicelli-Daley LA, Luk KC, Lee VMY. Addition of exogenous α-synuclein preformed fibrils to primary neuronal cultures to seed recruitment of endogenous α-synuclein to Lewy body and Lewy neurite–like aggregates. *Nat Protoc*. 2014;9(9):2135-2146. doi:10.1038/nprot.2014.143

222. Clemen CS, Winter L, Strucksberg KH, et al. The heterozygous R155C VCP mutation: Toxic in humans! Harmless in mice? *Biochem Biophys Res Commun*. 2018;503(4):2770-2777. doi:10.1016/j.bbrc.2018.08.038

223. Furman JL, Holmes BB, Diamond MI. Sensitive Detection of Proteopathic Seeding Activity with FRET Flow Cytometry. *J Vis Exp*. 2015;(106):53205. doi:10.3791/53205

224. Beilina A, Bonet-Ponce L, Kumaran R, et al. The Parkinson's Disease Protein LRRK2 Interacts with the GARP Complex to Promote Retrograde Transport to the trans-Golgi Network. *Cell Rep*. 2020;31(5):107614. doi:10.1016/j.celrep.2020.107614

225. Mangieri LR, Mader BJ, Thomas CE, et al. ATP6V0C Knockdown in Neuroblastoma Cells Alters Autophagy-Lysosome Pathway Function and Metabolism of Proteins that Accumulate in Neurodegenerative Disease. Srinivasula SM, ed. *PLoS ONE*. 2014;9(4):e93257. doi:10.1371/journal.pone.0093257

226. Garcia-Esparcia P, López-González I, Grau-Rivera O, et al. Dementia with Lewy Bodies: Molecular Pathology in the Frontal Cortex in Typical and Rapidly Progressive Forms. *Front Neurol*. 2017;8. doi:10.3389/fneur.2017.00089

227. Colla E. Linking the Endoplasmic Reticulum to Parkinson's Disease and Alpha-Synucleinopathy. *Front Neurosci*. 2019;13:560. doi:10.3389/fnins.2019.00560

228. Konno M, Hasegawa T, Baba T, et al. Suppression of dynamin GTPase decreases α-synuclein uptake by neuronal and oligodendroglial cells: a potent therapeutic target for synucleinopathy. *Mol Neurodegener*. 2012;7(1):38. doi:10.1186/1750-1326-7-38

229. Magnaghi P, D'Alessio R, Valsasina B, et al. Covalent and allosteric inhibitors of the ATPase VCP/p97 induce cancer cell death. *Nat Chem Biol*. 2013;9(9):548-556. doi:10.1038/nchembio.1313

230. Zhou HJ, Wang J, Yao B, et al. Discovery of a First-in-Class, Potent, Selective, and Orally Bioavailable Inhibitor of the p97 AAA ATPase (CB-5083). *J Med Chem*. 2015;58(24):9480-9497. doi:10.1021/acs.jmedchem.5b01346

231. Wang Q, Li L, Ye Y. Inhibition of p97-dependent Protein Degradation by Eeyarestatin I. *J Biol Chem*. 2008;283(12):7445-7454. doi:10.1074/jbc.M708347200

232. Chou TF, Brown SJ, Minond D, et al. Reversible inhibitor of p97, DBeQ, impairs both ubiquitin-dependent and autophagic protein clearance pathways. *Proc Natl Acad Sci*. 2011;108(12):4834-4839. doi:10.1073/pnas.1015312108

233. Birol M, Wojcik SP, Miranker AD, Rhoades E. Identification of N-linked glycans as specific mediators of neuronal uptake of acetylated α-Synuclein. Bates GP, ed. *PLOS Biol*. 2019;17(6):e3000318. doi:10.1371/journal.pbio.3000318

234. Chou T, Li K, Frankowski KJ, Schoenen FJ, Deshaies RJ. Structure–Activity Relationship Study Reveals ML240 and ML241 as Potent and Selective Inhibitors of p97 ATPase. *ChemMedChem*. 2013;8(2):297-312. doi:10.1002/cmdc.201200520

235. Ritz D, Vuk M, Kirchner P, et al. Endolysosomal sorting of ubiquitylated caveolin-1 is regulated by VCP and UBXD1 and impaired by VCP disease mutations. *Nat Cell Biol*. 2011;13(9):1116-1123. doi:10.1038/ncb2301

236. Nalbandian A, Llewellyn KJ, Badadani M, et al. A progressive translational mouse model of human valosin-containing protein disease: The *VCP* $^{R155H/+}$ mouse: Mouse Model for Human VCP Disease. *Muscle Nerve*. 2013;47(2):260-270. doi:10.1002/mus.23522

237. Aulas A, Vande Velde C. Alterations in stress granule dynamics driven by TDP-43 and FUS: a link to pathological inclusions in ALS? *Front Cell Neurosci*. 2015;9. doi:10.3389/fncel.2015.00423

238. Cooper AA, Gitler AD, Cashikar A, et al. α-Synuclein Blocks ER-Golgi Traffic and Rab1 Rescues Neuron Loss in Parkinson's Models. *Science*. 2006;313(5785):324-328. doi:10.1126/science.1129462

239. Rousseaux MWC, Vázquez-Vélez GE, Al-Ramahi I, et al. A Druggable Genome Screen Identifies Modifiers of α-Synuclein Levels via a Tiered Cross-Species Validation Approach. *J Neurosci*. 2018;38(43):9286-9301. doi:10.1523/JNEUROSCI.0254-18.2018

240. Jiang P, Gan M, Yen SH, McLean PJ, Dickson DW. Impaired endo-lysosomal membrane integrity accelerates the seeding progression of α-synuclein aggregates. *Sci Rep*. 2017;7(1):7690. doi:10.1038/s41598-017-08149-w

241. Flavin WP, Bousset L, Green ZC, et al. Endocytic vesicle rupture is a conserved mechanism of cellular invasion by amyloid proteins. *Acta Neuropathol (Berl)*. 2017;134(4):629-653. doi:10.1007/s00401-017-1722-x

242. Skowyra ML, Schlesinger PH, Naismith TV, Hanson PI. Triggered recruitment of ESCRT machinery promotes endolysosomal repair. *Science*. 2018;360(6384):eaar5078. doi:10.1126/science.aar5078

243. Chauhan S, Kumar S, Jain A, et al. TRIMs and Galectins Globally Cooperate and TRIM16 and Galectin-3 Co-direct Autophagy in Endomembrane Damage Homeostasis. *Dev Cell*. 2016;39(1):13-27. doi:10.1016/j.devcel.2016.08.003

244. Chen JJ, Nathaniel DL, Raghavan P, et al. Compromised function of the ESCRT pathway promotes endolysosomal escape of tau seeds and propagation of tau aggregation. *J Biol Chem*. 2019;294(50):18952-18966. doi:10.1074/jbc.RA119.009432

245. Watts GDJ, Wymer J, Kovach MJ, et al. Inclusion body myopathy associated with Paget disease of bone and frontotemporal dementia is caused by mutant valosin-containing protein. *Nat Genet*. 2004;36(4):377-381. doi:10.1038/ng1332

246. Forman MS, Mackenzie IR, Cairns NJ, et al. Novel Ubiquitin Neuropathology in Frontotemporal Dementia With *Valosin-Containing Protein* Gene Mutations. *J Neuropathol Exp Neurol*. 2006;65(6):571-581. doi:10.1097/00005072-200606000-00005

247. Kim HJ, Kim NC, Wang YD, et al. Mutations in prion-like domains in hnRNPA2B1 and hnRNPA1 cause multisystem proteinopathy and ALS. *Nature*. 2013;495(7442):467-473. doi:10.1038/nature11922

248. Weihl CC, Pestronk A, Kimonis VE. Valosin-containing protein disease: Inclusion body myopathy with Paget's disease of the bone and fronto-temporal dementia. *Neuromuscul Disord*. 2009;19(5):308-315. doi:10.1016/j.nmd.2009.01.009

249. de Boer EMJ, Orie VK, Williams T, et al. TDP-43 proteinopathies: a new wave of neurodegenerative diseases. *J Neurol Neurosurg Psychiatry*. 2021;92(1):86-95. doi:10.1136/jnnp-2020-322983

250. Lee HJ, Suk JE, Bae EJ, Lee JH, Paik SR, Lee SJ. Assembly-dependent endocytosis and clearance of extracellular a-synuclein. *Int J Biochem Cell Biol*. 2008;40(9):1835-1849.

doi:10.1016/j.biocel.2008.01.017

251. Flavin WP, Bousset L, Green ZC, et al. Endocytic vesicle rupture is a conserved mechanism of cellular invasion by amyloid proteins. *Acta Neuropathol (Berl)*. 2017;134(4):629-653. doi:10.1007/s00401-017-1722-x

252. Mori F, Tada M, Kon T, et al. Phosphorylated TDP-43 aggregates in skeletal and cardiac muscle are a marker of myogenic degeneration in amyotrophic lateral sclerosis and various conditions. *Acta Neuropathol Commun*. 2019;7(1):165. doi:10.1186/s40478-019-0824-1

253. Zhao N, Attrebi ON, Ren Y, et al. APOE4 exacerbates α-synuclein pathology and related toxicity independent of amyloid. *Sci Transl Med*. 2020;12(529):eaay1809. doi:10.1126/scitranslmed.aay1809

254. Davis AA, Inman CE, Wargel ZM, et al. *APOE* genotype regulates pathology and disease progression in synucleinopathy. *Sci Transl Med*. 2020;12(529):eaay3069. doi:10.1126/scitranslmed.aay3069

255. Wang X, Becker K, Levine N, et al. Pathogenic alpha-synuclein aggregates preferentially bind to mitochondria and affect cellular respiration. *Acta Neuropathol Commun*. 2019;7(1):41. doi:10.1186/s40478-019-0696-4

256. Jena KK, Kolapalli SP, Mehto S, et al. TRIM16 controls assembly and degradation of protein aggregates by modulating the p62-NRF2 axis and autophagy. *EMBO J*. 2018;37(18). doi:10.15252/embj.201798358

257. Eapen VV, Swarup S, Hoyer MJ, Paulo JA, Harper JW. Quantitative proteomics reveals the selectivity of ubiquitin-binding autophagy receptors in the turnover of damaged lysosomes by lysophagy. *eLife*. 2021;10:e72328. doi:10.7554/eLife.72328

258. Gershlick DC, Ishida M, Jones JR, Bellomo A, Bonifacino JS, Everman DB. A neurodevelopmental disorder caused by mutations in the VPS51 subunit of the GARP and EARP complexes. *Hum Mol Genet*. 2019;28(9):1548-1560. doi:10.1093/hmg/ddy423

259. Chen KS, Menezes K, Rodgers JB, et al. Small molecule inhibitors of α-synuclein oligomers identified by targeting early dopamine-mediated motor impairment in C. elegans. *Mol Neurodegener*. 2021;16(1):77. doi:10.1186/s13024-021-00497-6

260. Locke CJ, Fox SA, Caldwell GA, Caldwell KA. Acetaminophen attenuates dopamine neuron degeneration in animal models of Parkinson's disease. *Neurosci Lett*. 2008;439(2):129-133. doi:10.1016/j.neulet.2008.05.003

261. Chen JJ, Nathaniel DL, Raghavan P, et al. Compromised function of the ESCRT pathway promotes endolysosomal escape of tau seeds and propagation of tau aggregation. *J Biol Chem*. 2019;294(50):18952-18966. doi:10.1074/jbc.RA119.009432

262. Scotter EL, Chen HJ, Shaw CE. TDP-43 Proteinopathy and ALS: Insights into Disease Mechanisms and Therapeutic Targets. *Neurotherapeutics*. 2015;12(2):352-363. doi:10.1007/s13311-015-0338-x

263. Wu JJ, Cai A, Greenslade JE, et al. ALS/FTD mutations in UBQLN2 impede autophagy by reducing autophagosome acidification through loss of function. *Proc Natl Acad Sci*. 2020;117(26):15230-15241. doi:10.1073/pnas.1917371117

264. Iguchi Y, Eid L, Parent M, et al. Exosome secretion is a key pathway for clearance of pathological TDP-43. *Brain*. 2016;139(12):3187-3201. doi:10.1093/brain/aww237

265. Kuiperij HB, Versleijen AAM, Beenes M, et al. Tau Rather than TDP-43 Proteins are Potential Cerebrospinal Fluid Biomarkers for Frontotemporal Lobar Degeneration Subtypes: A Pilot Study. *J Alzheimers Dis*. 2017;55(2):585-595. doi:10.3233/JAD-160386

266. Steinacker P, Barschke P, Otto M. Biomarkers for diseases with TDP-43 pathology. *Mol Cell Neurosci*. 2019;97:43-59. doi:10.1016/j.mcn.2018.10.003

267. Noto YI, Shibuya K, Sato Y, et al. Elevated CSF TDP-43 levels in amyotrophic lateral sclerosis: Specificity, sensitivity, and a possible prognostic value. *Amyotroph Lateral Scler*. 2011;12(2):140-143. doi:10.3109/17482968.2010.541263

268. Hoye ML, Koval ED, Wegener AJ, et al. MicroRNA Profiling Reveals Marker of Motor Neuron Disease in ALS Models. *J Neurosci Off J Soc Neurosci*. 2017;37(22):5574-5586. doi:10.1523/JNEUROSCI.3582-16.2017

269. Rizzuti M, Filosa G, Melzi V, et al. MicroRNA expression analysis identifies a subset of downregulated miRNAs in ALS motor neuron progenitors. *Sci Rep*. 2018;8:10105. doi:10.1038/s41598-018-28366-1

270. Kimonis V. Inclusion Body Myopathy with Paget Disease of Bone and/or Frontotemporal Dementia. In: Adam MP, Ardinger HH, Pagon RA, et al., eds. *GeneReviews®*. University of Washington, Seattle; 1993. Accessed January 23, 2022. http://www.ncbi.nlm.nih.gov/books/NBK1476/

271. Vogler TO, Wheeler JR, Nguyen ED, et al. TDP-43 and RNA form amyloid-like myo-granules in regenerating muscle. *Nature*. 2018;563(7732):508-513. doi:10.1038/s41586-018-0665-2

272. Vogler TO, Wheeler JR, Nguyen ED, et al. TDP-43 and RNA form amyloid-like myo-granules in regenerating muscle. *Nature*. 2018;563(7732):508-513. doi:10.1038/s41586-018-0665-2

273. Sigurdson CJ, Bartz JC, Glatzel M. Cellular and Molecular Mechanisms of Prion Disease. *Annu Rev Pathol Mech Dis*. 2019;14(1):497-516. doi:10.1146/annurev-pathmechdis-012418-013109

274. Eisele YS, Obermüller U, Heilbronner G, et al. Peripherally Applied Aβ-Containing Inoculates Induce Cerebral β-Amyloidosis. *Science*. 2010;330(6006):980-982. doi:10.1126/science.1194516

275. Ma LY, Liu GL, Wang DX, Zhang MM, Kou WY, Feng T. Alpha-Synuclein in Peripheral Tissues in Parkinson's Disease. *ACS Chem Neurosci*. 2019;10(2):812-823. doi:10.1021/acschemneuro.8b00383

276. Holmqvist S, Chutna O, Bousset L, et al. Direct evidence of Parkinson pathology spread from the gastrointestinal tract to the brain in rats. *Acta Neuropathol (Berl)*. 2014;128(6):805-820. doi:10.1007/s00401-014-1343-6

277. Kim S, Kwon SH, Kam TI, et al. Transneuronal Propagation of Pathologic α-Synuclein from the Gut to the Brain Models Parkinson's Disease. *Neuron*. 2019;103(4):627-641.e7. doi:10.1016/j.neuron.2019.05.035

278. Lohmann S, Bernis ME, Tachu BJ, Ziemski A, Grigoletto J, Tamgüney G. Oral and intravenous transmission of α-synuclein fibrils to mice. *Acta Neuropathol (Berl)*. 2019;138(4):515-533. doi:10.1007/s00401-019-02037-5

279. Sacino AN, Brooks M, Thomas MA, et al. Intramuscular injection of α-synuclein induces CNS α-synuclein pathology and a rapid-onset motor phenotype in transgenic mice. *Proc Natl Acad Sci*. 2014;111(29):10732-10737. doi:10.1073/pnas.1321785111

Appendix

Appendix Table. Protective genes for αS seeding

Group	Gene ID	FDR	log2(Fold change)
FRET+	SLC27A2	0.000118	4.3772
FRET+	IFI44L	0.000118	4.3532
FRET+	YAP1	0.000118	4.2783
FRET+	UBE2C	0.000118	4.241
FRET+	HPSE	0.000118	3.9899
FRET+	KIF1C	0.000118	3.7946
FRET+	PDPN	0.000118	3.7181
FRET+	LYPLA1	0.000118	3.6877
FRET+	HNRNPA0	0.000118	3.6485
FRET+	LAMTOR5	0.000118	3.6003
FRET+	SUGT1	0.000118	3.5984
FRET+	RBPMS	0.000118	3.5688
FRET+	CAMKK2	0.000118	3.5165
FRET+	OS9	0.000118	3.4672
FRET+	LRRC41	0.000118	3.419
FRET+	KDELR1	0.000118	3.3573
FRET+	CELF1	0.000118	3.3333
FRET+	ZNHIT1	0.000118	3.2808
FRET+	PPIH	0.000118	3.2753
FRET+	RABAC1	0.000118	3.2625
FRET+	HIBADH	0.000118	3.2511
FRET+	TRIM16	0.000118	3.1945
FRET+	NEK6	0.000118	3.1487
FRET+	TOMM34	0.000118	3.1085
FRET+	NPC2	0.000118	3.0687
FRET+	COL4A1	0.000118	3.0495
FRET+	STK25	0.000118	3.0438
FRET+	POSTN	0.000118	3.0277
FRET+	C1D	0.000118	2.9735
FRET+	PAPOLA	0.000118	2.9589
FRET+	NCOA2	0.000118	2.9439
FRET+	RAB35	0.000118	2.9415
FRET+	HSPH1	0.000118	2.8891
FRET+	TXNRD2	0.000118	2.8644
FRET+	DBF4	0.000118	2.8321
FRET+	STIP1	0.000118	2.8143
FRET+	IVNS1ABP	0.000118	2.7742
FRET+	SIVA1	0.000118	2.7282
FRET+	PDE10A	0.000118	2.7021
FRET+	MAP3K2	0.000118	2.602

Group	Gene ID	FDR	log2(Fold change)
FRET+	IFI44	0.000118	2.5343
FRET+	PIAS3	0.000323	3.2893
FRET+	C11orf58	0.000323	3.11
FRET+	SPAG5	0.000323	2.609
FRET+	CARM1	0.000323	2.5799
FRET+	GIPC1	0.000505	3.2611
FRET+	VAT1	0.000505	3.055
FRET+	LMAN2	0.000505	2.9969
FRET+	ARPP19	0.00081	3.1388
FRET+	VAV3	0.00081	3.0517
FRET+	MALT1	0.00081	3.0023
FRET+	CIB1	0.00081	2.722
FRET+	EHMT1	0.00081	2.6874
FRET+	PRSS21	0.00081	2.1081
FRET+	PIM2	0.000972	2.6236
FRET+	CAP1	0.001129	2.9592
FRET+	PRDX3	0.001238	3.5197
FRET+	SEC61B	0.001238	2.9665
FRET+	USP19	0.001238	2.8722
FRET+	DDX17	0.001357	2.9398
FRET+	PLK2	0.001357	2.8197
FRET+	GCN1L1	0.00147	3.3654
FRET+	MGEA5	0.00147	3.3354
FRET+	ECI2	0.001575	2.8595
FRET+	TNFSF13B	0.001575	2.4859
FRET+	PRSS23	0.001674	2.9191
FRET+	METAP2	0.001674	2.9024
FRET+	TRIM38	0.001794	2.7015
FRET+	PDIA5	0.001909	2.887
FRET+	ANP32B	0.001967	2.9086
FRET+	PRDX4	0.001967	2.854
FRET+	CCNI	0.001967	2.6154
FRET+	KDELR2	0.002019	2.8607
FRET+	USP16	0.002019	2.6986
FRET+	TMEM147	0.002019	2.6318
FRET+	SRSF10	0.00225	2.548
FRET+	EBP	0.002475	2.4016
FRET+	YIF1A	0.002569	2.6953
FRET+	STAMBP	0.002628	2.9476
FRET+	DNAJB4	0.002628	1.9888
FRET+	ERP29	0.002717	2.5051
FRET+	SH2B2	0.002863	2.4624
FRET+	HNRNPUL1	0.003359	2.202
FRET+	PTGES3	0.004252	2.132
FRET+	FAM3C	0.004432	2.3308
FRET+	SLC27A5	0.00495	2.5831
FRET+	FERMT2	0.005457	2.7082
FRET+	TACC2	0.005729	2.1163
FRET+	TMED10	0.005886	2.7171
FRET+	AHSA1	0.006365	3.1307

Group	Gene ID	FDR	log2(Fold change)
FRET+	CIB2	0.006403	2.4944
FRET+	LILRB4	0.006867	2.1038
FRET+	RRAGA	0.008058	2.8375
FRET+	TAB1	0.008286	2.8946
FRET+	SSSCA1	0.014078	2.0017
FRET+	HMGN4	0.014599	2.8039
FRET+	TIMM17A	0.014599	2.7675
FRET+	SLC35A1	0.015452	2.4395
FRET+	TGOLN2	0.017277	2.0313
FRET+	EHMT2	0.018675	2.414
FRET+	MERTK	0.021292	1.7698
FRET+	PPP1R13L	0.023562	2.7847
FRET+	TACC3	0.027298	2.1942
FRET+	SMAD5	0.02975	1.9546
FRET+	ADGRL2	0.032155	2.1509
FRET+	CBX1	0.032866	2.5533
FRET+	LRTOMT	0.035562	2.1702
FRET+	C7orf34	0.036319	1.4542
FRET+	KLHDC7A	0.036616	1.7663
FRET+	MORC2	0.04177	2.1945
FRET+	TCERG1	0.047095	2.2514
FRET-	PRC1	0.001238	-2.8323
FRET-	PSMD14	0.001238	-2.3874
FRET-	ATP6V0C	0.001238	-2.2861
FRET-	TRAPPC11	0.001238	-1.9267

Group	Gene ID	FDR	log2(Fold change)
FRET-	AURKB	0.002122	-2.3266
FRET-	RPL23A	0.002122	-1.9353
FRET-	GINS4	0.002122	-1.213
FRET-	TUBGCP3	0.00275	-1.8507
FRET-	VPS52	0.00275	-1.4399
FRET-	SNRNP35	0.00495	-1.1493
FRET-	PRIM1	0.005304	-1.581
FRET-	ATP6V0B	0.005304	-1.3902
FRET-	ACTL6A	0.005304	-1.0426
FRET-	CCT7	0.013531	-1.903
FRET-	MCM5	0.013923	-1.468
FRET-	BUB3	0.016599	-1.8184
FRET-	CDC45	0.018152	-2.4996
FRET-	ATP6V1A	0.018152	-1.5073
FRET-	MCM7	0.018152	-1.3744
FRET-	ARCN1	0.019127	-1.5577
FRET-	RPF2	0.019156	-1.3106
FRET-	TUT1	0.019208	-1.9006
FRET-	CDCA8	0.019208	-1.1978
FRET-	NAPA	0.024181	-2.0421
FRET-	RPL19	0.024386	-1.5775
FRET-	RPS6	0.024576	-1.5797
FRET-	SMU1	0.027073	-1.9513
FRET-	SNRPG	0.027073	-1.6738
FRET-	SNRPD2	0.027073	-1.5715

Group	Gene ID	FDR	log2(Fold change)
FRET-	HAUS8	0.030354	-2.1828
FRET-	VPS51	0.030354	-1.694
FRET-	VCP	0.030354	-1.6651
FRET-	TRRAP	0.030354	-1.6237
FRET-	PRPF19	0.030354	-1.3478
FRET-	ASH2L	0.030354	-1.2235
FRET-	UTP6	0.0344	-1.2987

Group	Gene ID	FDR	log2(Fold change)
FRET-	RPS3A	0.042381	-1.4925
FRET-	RACGAP1	0.044201	-1.4768
FRET-	USE1	0.044892	-1.1336
FRET-	CNOT1	0.045483	-1.0822
FRET-	ATP6V1G1	0.049	-1.4845
FRET-	TRAPPC3	0.049886	-1.7526
FRET-	YKT6	0.049886	-1.615